Masters Theses                                              Student Theses and Dissertations

Fall 2015

# The effects of short delay times on rock fragmentation in bench blasts

Margaret Ruth Hettinger

THE EFFECTS OF SHORT DELAY TIMES ON ROCK

FRAGMENTATION IN BENCH BLASTS


by


MARGARET RUTH HETTINGER


A THESIS

Presented to the Faculty of the Graduate School of the

MISSOURI UNIVERSITY OF SCIENCE AND TECHNOLOGY

In Partial Fulfillment of the Requirements for the Degree


MASTER OF SCIENCE IN EXPLOSIVES ENGINEERING

2015

Approved by


Catherine Johnson, Advisor
Paul Worsey
Nassib Aouad

المنارة للاستشارات

www.manaraa.com

# ABSTRACT

Optimized rock fragmentation is essential for minimizing downstream costs to mining operations. Photographic fragmentation analysis, vibration monitoring, and high-speed video all provide measurements of blast effectiveness and supply data that allows operations to modify blasts to achieve downstream goals.

This study evaluates the effects of short hole-to-hole delay times on rock fragmentation. Photographic fragmentation analysis and various delay times were used on the same bench blast, the effects of timing on fragmentation were determined. This analysis provides a representative understanding of timing effects on fragmentation in the field, different from previous blast models which either negate the effects of timing or geology. Four test blasts were conducted at a granite quarry in Talbotton, GA. For each test blast, the bench was divided into three timing zones. This allowed for multiple delay times to be evaluated in each shot and it provided visual comparison of the variable face movement and throw. Hole-to-hole delay times included 0 ms, 1 ms, 4 ms, 10ms, 16 ms, and 25 ms across the various zones. The 16 ms and 25 ms times were the baseline times against which the short delay results were evaluated. The 0 ms and 1 ms times included stress wave collision regions, and the 10 ms time was based on the speed of sound in the rock and burden distance. Each blast was monitored using high-speed video and seismographs. Dyno Consult provided additional seismograph and video monitoring, along with bore track and 3D laser profile data. Multiple photographs were taken of each of the zones for WipFrag analysis. Based on the fragmentation analysis the 25 ms and 10 ms delay times resulted in the smallest rock fragmentation, while the 1 ms delay gave the coarsest fragmentation.

## ACKNOWLEDGMENTS

# TABLE OF CONTENTS

## LIST OF ILLUSTRATIONS

# LIST OF TABLES

## 1. INTRODUCTION

Rock fragmentation is a fundamental goal of bench blasting where the most effective blasts can only be achieved through fragmentation optimization. The meaning of optimized fragmentation is site dependent, as there is no single fragment size that is the most cost effective for all mine sites, loading equipment, and processing facilities. Often times, and in the case of this thesis, the goal is to decrease the average particle size of the fragmented rock without overly increasing fines or, in other words, improve fragmentation. There are many ways to measure blast performance including, but by no means limited to, throw placement, diggability, downstream processing cost, and in-pit fragmentation analysis. Observing and measuring rock fragmentation is one of the first steps toward optimization. Photographic fragmentation analysis, vibration monitoring, and high-speed video all provide measurements of blast performance and supply useful data to the blaster and mine operator. Changes to the blast design, based on the blast performance measures, can be made to improve fragmentation based on the mine's goals. One of the blast design parameters that can be modified to improve fragmentation is timing.

There is some disagreement amongst researchers and blasters regarding the best delay times for increased rock fragmentation. Some studies indicate that utilizing short delay times, which allow for wave interaction and collision, will result in improved fragmentation. One problem with that hypothesis stems from the difficulty of applying delay times that will cause collision in the field; even delays that are based on the speed of sound in the local rock can have their resulting waves altered by unknown geologic discontinuities. Also, even when wave interaction occurs, it may not actually result in

improved fragmentation. The opposing school of thought is to use delay times that are much longer than those which could result in wave collision. These delay times are long enough for each hole to pre-stress the rock of the adjacent hole. Longer delay times are also necessary when the concern is burden movement, but this applies to inter-row delays, not inter-hole delays. Ultimately, either way, delay times must be designed based on site-specific parameters in order to achieve optimized fragmentation. Also, given that delay times affect fragmentation, fragmentation models, such as the Kuz-Ram, need to be modified to include delay timing.

The goal of this thesis is to investigate the possible effects of short hole-to-hole delay times on rock fragmentation in bench blasts. This thesis tests whether or not short hole-to-hole delay times improve rock fragmentation in full scale bench blasting. Six different delay times were tested during four blasts at a granite quarry in Talbotton, GA. These tests included two delay times within the potential stress wave collision region, another short delay time, an intermediate delay time, the mine's standard delay time, and another common long delay time. Hole-to-hole delay times were 0 milliseconds (ms), 1 ms, 4 ms, 10ms, 16 ms, and 25 ms. The 0 ms, 1 ms, and 4 ms delays were all considered to be short delay times, and the 0 and 1 ms times were the only ones with the potential for wave collision. The 16 ms and 25 ms times were the baseline long delay times against which the short delay results could be compared, 16 ms was the mine's standard inter-hole delay. The 16 ms delay had been previously established as a standard at the mine by trial and error. The intermediate, 10 ms delay, was used based on the recommendation of DynoConsult, which is based on an equation that input speed of sound in the rock and burden distance. Each shot was divided into three zones so that multiple delay times

could be tested on a single bench blast. All other blast parameters, including loading, powder factor, and stemming, were completed using the mine's standard blasting procedures.

WipFrag analysis of photographs taken for the designated zones on the bench of each shot was performed and quantitative measurements of the fragmentation distributions resulting from the various delay times were made and analyzed. This allowed for the effectiveness of the delays to be evaluated side by side in the most controlled way possible given the constraints of working in a full-scale production mine and in naturally variable rock. The WipFrag analysis also showed how the relatively small variation in the rock can affect the fragmentation size. In addition to the photographic image analysis, the shots were also monitored using high-speed video and seismographs.

The goals of this thesis are to measure the effects of short inter-hole delay times on blast performance. More specifically, the primary goal of testing was to determine if short hole-to-hole delays improve rock fragmentation in full scale bench blasting. Additionally, it was a goal to observe how short inter-hole delays affect throw.

## 2. LITERATURE REVIEW

### 2.1. INTRODUCTION TO ROCK FRAGMENTATION IN BENCH BLASTS

Rock fragmentation from blasting is dependent on a number of factors. These factors include the properties of the in situ rock, such as jointing and fracturing, properties of the explosives used, blast pattern design, and shot timing. The rock properties such as compressive strength, porosity, density, Young's modulus, Poisson's Ratio, and rock fracturing and jointing cannot be altered. Thus, any optimization to fragmentation will have to occur within the limitations placed by the rock mass. This leaves the explosive properties, blast design including timing design, and execution to influence fragmentation. Explosive properties that influence fragmentation include the Chapman-Jouget (C-J) pressure, density of the explosive, and the detonation velocity of the explosive. Blast pattern design elements include burden, spacing, powder factor, stemming length and type, hole depth and diameter, and sub-drill length (ISEE 2011). Figure 2.1. from the ISEE (2011) illustrates these blast parameters. The delay timing of a blast will also influence the fragmentation. This timing influence will be extensively covered in Section 2.2.
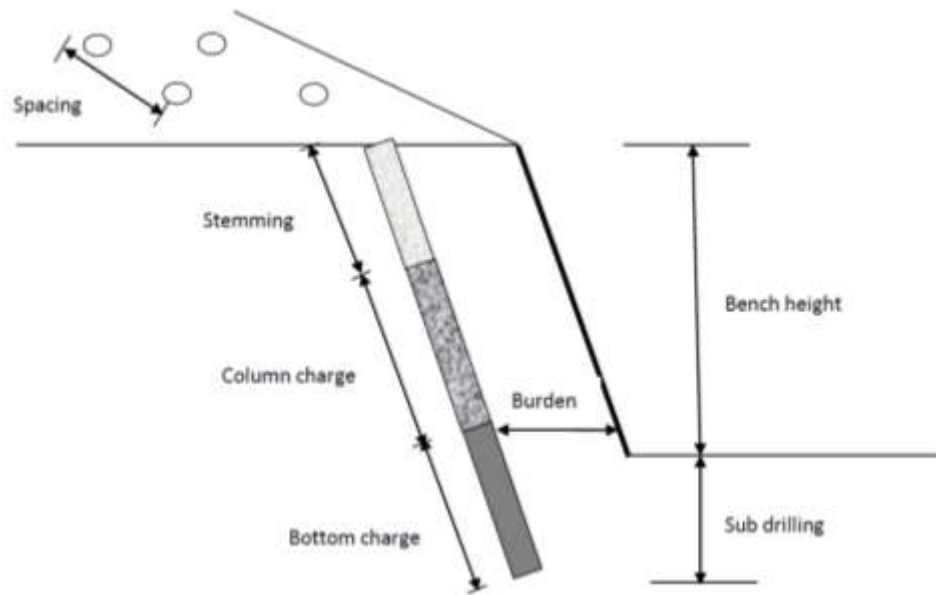
Figure 2.1. Blast Parameters (Johnson 2014)

A reasonable starting point for understanding the mechanisms by which rock
fragmentation occurs, is to examine how fragmentation happens around a single blast
hole. The process begins with the detonation of the explosives in the hole, which transmit
a radial shock wave into the rock mass. The detonation and this initial shock wave causes
crushing around the hole by exceeding the uniaxial compressive strength of the rock.
Relatively close to the hole, the shock wave will attenuate to a stress wave (ISEE 2011).
As the stress wave continues outward, breakage occurs in tension at rock fractures, joints,
and discontinuities. When the compressive wave reaches a free face, it reflects in tension
causing failure cracks and bench face spalling (Worsey 2014, Johnson 2014).
Immediately following the stress wave, the other major factor, the gas pressure comes
into play. The hole is pressurized by the gases, which leads to the growth of previously
created radial fractures, as well as the expansion of material flaws within a few borehole

diameters. As the fracture zone extends, dominant fractures continue to grow (Worsey 2014). Gas pressure is not able to dissipate until it reaches a significant phase change. This will typically occur at a free face. The gas pressure bows the bench face and pushes it forward (Johnson 2014).

While examining the fragmentation effects caused by single holes is essential; it is far from all encompassing. When a bench blast occurs, rock damage accumulates behind the stress wave and improves as stress waves from secondary holes move across areas that have already been traversed by the stress waves of the initial holes (ISEE 2011). Additional fragmentation occurs by collision between blasted rocks and the impact of the rocks with the ground (Worsey 2014b). Basic principles of blast optimization provide guidelines about how to alter fragmentation by modifying blast pattern geometry. Based on these, fragmentation can be improved (smaller particle size) by decreasing burden and, within limitations, decreasing spacing (effectively increasing powder factor). It is important to note that in this scenario, improved fragmentation is not necessarily optimized fragmentation, because reducing the pattern geometries can also cause an increase in fines and other less than desirable effects. Also, stemming type and length can affect fragmentation; this is particularly significant at the top of the bench and can result in unbroken cap rock and oversize (Worsey 2015).

## 2.2. BLAST MODELS AND RESEARCH ON TIMING EFFECTS

The understanding of rock fragmentation mechanisms and the methods for optimizing fragmentation have always been important for blasting engineers and mine operators, because rock fragmentation can have a significant influence on production

costs. The optimization of fragmentation through trial and error as well as blaster experience was used before many of the mechanics of fragmentation were understood.

**2.2.1. Classic Blast Timing Principles.** The utilization of correct delay sequencing is essential for muck pile formation and delay timing is necessary to maintain the balance between required confinement and the creation of relief, as crack extension and face movement both progress. The degree of confinement of a blast is directly related to the time it will take for the rock to respond; therefore as blast confinement increases, so must the delay time utilized. Blast timing should direct the rock displacement to create the desired muck pile shape and location (ISEE 2011). Traditional timing design principles suggest that decreased hole-to-hole delay times decreases fragmentation and increased row-to-row delay times increases fragmentation up to a certain limit (Worsey 2015).

Floyd (2013) suggests a number of typical timing ranges for optimum fragmentation based on rock mass type. These include an inter-hole delay of less than 0.3 milliseconds per foot (ms/ft) of spacing for blocky and massive rock with an inter-row delay of at least 2 to 3 times the inter-hole delay and an inter-row delay of 0.5 to 1.5 ms/ft of burden for highly jointed or highly bedded rock. Floyd's (2013) suggestions do not align well with some of the recommendations stated in other research. Modifying pre-existing timing plans and observing the results to achieve improved fragmentation is another way that blasters have improved fragmentation using timing. Grant (1990) reviewed a large number of published blast trials and found that optimized fragmentation was found at 3-5 ms/m of burden.

**2.2.2. Introduction to Wave Collision.** The ISEE Blasters' Handbook (2011) states that, under certain timing circumstances, stress waves can collide between two holes. Depending on where the stress waves collide, or interact, various results can occur which affect fragmentation. One wave may be overwhelmed by the other, thus causing effects of the first to be inhibited by those of the second. This occurs in the case that the first wave has already depleted before interacting with the stronger second wave. Yamamoto (1999), states that simultaneously detonating charges, referred to as zero millisecond delays by the ISEE, will result in wave collision halfway between the two holes. According to Yamamoto (1999), the greatest fragmentation between two holes occurs when the tensile trailing sections of the blast waves interact. Worsey (1981) disproves Yamamoto's conclusion based on micro-fracture density. Worsey (1981) used tests performed in resin blocks to show that, rather than initiating at the midway point between holes, fractures from adjacent holes intersect and merge there. While Yamamoto (1999) and the ISEE (2011) agree that wave collision occurs and has an effect, in contrast to Yamamoto, damage, in the case of the ISEE (2011) simulation, was increased by utilizing delay times that were significantly longer than those that would have had any stress wave interaction. Rossmanith (2003), puts forth that the location and size of the stress wave interaction very much depends on the ratio of the length of the pulses, the hole spacing, and the delay time used. Rossmanith's (2003) results are discussed further in Section 2.2.3.

Early models of wave interaction lacked experimental data. More recent research has begun to provide a clearer picture of what is actually happening. Many experimental tests and newer model simulations disagree with Rossmanith (2003) and Yamamoto

(1999) and agree with the ISEE (2011), that the greatest fragmentation occurs at delay times that are too long for wave interaction to occur. These models and tests are detailed in Sections 2.2.4.

**2.2.3. Blast and Fragmentation Simulations and Modeling.** Traditional blast design methods do not incorporate all of the variables that can be used to optimize fragmentation and can be accounted for when using electronic detonators. While every model has its limitations, blast and fragmentation modeling can provide information about the outcome of a blast that would have previously been unknown. According to Rossmanith (2003), laboratory scale tests have shown that the interaction of blast waves and subsequent cracks can be used to achieve optimized fragmentation. In order for the waves to utilize the superposition effect, delay times must be significantly shorter than conventional delay times. One component that laboratory and scale tests cannot incorporate well is rock jointing and faulting. In order for wave interaction to occur, delay times must be selected based on site specific rock properties, such as the sonic velocity of the rock and the presence of jointing and fractures. Since these features are typically not thoroughly and accurately characterized for each blast, designing a blast with the goal of interaction is difficult. This is also the major problem with modeling blasts using computational mechanics methods. For these methods to be employed, one must negate the effects of structural geology (Rossmanith 2003). Section 2.5 details how geology influences fragmentation.

Within the rock mass or body, P-waves and S-waves, propagate. P-waves are primary or longitudinal waves and S-waves are secondary or shear waves. Each of these waves has a leading (compressive +) and a trailing (tensile -) part. Close to the hole these

waves overlap, but as they travel out they will separate because their speeds are different. Rossmanith (2003) states that given two holes separated by a spacing, the fundamental event is the interaction of two stress waves: $P_1$-$P_2$, $S_1$-$S_2$, $P_1$-$S_2$, and $S_1$-$P_2$. A number of zones of interaction can be identified, as illustrated in the Lagrange diagram shown in Figure 2.2. The areas of stress wave interaction may cover the space between holes multiple times when non-brisant explosives that produce long stress waves are used.
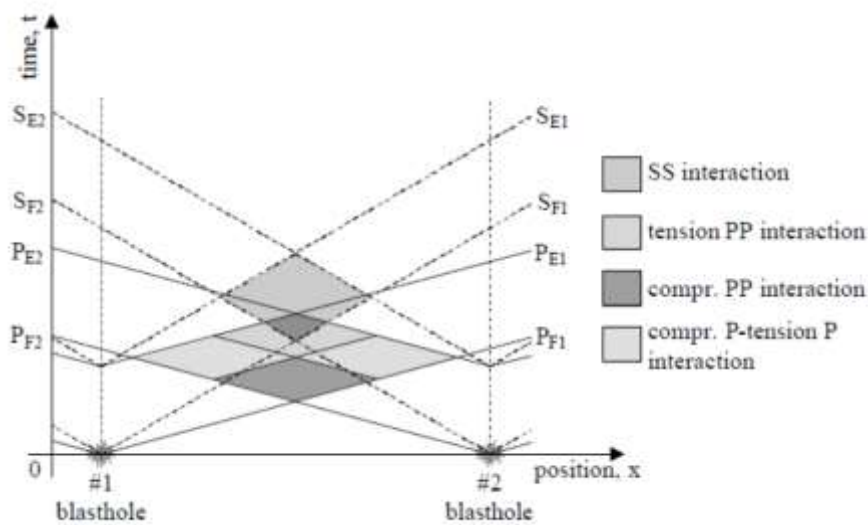


Figure 2.2. Lagrange Diagram of the Interaction of Stress Waves from Two Simultaneously Detonated Holes and Their Wave Interaction Patterns (Rossmanith 2003)

Another parameter that should be incorporated when designing a blast that utilizes electronic detonators is acoustic impedance. The acoustic impedance of the explosives, the rock, the ratio of the two, and the ratio between different rock strata are all important quantities to understand. The stress and strain field caused by the detonation of a blast hole is dependent on the ratios between the velocity of detonation and the wave speed in the rock mass (Rossmanith 2003).

Proposed by Cunningham in 1983, the Kuz-Ram model was one of the original models used to predict rock fragmentation size, and it is still a commonly used model in the industry. The model uses the combination of the Kuznetsov and Rosin-Rammler equations. The Kuznetsov empirical equation gives the relationship between the mean rock fragment size and the powder factor used. The Rosin-Rammler equation is used to predict the rock fragment size distribution. There are a several problems with the Kuz-Ram model. These include an inability to predict fines and a failure to account for shot timing. A number of models and modifications have been proposed in order to mitigate some of the problems with the Kuz-Ram model, and to improve rock fragment size distribution prediction. Two examples of extensions of the Kuz-Ram model are the Crush Zone Model (CZM) and the Two-Component Model (TCM). These models, known as the Julius Kruttschnitt Mineral Research Centre (JKMRC) models, aim to improve the prediction of fines (Gheibie 2009). All of the modified Kuz-Ram models still fail to incorporate timing as a parameter (Johnson 2014). Of course, as it has been previously stated, timing has an influence on fragmentation. So, any model that does not include timing as a variable, must only be used with the understanding that once timing is incorporated into the blast, the outcome may vary from the model.

**2.2.4. Further Research, Lab Scale Tests, and Field Tests.** Sjoberg's (2012) project tested Rossmanith's (2002) hypothesis that fragmentation is improved in areas of tensile tail interaction and the project developed computational tools for blast simulation. Sjoberg (2012) used the 3D finite-element code LS-DYNA to model blasts, with Euler formulation close to the blast hole and Lagrange formulations in the rock further from the hole. A Riedel-Hiermaier-Thoma (RHT) material model was used to simulate the rock

and an algorithm was developed to calculate fragmentation based on model interpretation. The hole diameter was 311 mm. Explosive column heights of 8 meters (m) and 11 m were used. The delays, amount of explosive, and distance between blast holes were varied as shown in Table 2.1. Based on the cases tested, Sjoberg (2012) concluded that there was a small effect from stress wave interaction, but that it was local and did not significantly improve fragmentation. Varying hole space and explosive quantity had the largest effect on fragmentation, and relatively long delay times where the stress wave would have passed the second hole resulted in the most fragmentation.

Table 2.1. Cases analyzed by Sjoberg (2012)

| Case no. | Ignition time | | Amount of explosive | | Distance between blast holes |
|---|---|---|---|---|---|
| | Hole 1 | Hole 2 | Hole 1 | Hole 2 | |
| 1 | 0 ms | 0 ms | 11 m | 11 m | 8.7 m |
| 2 | 0 ms | 1.5 ms | 11 m | 11 m | 8.7 m |
| 3 | 0 ms | 5 ms | 11 m | 11 m | 8.7 m |
| 4 | 0 ms | 0 ms | 11 m | 11 m | 12.3 m |
| 5 | 0 ms | 0 ms | 8 m | 8 m | 8.7 m |
| 6 | 0 ms | 0 ms | 8 m | 11 m | 8.7 m |

Johansson and Ouchterlony (2013) performed model scale tests to study the utilization of short delays to promote improved fragmentation caused by shock wave interactions. The tests were made on magnetic mortar blocks confined by U-shaped yokes, with the space between the yoke and the mortar block filled with fine-grained expanding grout comparable to the yoke characteristics to minimize the impedance mismatch. The block size was 650/660 x 205 x 300 mm (L x W x H). It had two rows of

holes each with five 10-mm holes per row. The spacing and burden was 110 and 70 mm. Decoupled 20 g/m PETN-cord was the explosive used. The two rows were shot separately and the first row caused back break into the second. Delay times were first selected based on the measured elastic P-wave velocity of 3,800 m/s which indicated an arrival time at the adjacent hole for the elastic wave of ~28 µs. They used hole-to-hole times that covered from before the P-wave from the adjacent hole arrived until well after the S-wave had passed. Table 2.2 shows the full range of delay times used by Johansson and Ouchterlony (2013) and the reason for their use based on the expected wave interaction or lack thereof. They found that their second row of holes had significantly different fragmentation results from the first, because of the backward penetration of cracks from the first row. The second row material was significantly smaller and more uniform. This indicates that the pre-stressing of the rock mass by preceding blast holes as a shot progresses plays an important role in the overall fragmentation distribution of the shot.

Table 2.2. Test Matrix Johansson and Ouchterlony (2013)

| Test no. | Block no. | Nominal delay time (µs) | Expected interaction | Campaign no. |
|---|---|---|---|---|
| 1 | 1 | 28 | P-wave velocity ($c_P$) interaction at neighbour hole | 1 |
| 2 | 6 | 146 | No shock wave interaction | 1 |
| 3 | 2 | ∞ | Single shots to determine shock wave arrival times at neighbour hole | 2 |
| 4 | 3 | 37 | Shock wave interaction at neighbour hole | 2 |
| 5 | 4 | 46 | Initial 'tensile' (negative) phase interaction with shock wave | 3 |
| 6 | 5 | 56 | Intermediate 'tensile' (negative) phase interaction with shock wave | 3 |
| 7 | 8 | 46 | Repetition because test no. 5 gave anomalous results | 4 |
| 8 | 7 | 86 | Vanbrabant's recommendations | 4 |
| 9 | 11 | 73 | 2nd variety of Vanbrabant's scheme | 5 |
| 10 | 9 | 146 | No shock wave interaction and confined | 5 |
| 11 | 13 | 73 | Vanbrabant 2nd scheme and confined | 5 |
| 12 | 14 | 146 | No shock wave interaction and confined | 6 |
| 13 | 10 | 73 | Vanbrabant 2nd scheme and confined | 6 |
| 14 | 12 | 73 | Vanbrabant 2nd scheme | 6 |
| 15 | 15 | 0 | Instantaneous initiation | 6 |

Katsabanis has published a number of papers regarding the effects of timing on rock fragmentation and in 2014 published a review of past research about the timing parameters necessary for fragmentation optimization, which covered much of his own previous research, several other studies of significance, and new experiments in grout specimens. Studies completed by the USBM (Stagg and Nutting 1987, Stagg and Rholl 1987, Otterness et al.1991), included reduced scale tests and full scale tests. While not many conclusions can be made based on the early tests, it seemed that very short delays were associated with coarse fragmentation. In 1996, Katsabanis and Liu studied delay effects on a small granite bench using manual digitization of high-speed films. This method only allowed large differences to be observed because its accuracy was compromised by penalizing small fragments. Zero delay times resulted in boulders and the optimum delay was found to be 2.4 ms/ft (8 ms/m) of burden (Katsabanis and Liu 1996).

Katsabanis et al. (2006) performed small scale tests in high quality granodiorite using an equilateral triangular pattern that had 10.2 cm between 11 mm in diameter holes. Each hole was 18 cm long. 23 holes were drilled in each 92 cm x 36 cm x 21 cm (length x width x height) block. The holes were each loaded with three strands of 5.3 g/m (25 grain/ft) detonating cord and coupled to the rock with water. Lengths of detonating cord and seismic detonators fired with a sequential blasting machine were used to achieve delay times from 0 to 4000 μs. After each shot, fragments were collected and screened to determine the fragmentation sizing. Results of the tests showed that the coarsest fragmentation occurred when all charges were initiated simultaneously and that fragmentation became finer as delay time increased, up to 1 ms between holes. There was

little difference between delays varying from as fast as 10 µs to as long as 1 ms. This gave an ideal range of delays for fragmentation optimization between 0.03 ms/ft (0.11 ms/m) of burden to 3.4 ms/ft (11 ms/m) of burden. Fragmentation became coarser at very long delays because the fragments become separated by open cracks. This work shows that the selection of fast firing times is not ideal for fragmentation optimization (Katsabanis et al. 2006).

Katsabanis et al. (2014) sought to eliminate some of the problems that were present in previous research. These were scatter in measurements, unwanted edge effects, and few data points covering the entire range of delays. To solve these problems, small scale tests were conducted, simulating a rock bench, using a grout resembling rock encased in a yoke that eliminated unwanted reflections. The blocks were 60 cm x 40 cm x 25 cm and were drilled with a 7.5 cm x 10.5 cm (burden x spacing) pattern of 12 mm diameter holes. Each hole was 23 cm long and was loaded with two strands of 10 g/m (50 grain/ft) detonating cord coupled to the block with water. Delay times were obtained using lengths of detonating cord for those times less than 100 µs and sub-millisecond electronic detonators were used for delays greater than 100 µs. Fragments from each shot were collected and screened to determine the fragmentation sizing. Very short delays produced the worst fragmentation. The best fragmentation was achieved between 4 ms/m of burden and 10 ms/m of burden. Then, at long delay times fragmentation became coarser and back break was increased (Katsabanis et al. 2014).

Johnson (2014) investigated the effects on fragmentation of head on collision of shock waves in a rock mass and of detonation waves within the explosive column. Twenty seven small scale tests in 15 x 7 ¾ x 7 ¾ inch concrete blocks were performed.

Each of the blocks was wrapped in geotextile fabric and wire mesh so that in situ fracturing could be examined. 50 gr/ft detonating cord was used.  Three types of tests were completed. Six concrete blocks were used to test single initiation as a baseline for comparison with the second test. These tests had detonating cord initiated from one end so that no wave collision would occur. Six blocks were used to test colliding detonating waves. In these tests, detonating cord was initiated from both ends. This resulted in the collision of detonation waves through the center of the block. The third set of tests consisted of 15 blocks and tested colliding shock waves. These experiments had no explosives in the center of the block. This allowed only the shock waves to move through the block and collide in the center. This test was similar to what happens between blast holes. The second test set resulted in the same radial crack formation as in test one, but had the addition of a horizontal crack through the center. For the third set of tests, both instantaneous detonation of the two holes and various changes in initiation time were tested. Here the largest fragments were found in the center of the blocks where there was no explosive, but there was shock wave collision.

Collision of shock waves between blast holes was found to decrease fragmentation. The directional particle movement between holes resulted in  an increase in the concrete density at the collision point, which resulted in decreased fragmentation and increased throw because of the impedance mismatch at the center point. Simulations were done which backed up the small scale experimental data, but no full scale bench blast tests were completed (Johnson 2014).

The results of tests done by Sjoberg (2012), Johansson and Ouchterlony (2013), Katsabanis et al. (1996, 2006, 2014), and Johnson (2014) contradict Rossmanith (2003)

and Yamamoto (1999) and agree with the ISEE (2011). These results point to the conclusion that the best fragmentation results are achieved using delay times that are much longer than those which can produce wave interaction. Additionally, very long delay times should be avoided as they result in coarser fragmentation and increased back break.

Yang and Rai (2011) studied the effects of inter-row delay timing on fragmentation and fragment size distribution in full scale at the Century Cements limestone quarry in Raipur, India. Previous research at the same quarry led them to test the timing on straight V and diagonal patterns, because these had provided better results than other pattern types. Inter-row delay times of 17 ms and 25 ms were tested on both pattern types. These times gave effective firing delays of about 2.4 ms/ft (8 ms/m) of burden and 3.7ms/ft (12 ms/m) of burden, respectively.

The digital image analysis software Fragalyst was used to measure fragment size and distribution. Photos were taken every hour to capture the entirety of the excavation and a large number of images were analyzed for each muck pile. This study provides a good example of the effective use of a digital image analysis program. (The use of digital image analysis for rock fragmentation characterization is detailed in Section 2.6.) For both of the pattern types tested, the 17 ms delay resulted in better fragmentation. It was concluded that the 17 ms delay allowed for more in-flight, inter-rock collisions than the 25 ms delay time (Yang and Rai 2011). While this study provides insight into how various inter-row delays influence fragmentation, because of the use of a shock tube based pyrotechnically delayed initiation system, the timing accuracy was much lower than what would have been achieved using an electronic system. Thus, if the study were

to be repeated utilizing electronic detonators, the results might not be the same. Additionally, the delay times tested did not represent a range of short and long times, but rather two fairly similar mid-range times.

### 2.3. TIMING INFLUENCE ON THROW

Delay time influences how the blasted rock will move, and blasts can be designed so that the desired throw is achieved. In addition to timing, other blast design parameters such as burden; spacing; hole diameter, depth, and angle; pattern type; and explosive type can influence rock movement. Bench blasting is one of the most efficient blast geometries for fragmentation and throw. Different types of bench blasting, such as quarry blasts and cast blasts, have different goals in terms of throw and, therefore, have differing design parameters, which include varying delay times. Typically in a quarry blast the aim is to spread the rock on the quarry floor in such a way that diggability is optimized for the quarry's available excavation equipment. There are a number of ways that cast blasting differs from quarry blasting. In terms of the muck pile, cast blasts aim to throw as much muck as possible to the final location so that the minimum amount of handling is required. They also aim to achieve looseness and fragmentation that allows for easy digging by the dragline. In cast blasting, it is important to use sufficient inter-row delay times to allow for necessary burden relief (ISEE 2011). Short hole-to-hole timing is necessary so that holes interact and a higher percent cast is achieved (Worsey 2015 b). Grant (1990) states that for a front row of holes, the greatest throw is achieved when all holes are fired simultaneously. Small scale tests performed by Johnson (2014) found an increase in throw when adjacent holes were simultaneously detonated.

## 2.4. BENEFITS OF ELECTRONIC DETONATORS

It must be understood that rock damage and crack propagation occurs significantly behind the stress wave in order to utilize detonators in a way that allows for the optimization of fragmentation based on those effects. No other type of commercial blasting detonator has the accuracy along with precision necessary to take advantage of timing plans that correctly match the best time for optimized fragmentation. One of the key ways that electronic detonators differ from their predecessors is that, rather than using relatively inaccurate pyrotechnic delays, they utilize an integrated circuit chip to control the delay time. This electronic chip allows for their nearly complete accuracy and precision. Typical electronic detonators have an accuracy of plus or minus 1 ms for all delay times and delays can range up to 20,000 ms (ISEE 2011). Some manufacturers sell detonators that are said to provide even more accuracy with precision, and a larger delay range. An example of these is Orica's (2015) newest detonator which is specified as having timing that has precision as a coefficient of variation of 0.005% and a maximum delay time of 30,000 ms. Studying the effects of short delay times would be ineffective and nearly useless without the ability to utilize accurate electronic delays. The scatter that would be present when using detonators with pyrotechnic delays would most likely result in some holes firing out of planned order or at otherwise incorrect times. These timing inaccuracies would affect the fragmentation of the shot and would likely negate any possibility of wave interaction.

## 2.5. THE INFLUENCE OF GEOLOGIC STRUCTURES ON FRAGMENTATION

The properties of the rock mass being shot can have a significant influence on the fragmentation outcomes of the blast. Rock properties such as compressive strength, porosity, density, Young's modulus, Poisson's Ratio, and rock fracturing and jointing can all influence fragmentation. Rock structures, fracture planes, and voids can attenuate fragmentation crack network formation and can cut into the energy distribution of the pattern. Both of these can cause less than optimum fragmentation results from a blast. It is important for rock structures to be identified and mapped because if blast hole pattern dimensions exceed those of structure spacing, fragmentation will be poor (ISEE 2011).

Abu Bakar et al. (2013) reviewed the influence of geological discontinuities on fragmentation. Most rock masses have fissures and they act to reduce induced stress on the rock and radial cracks from blasting are arrested at the fissures when stress concentration becomes too low. Previous stress-time history and the differences in principle stresses can change the fracture pattern caused by blasting. Energy loss in joints increases as joint size increases and the infilling of joints can affect the wave transmission through the joint depending on how well the infill material matches the impedance of the rock mass. For small joints with well-matched infill material, the wave transmission will be better than for larger joints or those with mismatched infill material.

Jointing controls rock fragmentation in a number of ways. Jointing will reduce and reflect waves, thus limiting their effects, as well as control the radial fracturing zone. Joints will often stop the extension of fractures, as a fracture will tend to follow along the joint rather than passing through it. Also, gases can escape into the joint causing reduced

fragmentation because of the venting. Finally, jointing can reduce rock mass strength (Worsey 2014 c).

Rock mass strength influences fragmentation, but it can be difficult to characterize in rock that is not homogenous. One thing that affects rock mass strength is bedding planes. Their presence in a rock mass will lower its strength and allow for easier fragmentation. Additionally, as the number of bedding planes in a rock mass increases, the ability for those bedding planes to control the maximum fragmentation size also increases. Bedding at the bottom of a bench allows for easier movement and better fragmentation. Weathering of the rock mass can also affect fragmentation by creating zones of rock with strengths that differ from the rock below or surrounding a contact zone. Weathering which results in weakened rock can cause confinement problems, and weathering that exposes a hard layer that ends up being the bench surface can result in cap rock problems. Small voids can also affect the rock strength if many of them are present. Large voids can have an effect on fragmentation because they allow for the venting of gas and therefore a reduction in gas pressure (Worsey 2014 c).

## 2.6. ROCK FRAGMENTATION ANALYSIS METHODS

Rock fragmentation distribution can be evaluated in a number of different ways. These methods vary from those that are very simple to perform and qualitative to the impractically difficult in production situations, but very quantitatively accurate. Fragmentation can be evaluated qualitatively on a shot to shot basis by blaster observation and loader operator feedback about sizing and diggability. This method lacks data and is subject to a significant amount of human error and bias. Sieving of shot rock

is a very accurate quantitative method of determining fragmentation size, but it is time consuming, impractical, and expensive in active mining operations. Digital image analysis provides a middle ground between the previous methods with a quantitative measure of fragmentation sizing that is minimally disruptive to the mining process, and is therefore a practically applicable method of obtaining the fragmentation results of bench blasts. Digital image analysis of shot rock can be performed using images of the muckpile taken with handheld/portable cameras, with belt mounted systems, or loader mounted systems (Motion Metrics 2015).

There are various software packages and image capture systems designed to facilitate digital image analysis for fragmentation sizing. These include WipFrag, Split, PortaMetrics, GoldSize, Fragscan, PowerSieve, and BLASTFRAG (Split Engineering 2015, Motion Metrics 2015, Sanchidrian 2009, Johnson 2014). Many of the image analysis systems operate in a similar manner and most require some type of scaling item to be placed in the photo. For example, WipFrag takes an image of a muckpile or other broken rock and converts that image into a net of rock fragments. This net is measured and used to provide a sieve simulation of the fragments. This provides fragmentation statistics, such as the D10, mean, D50, and D90, and graphs of the fragmentation sizing (WipFrag 2015). WipFrag (2015) states that, "images must be clear, evenly lit and must be acquired systematically in order to minimize editing and to optimize results." Even when using high quality photos, rock outline editing is typically necessary to distinguish fragments, identify fines, and identify shadow or other areas to be excluded from the analysis. Systematic photo acquisition is important both immediately after the shot and throughout the mucking process to ensure all areas of interest are accounted for. Photos

must be collected throughout mucking to eliminate the sampling bias caused by the typically more course fragmentation found on the surface of muck piles (Johnson 2014).

There are a few problems associated with digital image analysis methods that should be understood when utilizing them for fragmentation optimization, but that do not negate the usefulness of the analysis. These include the previously mentioned manual editing of rock outlines to ensure correct delineation of fragments. This introduces human error into the analysis, especially when particle sizes are small. In images with larger particle size or where the image resolution is high, this error is minimized. Other issues include errors associated with the calculations used to transform rock surface measurements into volumes, the limitations of the resolution of image systems, shape effects causing fragments to be assigned mesh sizes differently in the image analysis than they would be in sieving, and density assumptions. When utilizing image analysis to do side-by-side comparisons, some of these problems, such as the volume calculations, are irrelevant because any error introduced will apply to all of the images and the difference in size distribution from photo to photo will still be evident. Additionally, despite the issues, when tested, the size distributions found using digital image analysis of muck piles matches those of sieved material well. Coarse materials tend to result in fewer errors than fine materials (Sanchidrian 2009).

## 2.7. IMPACT OF FRAGMENTATION ON BLAST PERFORMANCE AND DOWNSTREAM COST EFFECTS

There are a large number of ways to evaluate the effectiveness of a blast depending on the desired outcomes. Historically, blast effectiveness has been measured based on in-pit results, but given that these results do not fully encompass the areas that

blast performance affects, it is necessary to evaluate a blast based on downstream results. Effective rock fragmentation is key to minimizing downstream costs by optimizing crusher and grinder throughput, minimizing wear on equipment, maximizing dig rate and payload, decreasing energy consumption of equipment, and controlling fines production. Photographic fragmentation analysis, vibration monitoring, and high-speed video provide quantitative measurements of blast effectiveness and supply data that allows operations to modify blasts to achieve downstream goals (ISEE 2011).

## 2.8. LITERATURE REVIEW SUMMARY

Rock fragmentation in bench blasting is dependent on many factors. Some of these, such as the rock mass characteristics, cannot be modified. Other variables, such as the blast design and delay timing, can be modified to optimize the fragmentation of a shot. Understanding the mechanics of a single blast hole is important when designing for fragmentation, but it is not all encompassing. Fragmentation also occurs because of pre-stressing of holes and the impact of rocks on each other and the ground. Increased powder factor will lead to smaller fragment sizes.

Blast timing should direct the rock displacement and create the desired muck pile shape. There is some disagreement among blasters and researchers about what delay times are ideal for fragmentation optimization. Some researchers argue that short times, that cause wave collision, result in the best fragmentation. The majority assert that the best fragmentation occurs at delay times much longer than those that have the potential for wave collision. Another blast outcome that is affected by delay timing is throw. Short hole-to-hole timing is necessary to achieve the greatest throw. In order to study the

effects of short delays, electronic detonators are needed for their superior accuracy and precision.

There are several ways to analyze rock fragmentation, but digital image analysis has many advantages. WipFrag is a program which allows the user to take an image of a muck pile and convert that image into a net of rock fragments, which can then be virtually sieved. This provides fragmentation statistics, such as the D10, mean, D50, and D90, and graphs of the fragmentation sizing.

### 3. EXPERIMENTAL SETUP

All four test blasts were conducted on the North 2nd Bench of an actively mining granite quarry in Talbotton, GA. The test blasts were full-size production shots conducted between April 16, 2015 and September 15, 2015. The tests included all shots on this bench during this timeframe. Each blast shot approximately 48,000 cubic yards of rock. The mine ran two Caterpillar 990 loaders, four 70 ton haul trucks, and one 50 ton haul truck. The last photographs for WipFrag analysis were taken on September 29, 2015.

#### 3.1. STANDARD BLAST DESIGN

The mine's standard inter-hole delay time was 16 ms and the inter-row delay was 142 ms. Each shot consisted of two rows of 5.75 inch holes with a total of 85 or 86 holes per blast. The burden and spacing were 13 feet and 17 feet, respectively. The mine's standard blast design was used for all of the shots. The only modifications made were to the hole-to-hole delay times. Other than the delay time variable all blast design parameters, including loading, powder factor, planned burden and spacing, and stemming were held constant. The zones in which the various delay times were used and additional details about each shot are detailed in Section 3.2 and Sections 3.4 through 3.7, respectively. The burden measurements from Boretrack and 3D Laser Profile data will be discussed in the individual shot sections. The bench height was approximately 70 feet and holes were drilled with a 3 foot sub-drill, at a 5 degree angle. The shots had only one open face. The typical stemming height was 8 to 9 feet and the stemming material used was good quality angular ¾" crushed rock as shown in Figure 3.1.

Figure 3.1. Typical Angular ¾" Stemming Material

Holes were loaded with either Titan 1000 SME or Titan 1000 SD. The two emulsion types were very similar. They both had a density of 1.20 g/cc, energy of 680 cal/g, and relative bulk strength of 1.13. The Titan 1000 SD had a slightly higher velocity and detonation pressure. Detailed information about the two emulsion types, as well as full loading details for each shot, is included in Appendix B. It would have been ideal if all holes could have been loaded with the exact same emulsion. Because of the loading capacity of the available powder trucks in the area, Zones 1 and 2 were loaded with Titan 1000 SME and Zone 3 was loaded with Titan 1000 SD. Dual electronic, Digishot, detonators were used to initiate each hole and allowed for the use of any desired delay time. Detonators with boosters were placed near the top and bottom of the hole and had a 2 ms delay between the bottom and top detonators. The bottom detonator was fired first and the top detonator was there as a back-up. The detonators were approximately 30 feet apart and given the detonation velocity of the explosive, the top detonator was overcome by the column detonation before firing. A typical bench and standard hole loading are shown in Figures 3.2. and 3.3.

Figure 3.2. Hole Loading During Test Shot 1, with Titan 1000 SME Truck in Background



Figure 3.3. Loading a Hole for Test Blast 1 with Titan 1000 SME

## 3.2. TIMING ZONES

For each test blast the bench was divided into three zones. Separating the bench into zones allowed for three different delay times to be evaluated on each shot. It also provided visual comparison of the variable face movement and throw. The separations were identified using buckets on top of the bench, as well as on the floor below. Shock tube "flash bulbs" were used to indicate the column detonation of the opening hole in each zone and could be seen clearly on the high-speed video. Figure 3.4. shows the set-up of a shock tube "flash bulb." In addition to the separation buckets, a bucket was hung over the face in the center of each zone, approximately 30 feet down to investigate face velocity.



Figure 3.4. Shock Tube "Flash Bulb" (hole outside of photo in lower left)

On the floor below the shot, in the center of each zone, neon painted rocks were placed at 150, 200, 250, and 300 feet from the face. These rocks allowed for observation of the throw distance achieved in each zone.  The layout of the zones, buckets, and marker rocks are shown in Figure 3.5. An image of the neon rocks and face bucket is shown in Figure 3.6. and an example of the zone marker bucket on the bench floor below is shown in Figure 3.7.
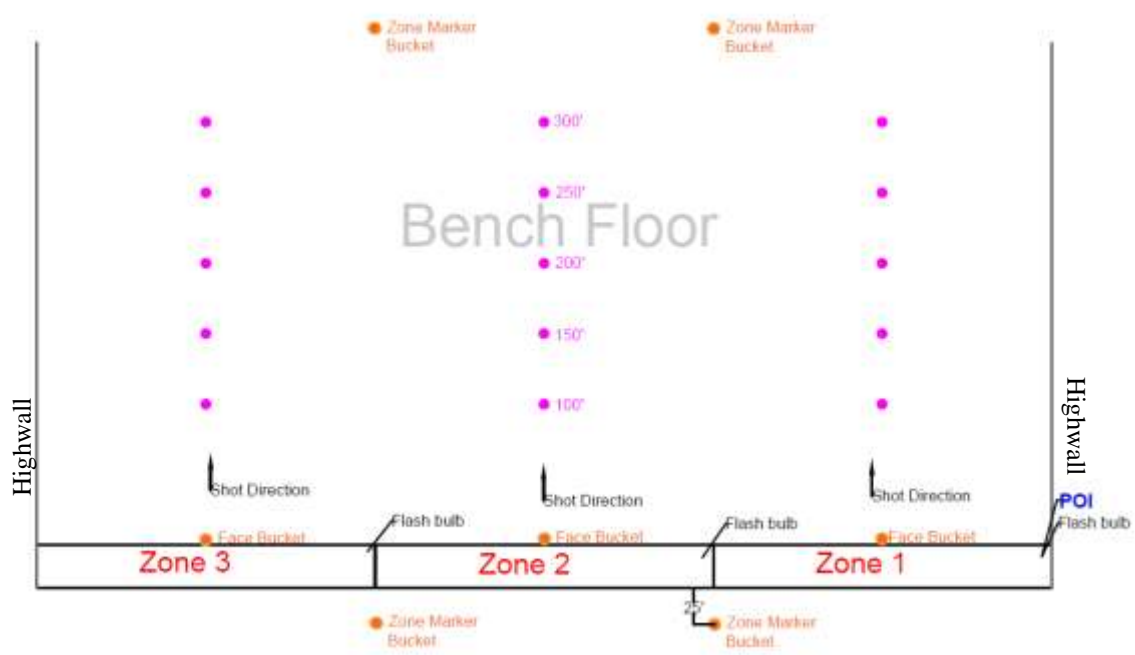


Figure 3.5. Top View of Bench Showing Zone Layout, Buckets, and Marker Rocks

Figure 3.6. Measurement Rocks and Face Bucket

Figure 3.7. Zones 1 and 2 Demarcation Below Test Shot 1

The mucking of each shot took several weeks and as a result, mucking of Zone 3 had typically not begun when the second set of photographs were taken. This affected the number of Zone 3 Photos available for WipFrag analysis on Shots 2 and 3. On Shot 1, Zone 3 was not evaluated, and on Shot 4 only two sets of photos were taken because of time constraints. Figure 3.8. shows the mucking process.



Figure 3.8. Shot Mucking (Catipillar 990 Loader)

**3.3. INSTRUMENTATION**

There were several ways in which information for each text blast was collected. The main source of shot data was collected via photographs taken for digital image analysis in WipFrag. Photographs were taken systemically for each timing zone, immediately after each shot and throughout the mucking process. The WipFrag analysis and results are detailed extensively in Section 4. The analysis photos and graphs can be found in Appendix A. Photographs were also used to document bench and floor conditions and the set-up of zone markers, seismographs, and other instrumentation. Additionally, still photographs were taken of each blast as it was shot. These photos are included in Appendix D.

High-speed video was taken of each shot. The first two shots were recorded by DynoConsult. For the second two shots, an MREL Blaster's Ranger II camera was used. The shock tube "flash bulbs," as discussed in Section 3.2., showed the start of each zone on the high-speed video recording and the buckets hung over the face showed the face movement. The Ranger II high-speed camera set-up is shown in Figure 3.9.



Figure 3.9. MREL Blaster's Ranger II Camera Set-up with Dr. Johnson

Seismographs were used to monitor each blast as well as to calculate the speed of sound in the rock and the airblast speed. Several White Mini Seis II were deployed by DynoConsult. Once available, two White Mini Seis III were used in addition to those provided by Dyno Consult. The two Mini Seis III were used to determine the speed of sound in rock, used in the determination of the 10 ms delay time, and the airblast speed. The speed of sound in the rock mass and airblast speed were found by tethering the two seismographs together at a known distance. The seismograph closest to the blast was the master which triggered the slave seismograph to begin recording at the same time. There were no concerns regarding the overpressure at the mine, because there were no close neighbors to the mine. The airblast recording is useful should short delay times be used in situations with neighbors in close proximity. The specific placement of seismographs is detailed in Section 3.4., the seismograph reports are included in Appendix C., and seismograph results are detailed in Section 4.4.

## 3.4. TEST BLASTS

The test blasts were completed on April 16, June 4, July 30, and September 15, 2015. Each blast was set-up using the blast design, zones, and instrumentation as stated earlier in Section 3. The various delay times that were tested and the zones in which they were shot are summarized in Table 3.1.

Table 3.1. Delay Times and Zones

| Test | Shot Date | Zone | Timing (ms) |
|------|-----------|------|-------------|
|      | 4/16/2015 | 1 | 16 |
|      | 4/16/2015 | 2 | 4 |
| 1    | 4/16/2015 | 3 | 16 |
|      | 6/4/2015  | 1 | 4 |
|      | 6/4/2015  | 2 | 16 |
| 2    | 6/4/2015  | 3 | 25 |
|      | 7/30/2015 | 1 | 1 |
|      | 7/30/2015 | 2 | 25 |
| 3    | 7/30/2015 | 3 | 16 |
|      | 9/15/2015 | 1 | 10 |
|      | 9/15/2015 | 2 | 25 |
| 4    | 9/15/2015 | 3 | 0 |

**3.4.1. Test Shot 1.** The first test blast was conducted on April 16, 2015. The shot occurred at 1:05 PM on the North 2nd Bench. The shot had 85 holes that were angled 5° toward the face, and were designed to be drilled to a depth of 72 feet. The designed drill depth included a 3 foot sub-drill and the bench height was 69 feet. The planned burden was 13 feet and the spacing was 17 feet. Based on the Boretrack and 3D Laser Profile data, the actual front row burden varied from approximately 10 feet to greater than 37 feet. The most significant portion of the overburdening occurred at the toe. Figure 3.10 shows an example of a boretrack with face profile from the first test blast that has significant overburdening at the toe. Table 3.2. provides the hole and face profile data.

0    4ft    Scale 1:633.8
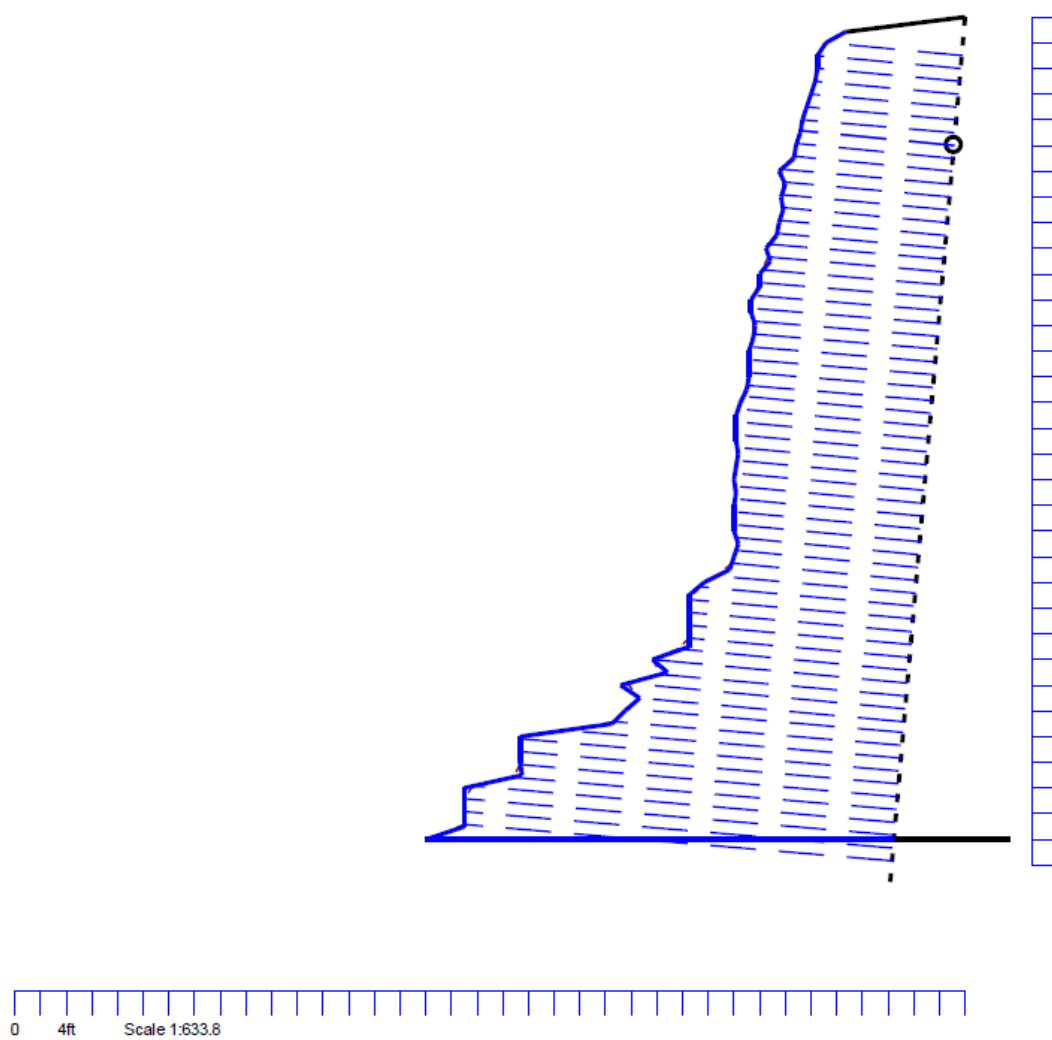
Figure 3.10. Face Profile and Boretrack from Test 1

Table 3.2. Hole and Face Profile Data

| Hole Diameter | 6.00 in |
|---|---|
| Hole Length | 67.6 ft |
| Stemming | 10.0 ft |
| Back Fill: | 0.0 ft |
| Subdrill | 3.4 ft |
| Hole Angle | 5° |
| Profile Cross-Section | 1144.5 ft² |
| Borehole Volume: | 17165.0 ft3 |
| Minimum Burden | 12.08 ft @10.0 ft |
| Maximum Burden | 35.33 ft @67.0 ft |
| Ave Burden | 18.1 ft |

This shot utilized 16 ms inter-hole delays in Zones 1 and 3, and 4 ms delays in Zone 2. 16 ms was the mine's standard delay time and 4 ms was chosen as a fast delay time outside of the stress wave collision region. For this test, Zone 3 was not included in the analysis because the 16 ms timing was evaluated in Zone 1, and it was to be evaluated in Zone 3 on later shots. 16 ms was used in two zones on the first test blast so that the mine supervision could get comfortable with modifying delay times. Figure 3.11. shows the location of the shot and the seismographs provided by DynoConsult. The details of the seismograph recordings can be found in Appendix C.

Figure 3.11. Shot 1 and Seismograph Locations

**3.4.2. Test Shot 2.** The second test blast was conducted on June 4, 2015. The shot occurred at 12:50 PM on the North 2$^{nd}$ Bench. The shot had 86 holes that were angled 5° toward the face, and were designed to be drilled to a depth of 73 feet. The designed drill depth included a 3 foot sub-drill and the bench height was 70 feet. The planned burden was 13 feet and the spacing was 17 feet. Based on the Boretrack and 3D Laser Profile data, the actual front row burden for Zone 1 varied from 10.01 to 37.42 feet. The front row burden for Zone 2 varied from 9.33 to 44.77 feet, and for Zone 3 it varied from 9.23 to 51.86 feet. The most significant overburdening occurred at the toe, and it did not significantly continue up the face. Typically, under-burdening occurred at the top of the face. An example of the Boretrack and 3D Laser Profile recording from Zone 2 is included in Appendix C.

Test blast 2 used 4 ms inter-hole delays in Zone 1, 16 ms inter-hole delays in Zone 2, and 25 ms inter-hole delays in Zone 3. Switching the 4 ms delays from Zone 2 on the first shot to Zone 1 on the second shot, and the 16 ms delays from Zone 1 on the first

shot to Zone 2 on the second shot, was designed to allow for comparison of the same delay times across zones. These comparisons are detailed in Section 4.

**3.4.3. Test Shot 3.** The third test blast was conducted at 1:40 PM on July 30, 2015. The shot had 85 holes that were angled 5° toward the face, and were designed to be drilled to a depth of 72 feet. The designed drill depth included a 3 foot sub-drill and the bench height was 69 feet. The planned burden was 13 feet and the spacing was 17 feet. Summary Boretrack and 3D Laser Profile data was received for this shot, the full Boretrack data was not available.

This shot was the first to use a delay time that had the possibility of causing stress wave collision. This 1 ms inter-hole delay was used in Zone 1. Zone 2 used a 25 ms inter-hole delay and Zone 3 used a 16 ms inter-hole delay. The use of 25 ms and 16 ms delays in different Zones than they were used on previous shots, allowed for comparison of the delay effects across the different zones.

As with all of the blasts, seismographs were set-up to record ground vibration and airblast from the shot. On this blast, two Mini Seis III seismographs were tethered together to facilitate the calculation of the speed of sound in the rock and the airblast speed. Figure 3.12., shows the location of the blast and approximate seismograph locations. The results of the calculations are detailed in Section 4.4. and the full seismograph reports can be found in Appendix C.

Figure 3.12. Approximate Sesimograph Locations Relative to Shot 3

**3.4.4. Test Shot 4.** The fourth test blast was completed at 2:40 PM on September 15, 2015. The shot had 85 holes that were angled 5° toward the face, and were designed to be drilled to a depth of 70 feet. The designed drill depth included a 3 foot sub-drill and the bench height was 67 feet. The planned burden was 13 feet and the spacing was 17 feet. This shot used hole-to-hole delays of 10 ms in Zone 1, 25 ms in Zone 2, and 0 ms in Zone 3. The 0 ms delay was the second delay time that had the potential for stress wave interaction. The 10 ms delay was selected on the recommendation of DynoConsult. The recommendation was based on the following equation:

$$15.6 \div sonic\ velocity \ \times burden = delay\ time \qquad (1)$$

Where sonic velocity is kilometers per second (km/s), burden is in meters (m), and delay time is in milliseconds (ms).

Using the sonic velocity of 5.8396 km/s, found during Test Blast 3, and the burden of 3.9642 m, the recommended delay time was found to be 10.5852 ms.

### 3.5. EXPERIMENT SUMMARY

Four full scale test blasts were completed at a granite quarry. The blast design for all of the shots consisted of 85 or 86, 5.75" holes, with of burden and spacing of 13 feet and 17 feet, respectively. A 142 ms inter-row delay was used. All of the blast parameters were held constant, except for the hole-to-hole delay times. Each bench was divided into three zones so that three delay times could be tested during each shot. 0 ms, 1 ms, 4 ms, 10 ms, 16 ms, and 25 ms delay times were tested across the zones. Various marking devices were used to measure throw and show face movement of each zone. Shots were monitored using seismographs and recorded with high-speed video cameras, and analyzed with photographic fragmentation analysis in WipFrag.

# 4. ANALYSIS, RESULTS, AND DISCUSSION

The method by which the fragmentation for each zone and delay time was evaluated was through digital image analysis using WipFrag commercial software. A total of 28 photographs were analyzed in WipFrag. Each of the photographs was extensively manually edited to ensure that the rock outlines, as they were shown and evaluated in the program, truly represented the actual rocks in the field. In addition to the WipFrag analysis of fragmentation, observations of several blast performance parameters were made.

## 4.1. WIPFRAG FRAGMENTATION ANALYSIS

The digital image analysis program WipFrag was used to determine the fragmentation distribution of each of the blast zones using photographs taken of each zone immediately after the shot and throughout the mucking process. The rock outlines generated by WipFrag were edited to ensure that they were true to the actual fragments. The zone separations were identified using the zone marker buckets, previously shown in Figure 3.5. The first set of photos for each shot was taken while on site, immediately after the blast, and subsequent photos were received throughout the mucking process. The second set of photos typically did not include Zone 3, because mucking had not yet begun on Zone 3 at the time the photographs were taken. Therefore the muck pile had not changed since immediately after the shot. Most blasts had three sets of photographs taken. The first was taken right after the shot, the second set was taken one to two weeks after the shot, and the third set was taken one to two weeks after the second. Typically, one photograph per zone per photograph capture date was analyzed. Uniform times

between photograph sets would have been ideal, but the ability to get photographs was constrained by the availability of DynoConsult.

Using WipFrag, a net of rock outlines was created for each of the photographs. The rock outline and the scaling object in the photo allowed the program to virtually sieve the exposed surface of the rock fragments and generate a graph of the fragmentation distribution. An example of a portion of a net is shown in Figure 4.1. Each of the rock fragments is outlined in blue, the grey box shows the scale object, and the white sections are defined as fines. Figure 4.2. is an example of the fragmentation graph generated for each of the photos analyzed throughout this study. All of the photos used and their corresponding graphs are included in Appendix A. A summary of the data collected through WipFrag analysis is shown in Table 4.1.
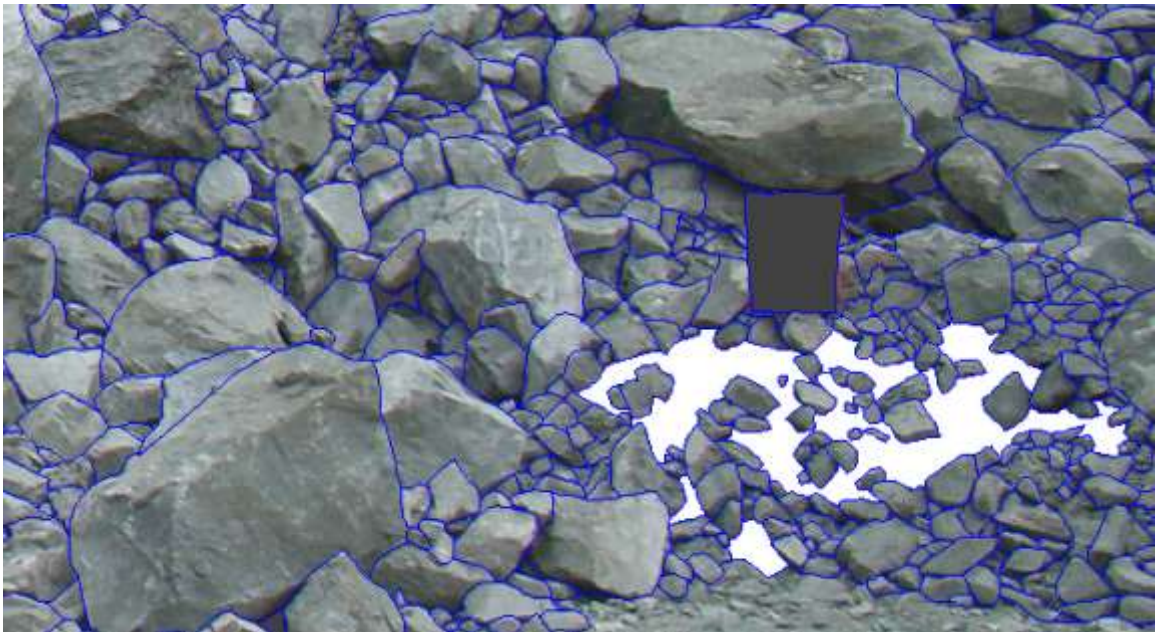


Figure 4.1. WipFrag Net Example
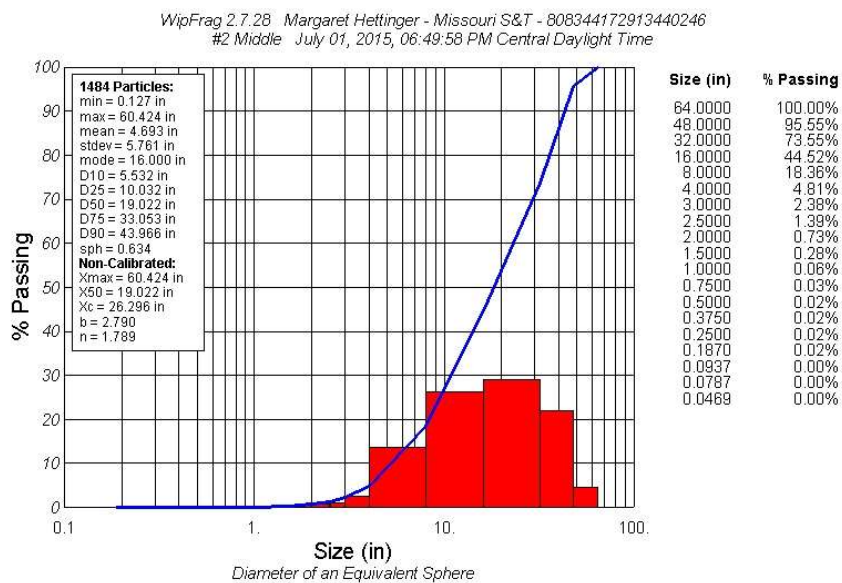
Figure 4.2. WipFrag Graph from Test Shot 2 Zone 2

Table 4.1. WipFrag Data

| Timing (ms) | Shot Date | Photo Date | Photo | Zone | D10 (in.) | Mean (in.) | D50 (in.) | D90 (in.) | Max (in.) |
|---|---|---|---|---|---|---|---|---|---|
| 16 | 4/16/2015 | 4/16/2015 | DSC04758w | 1 | 4.268 | 3.297 | 10.519 | 22.048 | 26.543 |
| 4 | 4/16/2015 | 4/16/2015 | DSC04789 | 2 | 5.982 | 4.771 | 20.206 | 46.069 | 64.835 |
| 16 | 4/16/2015 | 4/24/2015 | DSCF1839w | 1 | 0.162 | 4.535 | 6.947 | 18.404 | 34.267 |
| 4 | 4/16/2015 | 4/24/2015 | DSCF1848w | 2 | 3.955 | 5.802 | 12.253 | 28.858 | 38.881 |
| 16 | 4/16/2015 | 5/1/2015 | zone1b 5-1-15w | 1 | 0.126 | 2.126 | 4.588 | 29.895 | 56.543 |
| 4 | 4/16/2015 | 5/1/2015 | zone2d 5-1-15 | 2 | 2.393 | 2.132 | 6.408 | 15.198 | 19.917 |
| 4 | 6/4/2015 | 6/4/2015 | DSC02034 | 1 | 1.411 | 0.878 | 7.187 | 26.302 | 28.202 |
| 16 | 6/4/2015 | 6/4/2015 | DSC02046 | 2 | 1.617 | 0.986 | 9.985 | 37.832 | 36.848 |
| 25 | 6/4/2015 | 6/4/2015 | DSC02062 | 3 | 0.932 | 0.591 | 4.836 | 14.714 | 16.503 |
| 4 | 6/4/2015 | 6/10/2015 | #1 Middle | 1 | 4.201 | 4.19 | 12.587 | 31.487 | 52.938 |
| 16 | 6/4/2015 | 6/10/2015 | #2 Middle | 2 | 5.761 | 4.693 | 19.022 | 43.966 | 60.424 |
| 4 | 6/4/2015 | 6/25/2015 | Zn1a 6-25-15 | 1 | 0.245 | 3.296 | 4.851 | 17.642 | 36.036 |
| 16 | 6/4/2015 | 6/25/2015 | Zn2a 6-25-15 | 2 | 0.25 | 3.05 | 5.565 | 15.378 | 31.819 |
| 25 | 6/4/2015 | 6/25/2015 | Zn3a 6-25-16 | 3 | 1.931 | 2.775 | 8.462 | 26.362 | 33.775 |
| 1 | 7/30/2015 | 7/30/2015 | DSC02118 | 1 | 2.772 | 2.276 | 9.958 | 31.626 | 39.982 |
| 1 | 7/30/2015 | 8/5/2015 | Zone 1 A_1598x1063 | 1 | 4.678 | 4.835 | 14.102 | 49.217 | 63.916 |
| 1 | 7/30/2015 | 8/19/2015 | IMG_0059_1129x1505 | 1 | 2.707 | 4.204 | 10.38 | 29.713 | 42.121 |
| 25 | 7/30/2015 | 7/30/2015 | DSC02128w_1835x926 | 2 | 2.912 | 3.079 | 7.816 | 24.782 | 30.585 |
| 25 | 7/30/2015 | 8/5/2015 | Zone 2 A_1598x1063 | 2 | 4.708 | 4.938 | 13.504 | 31.124 | 39.008 |
| 25 | 7/30/2015 | 8/19/2015 | IMG_0061_1129x1505 | 2 | 0.312 | 3.559 | 5.056 | 22.667 | 37.669 |
| 16 | 7/30/2015 | 7/30/2015 | DSC02139_1599x1062 | 3 | 3.122 | 2.958 | 10.967 | 25.227 | 24.292 |
| 16 | 7/30/2015 | 8/19/2015 | IMG_0065_1129x1505 | 3 | 4.86 | 5.707 | 13.897 | 29.24 | 33.657 |
| 10 | 9/15/2015 | 9/15/2015 | DSC02277_1599x1062 | 1 | 1.953 | 1.824 | 7.645 | 21.779 | 25.365 |
| 10 | 9/15/2015 | 9/29/2015 | IMG_0670_1505x1129 | 1 | 2.826 | 4.082 | 10.867 | 27.248 | 32.766 |
| 25 | 9/15/2015 | 9/15/2015 | DSC02283_1599x1062 | 2 | 1.379 | 1.315 | 4.532 | 13.097 | 13.786 |
| 25 | 9/15/2015 | 9/29/2015 | IMG_0673_1505x1129 | 2 | 2.457 | 2.962 | 8.472 | 26.372 | 44.291 |
| 0 | 9/15/2015 | 9/15/2015 | DSC02294_1599x1062 | 3 | 2.607 | 3.395 | 8.4 | 20.621 | 20.406 |
| 0 | 9/15/2015 | 9/29/2015 | IMG_0677_1505x1129 | 3 | 4.208 | 3.94 | 12.153 | 30.843 | 37.088 |

## 4.2. WIPFRAG RESULTS

In order to evaluate the effects of each delay time, and how the various zones responded to each delay time, a number of tables and graphs were generated. These graphs allowed for easier visualization of the data. Based on the mean averages for each delay time, Table 4.2. lists the delay times in order of the smallest maximum fragmentation size to the largest, and Figure 4.3. visualizes that same data. These show that the smallest maximum fragment size was achieved with the 0 ms delay, but was very closely followed by the 10 ms delay. Figure 4.4. shows the size distributions in the order of the shortest to longest delay times.
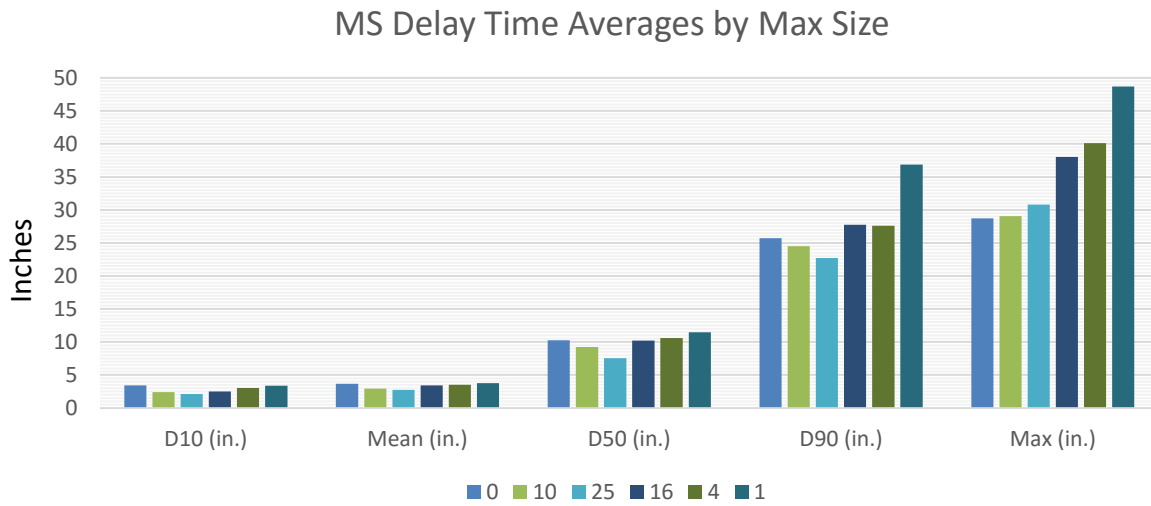
## MS Delay Time Averages by Max Size



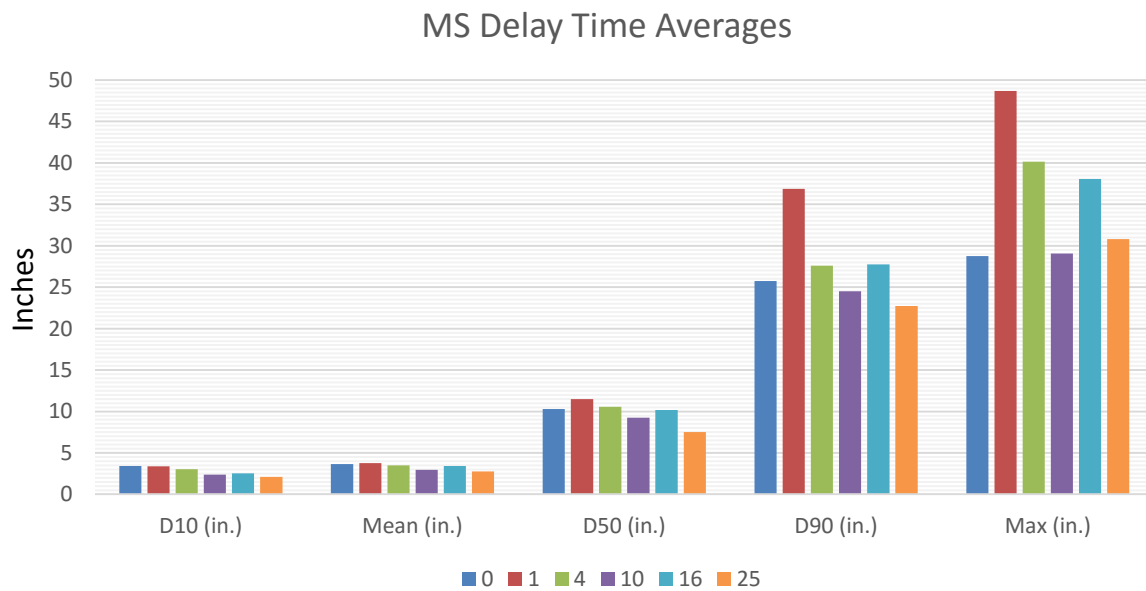Figure 4.3. Delays by Maximum Size

## MS Delay Time Averages



Figure 4.4. Averages in Order of Delay Time (10 ms and 25 ms performed the best)

Table 4.2. Delay Time by Max. Fragment Size

| # of Photos | Timing (ms) | D10 (in.) | Mean (in.) | D50 (in.) | D90 (in.) | Max (in.) |
|---|---|---|---|---|---|---|
| 2 | 0 | 3.41 | 3.67 | 10.28 | 25.73 | 28.75 |
| 2 | 10 | 2.39 | 2.95 | 9.26 | 24.51 | 29.07 |
| 7 | 25 | 2.09 | 2.75 | 7.53 | 22.73 | 30.80 |
| 8 | 16 | 2.52 | 3.42 | 10.19 | 27.75 | 38.05 |
| 6 | 4 | 3.03 | 3.51 | 10.58 | 27.59 | 40.13 |
| 3 | 1 | 3.39 | 3.77 | 11.48 | 36.85 | 48.67 |

## 4.3. FRAGMENTATION ANALYSIS DISCUSSION

There are advantages and disadvantages of using the maximum fragment size versus the D90 size as a determination of the largest particle sizes. On one hand, the maximum size could come from a rock whose size is an outlier, whereas, on the other hand, the D90 size is calculated based on the sieve sizes rather than a measured value. Results show that all of the values for the 10 ms delay time, other than the maximum size, are smaller than those for the 0 ms delay time and that the maximum size was less than a third of an inch larger. Thus, it can be concluded that the 10 ms delay time achieved better overall fragmentation than the 0 ms delay time. The 25 ms delay time had even smaller D10, Mean, D50, and D90 sizes, but had a larger maximum fragment size than either the 0 ms or 10 ms sizes. Given the greater number of photographs analyzed, its smaller size in values other than the maximum, and its use in multiple zones, the 25 ms delay time, was the best overall at increasing fragmentation. Even if the 25 ms delay time is evaluated only on its performance in Zone 2, it performed better in all values other than the maximum. The results disagree with Floyd's (2013) recommendation of an inter-hole delay of less than 0.3 milliseconds per foot (ms/ft) of spacing. The best performing time, 25 ms, had 1.47 ms/ft of spacing, and the second best, 10 ms, had 0.59

ms/ft of spacing. The worst performing times were closer to his recommended delay time with 0.8 ms/ft of spacing for the 1 ms delay and 0.31 ms/ft of spacing for the 4 ms delay, respectively. The overall poor performance of short delay times agrees with the conclusion made by Johnson (2014), that short delay times do not improve fragmentation. The tests performed by Johnson (2014), like much of the previous fragmentation research, were scale tests that require full size testing to confirm their results.

Delay times used in multiple zones had larger standard deviations than those only used in one zone. This could be due to the rock differences that are present in the varying zones, the use of a different emulsion in Zone 3, or it may have been caused by the greater number of images available for delay times that were used in multiple zones. Table 4.3. lists the standard deviation of the fragmentation distribution averages.

Table 4.3. Fragment Size Standard Deviation

| Timing (ms) | D10 (in.) | Mean (in.) | D50 (in.) | D90 (in.) | Max (in.) |
|---|---|---|---|---|---|
| 0 | 0.80 | 0.27 | 1.88 | 5.11 | 8.34 |
| 1 | 0.91 | 1.09 | 1.86 | 8.78 | 10.81 |
| 4 | 1.90 | 1.64 | 5.18 | 10.10 | 14.96 |
| 10 | 0.44 | 1.13 | 1.61 | 2.73 | 3.70 |
| 16 | 2.14 | 1.42 | 4.41 | 9.02 | 12.44 |
| 25 | 1.35 | 1.33 | 2.93 | 6.07 | 10.69 |

In order to evaluate the effects that the different zones had on the fragmentation size. The average fragmentation sizes for each zone were found. Table 4.4. lists the averages for each zone. Figure 4.5. visualizes the Table 4.4. data.

## Fragmentation Size Average by Zone
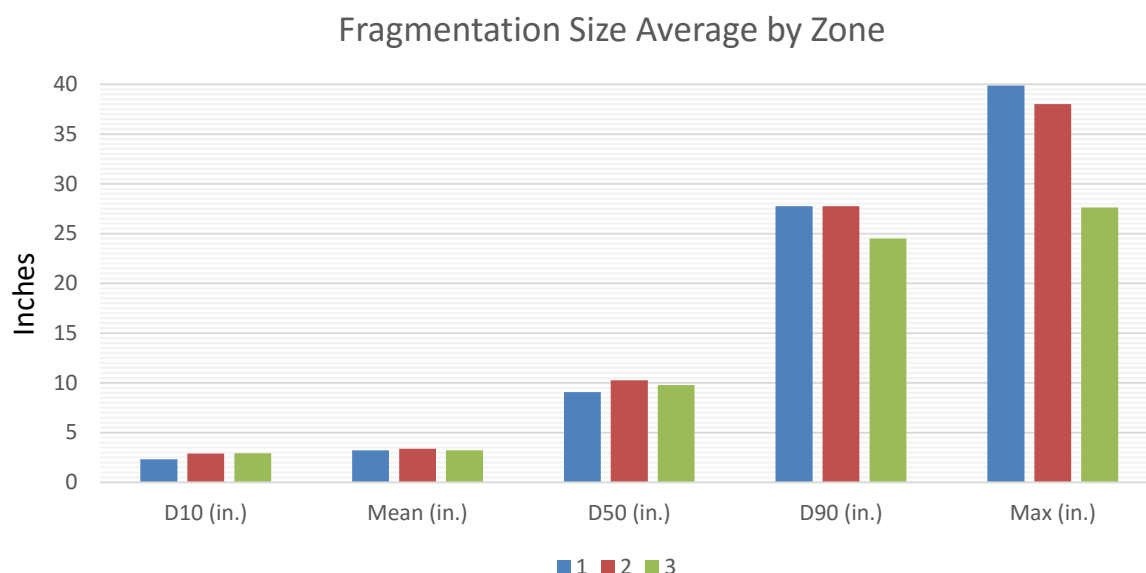


Figure 4.5. Fragmentation by Zone

An overall observation shows that Zone 3 had smaller fragmentation than Zones 1 and 2. Zone 3 used delay times of 0 ms, 16 ms, and 25 ms. The maximum fragment size from the 16 ms delay in Zone 3 was smaller than the one that resulted from the 16 ms delay when it was used in Zones 1 and 2. This did not hold true for both Zones 1 and 2 in the corresponding D10, mean, D50, or D90 size. Also, the D10, Mean, D50, D90, and Maximum sizes for the 25 ms delay time were on average smaller for Zone 3 than they were when the 25 ms delay was used in Zone 2. This shows that the rock type in Zone 3 may have resulted in improved fragmentation in that zone independent of the delay time effects. Comparing delay time effects on fragmentation just on the times used in Zone 3, results in 25 ms being the smallest for the D10, mean, D50, D90 and Max sizes.

Table 4.4. Average Fragmentation for Each Zone

| # of Photos | Zone | D10 (in.) | Mean (in.) | D50 (in.) | D90 (in.) | Max (in.) |
|---|---|---|---|---|---|---|
| 11 | 1 | 2.30 | 3.23 | 9.06 | 27.76 | 39.88 |
| 11 | 2 | 2.88 | 3.39 | 10.26 | 27.76 | 38.01 |
| 6 | 3 | 2.94 | 3.23 | 9.79 | 24.50 | 27.62 |

Since the number of photos analyzed was limited, and because 0 ms was only used in Zone 3, there is some uncertainty in conclusions made regarding the 0 ms delay time. The decision to use Zone 3 for the 0 ms delay time was based on concerns from DynoConsult that the other zones were under-burdened. Given the lack of data for 0 ms in other zones, the otherwise superior results of the 10 ms and 25 ms delays, and the limited number of photographs analyzed, it cannot be concluded that the 0 ms time would typically have the best fragmentation results based on the maximum size alone.

In order to show the variation in fragmentation for individual delay times, Table 4.5. was generated. Table 4.6. and Figure 4.6. show the average sizes by zone for 16ms delays. Table 4.7. and Figure 4.7. show the average sizes by zone for 25 ms delays. Table 4.8. and Figure 4.8. show the average sizes by zone for 4 ms delays. These tables and figures illustrate that the zones result in some variation in fragmentation size.
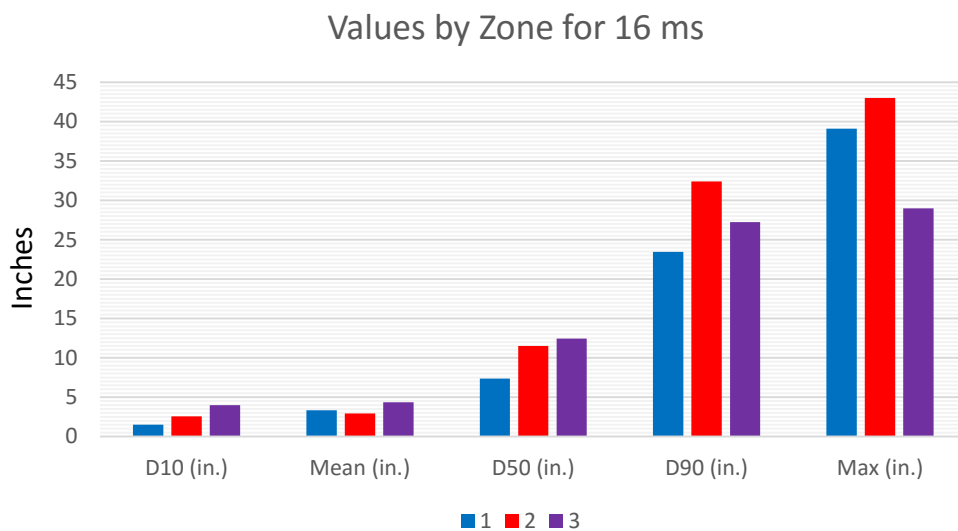
Figure 4.6. Values by Zone for 16 ms Delay
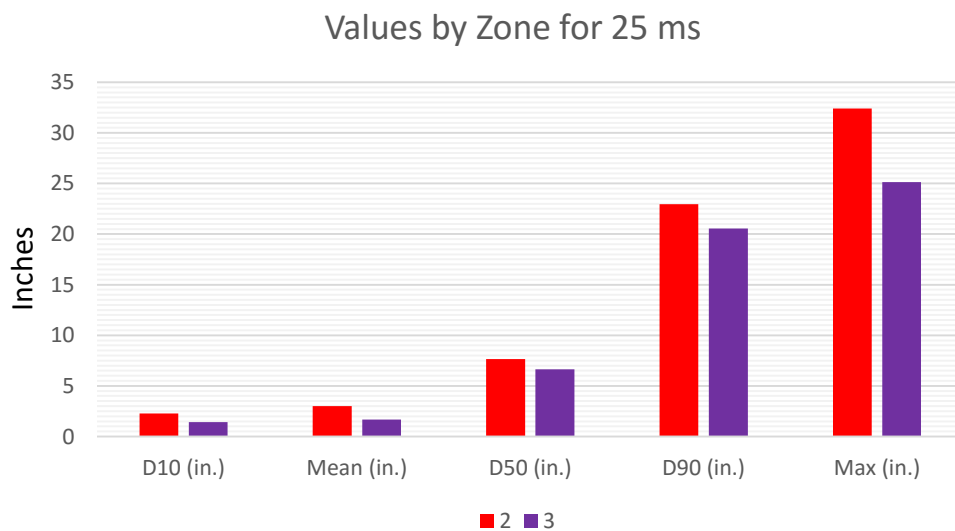


Figure 4.7. Values by Zone for 25 ms Delay

Values by Zone for 4 ms
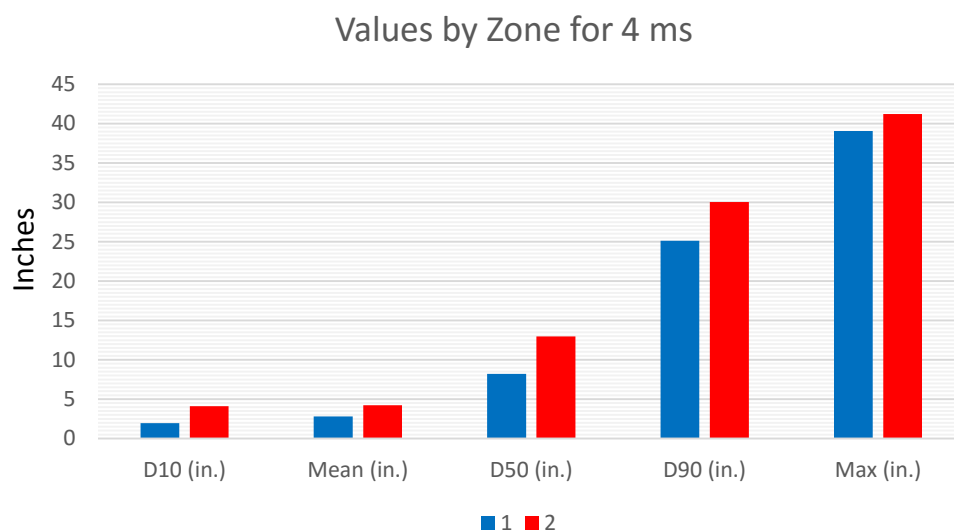


Figure 4.8. Values by Zone for 4 ms Delay

Table 4.5. Values Sorted by Timing

| Shot Date | Zone | Timing (ms) | # of Images | D10 (in.) | Mean (in.) | D50 (in.) | D90 (in.) | Max (in.) |
|---|---|---|---|---|---|---|---|---|
| 9/15/2015 | 3 | 0 | 2 | 3.41 | 3.67 | 10.28 | 25.73 | 28.75 |
| 7/30/2015 | 1 | 1 | 3 | 3.39 | 3.77 | 11.48 | 36.85 | 48.67 |
| 4/16/2015 | 2 | 4 | 3 | 4.11 | 4.24 | 12.96 | 30.04 | 41.21 |
| 6/4/2015 | 1 | 4 | 3 | 1.95 | 2.79 | 8.21 | 25.14 | 39.06 |
| 9/15/2015 | 1 | 10 | 2 | 2.39 | 2.95 | 9.26 | 24.51 | 29.07 |
| 4/16/2015 | 1 | 16 | 3 | 1.52 | 3.32 | 7.35 | 23.45 | 39.12 |
| 6/4/2015 | 2 | 16 | 3 | 2.54 | 2.91 | 11.52 | 32.39 | 43.03 |
| 7/30/2015 | 3 | 16 | 2 | 3.99 | 4.33 | 12.43 | 27.23 | 28.97 |
| 6/4/2015 | 3 | 25 | 2 | 1.43 | 1.68 | 6.65 | 20.54 | 25.14 |
| 7/30/2015 | 2 | 25 | 3 | 2.64 | 3.86 | 8.79 | 26.19 | 35.75 |
| 9/15/2015 | 2 | 25 | 2 | 1.92 | 2.14 | 6.50 | 19.73 | 29.04 |

Table 4.6. Values by Zone for 16 ms Delay

| Zone | D10 (in.) | Mean (in.) | D50 (in.) | D90 (in.) | Max (in.) |
|---|---|---|---|---|---|
| 1 | 1.52 | 3.32 | 7.35 | 23.45 | 39.12 |
| 2 | 2.54 | 2.91 | 11.52 | 32.39 | 43.03 |
| 3 | 3.99 | 4.33 | 12.43 | 27.23 | 28.97 |

Table 4.7. Values by Zone for 25 ms Delay

| Zone | D10 (in.) | Mean (in.) | D50 (in.) | D90 (in.) | Max (in.) |
|---|---|---|---|---|---|
| 2 | 2.281 | 2.99858333 | 7.647 | 22.96275 | 32.39625 |
| 3 | 1.43 | 1.68 | 6.65 | 20.54 | 25.14 |

Table 4.8. Values by Zone for 4 ms Delay

| Zone | D10 (in.) | Mean (in.) | D50 (in.) | D90 (in.) | Max (in.) |
|---|---|---|---|---|---|
| 1 | 1.95 | 2.79 | 8.21 | 25.14 | 39.06 |
| 2 | 4.11 | 4.24 | 12.96 | 30.04 | 41.21 |

## 4.4. OTHER RESULTS

Seismographs were set up for each of the test blasts. Table 4.9 summarizes the locations and results of the White Mini Seis III Seismographs. A summary of the results from the seismographs provided by DynoConsult and the full seismograph reports for all recordings can be found in Appendix C. During the third test blast, the Mini Seis III seismographs were tethered together and used to find the speed of sound in the rock, as well as the airblast speed. An additional recording of the speed of sound in rock and the airblast speed was attempted during the fourth test blast, but some unknown event pre-triggered the master seismograph on the same event that it recorded the shot data. This eliminated the chance to find a speed of sound in rock or airblast time difference, because typically the speed would be determined using the difference between when the master seismograph tripped in the pre-trigger time and when the slave seismograph started recording the blast vibration. Table 4.10. Summarizes the speed of sound in rock mass calculations found using the July 30, 2015 seismograph recordings. The speed of sound

in the rock mass was similar to the standard expected speed in granite of 5.950 km/s (The

Physics Hypertextbook). Table 4.11. summarizes the airblast calculations.

Table 4.9. Mini Seis III Locations and Results

| Shot Date | Seismo ID | Shot Northing | Shot Easting | Distance to Shot (ft) | Location Relative to Shot |
|---|---|---|---|---|---|
| 6/4/2015 | 7173 | N 32°38'02.3" | W84°30'01.5" | 200 | behind |
| 6/4/2015 | 7174 | N 32°38'02.3" | W84°30'01.5" | 400 | behind |
| 7/30/2015 | 7173 | N 32°38'02.29980" | W84°30'01.09980" | 389 | below in front |
| 7/30/2015 | 7174 | N 32°38'02.29980" | W84°30'01.09980" | 594 | below in front |
| 9/15/2015 | 7173 | N 32°37'57.49980" | W84°30'01.80000" | 500 | below in front |
| 9/15/2015 | 7174 | N 32°37'57.49980" | W84°30'01.80000" | 871 | below in front |

| Shot Date | Seismo ID | Acoustic (dBL) | R PPV | V PPV | T PPV | Max PPV | R Frequency | V Frequency | T Frequency |
|---|---|---|---|---|---|---|---|---|---|
| 6/4/2015 | 7173 | 140.2 | 6.03 | 4.11 | 2.8 | 6.03 | 17.1 | 26.9 | 15.5 |
| 6/4/2015 | 7174 | 136.1 | 3.53 | 1.13 | 1.86 | 3.53 | 23.3 | 51.2 | 1.86 |
| 7/30/2015 | 7173 | 148.2 | 1.36 | 1.07 | 0.657 | 1.36 | 21.3 | 14.6 | 42.7 |
| 7/30/2015 | 7174 | 148.2 | 0.872 | 0.953 | 0.501 | 0.953 | 22.3 | 36.6 | 18.3 |
| 9/15/2015 | 7173 | 148.2 | 0.769 | 0.747 | 1.29 | 1.29 | 40.2 | 20.7 | 20.3 |
| 9/15/2015 | 7174 | 148.1 | 0.435 | 0.391 | 0.706 | 0.706 | 23.8 | 23.3 | 19.1 |

Table 4.10. Speed of Sound in Rock Mass

| Date Measured | Distance (ft) | Time (s) | Speed (ft/s) | Speed (ft/ms) | Speed (km/s) |
|---|---|---|---|---|---|
| 7/30/2015 | 205 | 0.0107 | 19158.88 | 19.16 | 5.84 |

Table 4.11. Airblast Speed

| Date Measured | Distance (ft) | Time (s) | Speed (ft/s) | Speed (ft/ms) |
|---|---|---|---|---|
| 7/30/2015 | 205 | 0.1777 | 1153.63 | 1.15 |

All of the test blasts had stemming ejection occur across various parts of the

zones. There were a number of possible causes of stemming ejection. On the first test

blast, there was a significant amount of stemming ejection that began just before the start

of Zone 2 and continued into Zone 3. Figure 4.9. shows the stemming ejection as it

occurred during the shot. The likely cause of this was the increased broken ground, as recorded by the driller, on a number of holes through this section. Holes 35 through 42 all had broken ground between 9 and 11 feet. It is unknown if stemming was extended through the broken ground, but assuming it was not, this would be a major cause of stemming ejection because the powder column came up into the broken areas, reducing the top confinement.



Figure 4.9. Shot 1 Stemming Ejection

For all shots in holes where the emulsion did not rise to the planned height, bagged emulsion was added to the top of the powder column. Powder loss because of fractured ground and the extra emulsion added to the top of holes may have contributed to the stemming ejection problem. Overbreak from the holes on the bench above likely contributed to stemming ejection.  holes Since an individual hole loading breakdown was not completed for any of the blasts, it is unknown which holes had emulsion bags added to them.  Stemming ejection for each of the test blasts can be seen in the shot photographs included in Appendix D.

**4.4.1. Timing Effects on Throw.** The short delay times, especially the 0 ms delay, greatly increased the throw distance in the zone that they were used. This agrees with Johnson's (2014) conclusion that 0 ms delays increase throw because of the increased rock density that results from wave collision between holes. This also agrees with Worsey's (2015 b) assertion that short hole-to-hole timing is necessary so that holes interact to achieve greater throw. Figures 4.10. and 4.11. show the increased throw in Zone 3, resulting from the 0 ms delay, during the fourth test blast.



Figure 4.10.  Increased Throw from 0 ms Delay

Figure 4.11. Increased Throw from 0 ms Delay (far 1/3 of photograph)

**4.4.2. High-speed Video and Face Movement.** High-speed video was taken of each shot. The first two shots were recorded by DynoConsult. For the second two shots, an MREL Blaster's Ranger II camera was used. Figure 4.12. shows the start of Zone 1 during the first test blast, Figure 4.13. shows the start of Zone 2, and Figure 4.14. shows the face after all of the zones have started moving. During this shot, a significant amount of stemming ejection can be seen beginning just before the start of Zone 2 and continuing into Zone 3. Figure 4.15 show the face of the second test blast after all zones have started moving.

Figure 4.12. Zone 1 "Flash Bulb" Start



Figure 4.13. Zone 2 "Flash Bulb" Start



Figure 4.14. Test Blast 1 Movement

Figure 4.15. Test Blast 2 Movement

For the third test blast, the MREL Blaster's Ranger II camera was used for the
first time during these tests. Due to the size of the camera lens available and the
necessary safe distance for the set-up of the camera, only part of the face was able to be
seen in the recording. This provided a much closer look at the face. Figure 4.16. shows
Zone 1 and part of Zone 2 that was captured.
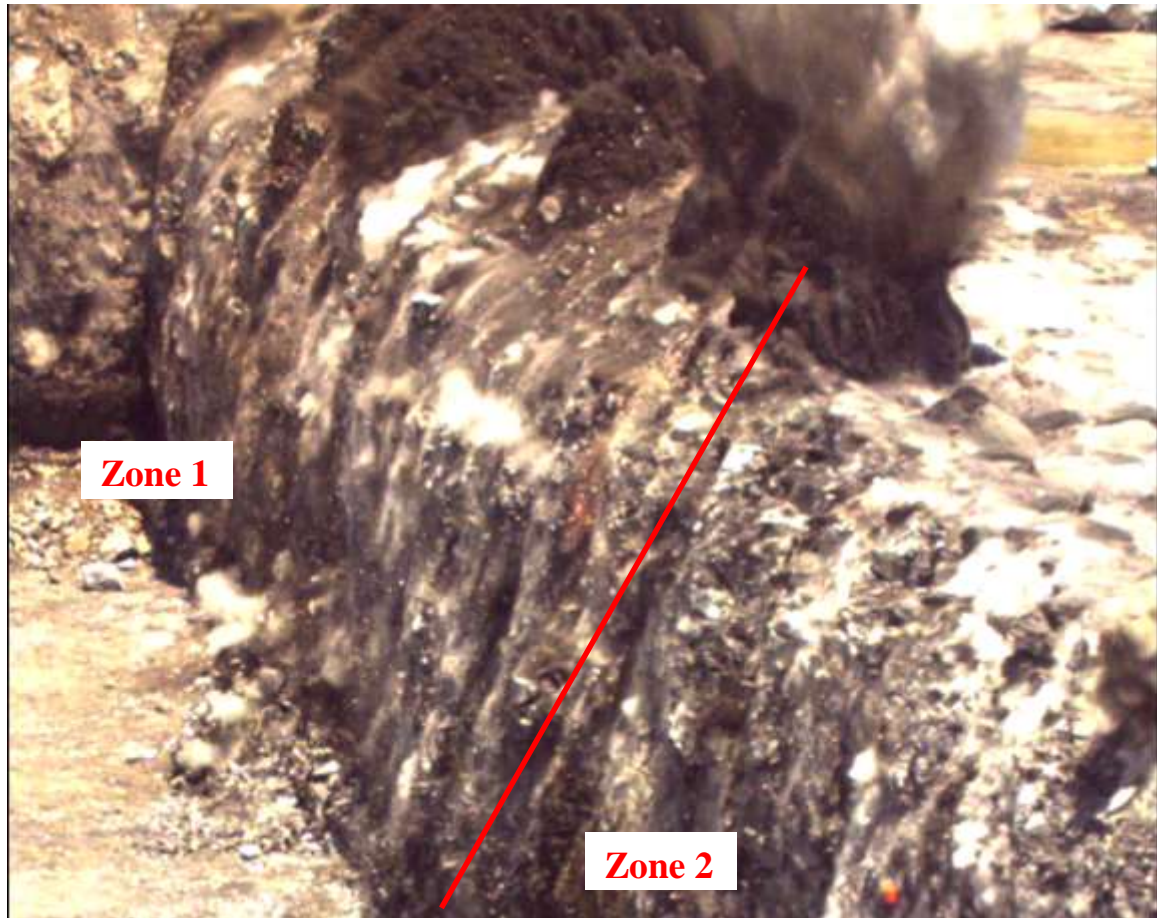
Figure 4.16. Test Blast 3 Movement

For the final test blast the recording was taken from across the pit. The video captured the end of Zone 2 and all of Zone 3. The instantaneous detonation of the entire first row of Zone 3 can clearly be seen as the entire face moves out as one mass. Figure 4.17 shows Zone 3 moving outward. Observations of the face movement were made, but because the view was either too far out or too close, velocities were not calculated.

Figure 4.17. Test Blast 4 Movement

## 4.5. DISCUSSION

This thesis used photographic fragmentation analysis of muck piles created using various delay times on the same bench blast to evaluate the effects of inter-hole timing on rock fragmentation. This analysis provided a representative understanding of timing effects on fragmentation in the field and differentiated itself from many previous blast models which had either negated the effects of timing or geology. While blasting in a full-scale operating mine site introduced a number of uncontrollable variables to the tests, testing in the full scale is necessary to determine if timing options are viable for use in real world mining applications. Scale tests and computer models provide consistency, but that consistency does not necessarily translate to applications in naturally variable material, like a quarry bench.

The analysis of the 0 ms delay time was not as complete as anticipated because of unavoidable time constraints. In the original analysis, it had the smallest maximum size, but when photographs were received later in the mucking process, after all of the analysis

had been completed, they showed a significant amount of oversize. Photographs of the muck piles were received for test blast 4 after all WipFrag analysis and average calculations had been completed. Full evaluation of these results was outside of time constraints and graduation deadlines. These photographs provided some additional insight into the fragmentation results in Zone 3 of that shot, which used the 0 ms delay timing. Feedback from the mine operators was that Zone 3 was digging tight and had a significant amount of oversize. The observations made by DynoConsult were that fragmentation was good between holes, but the burden had been pushed out in one mass resulting in the apparent oversize. Figure 4.18 shows the DynoConsult's view in the field of Zone 3 during the mucking process. This apparent good fragmentation between holes fits with the conclusions of Rossmanith (2003) and Yamamoto (1999), that fragmentation will be improved between holes where wave interaction occurs. This is not necessarily practical in the field, because oversize remains in the burden areas when they are pushed out in a single mass. While a full WipFrag analysis was not able to be performed on the photographs received on October 20, 2015, measurement of some of the larger fragments in these photographs found them to be in excess of 60 inches as shown in Figure 4.19. Previously, the maximum size found for the 0 ms delay was 28.75 inches.

Additionally, from a practical perspective the 0 ms delay time presents additional concerns. For example, for many applications, shooting that many pounds of explosives per delay may not be legally allowed. More relevant to fragmentation, is the issue that shooting the holes on a 0 ms delay does not allow for the pre-stressing of the rock mass by preceding blast holes as a shot progresses, which was found to have an influence on fragmentation by Johansson and Ouchterlony (2013).

Figure 4.18. Late Photograph of Zone 3 from the Last Test Blast
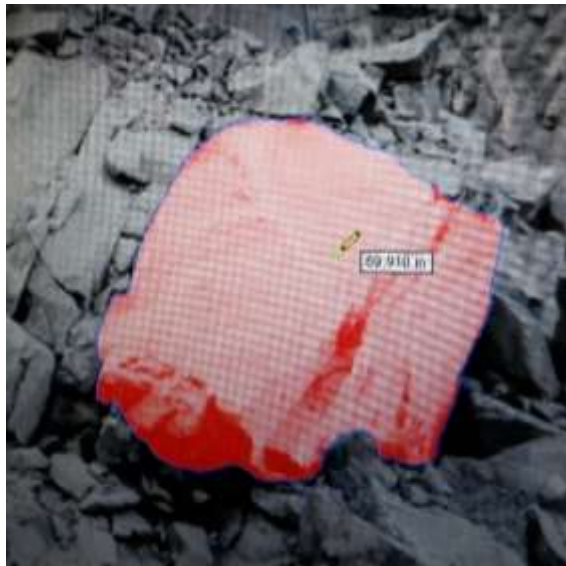


Figure 4.19. October 20, 2015 Large Fragment Example

## 4.6. ANALYSIS, RESULTS, AND DISCUSSION SUMMARY

The fragmentation in each zone was evaluated through digital image analysis of 28 photographs using WipFrag. Photographs were taken of each zone immediately after the shot and throughout the mucking process. The outlines generated by WipFrag were edited to ensure that they were true to the actual rocks. 0 ms, 1 ms, 4 ms, 10 ms, 16 ms, and 25 ms delay times were tested. The analysis of the fragmentation results of all of the delay times showed that the 25 ms delay time was the best overall at improving fragmentation. Short delay times performed the worst. Fragmentation varied by zone, and Zone 3 had the smallest fragmentation sizes. Stemming ejection occurred during all shots. The 0 ms delay resulted in the greatest throw. Seismographs and high-speed video cameras were used to record each of the test blasts. Testing in full scale was necessary to determine the practicality of the delay times for use in mining operations. Late photographs from Zone 3 of the final test blast showed the maximum particle size to be much larger than those which were included in the analysis.

# 5. CONCLUSION

The 25 ms and 10 ms delay times had the best fragmentation. Through photographic fragmentation analysis in WipFrag, it was found that the 25 ms delay had the smallest D10, Mean, D50, and D90 sizes. Given the greater number of photographs analyzed, its smaller size in values other than the maximum, and its use in multiple zones, the 25 ms delay time, was the best overall at improving fragmentation.

Short hole-to-hole delay times do not improve rock fragmentation in full scale bench blasting. The best performing delay times were outside of the short delay range and the worst performing delays were the shortest. The 1 ms delay time had the worst fragmentation results. A full analysis of the photographs for the 0 ms delay time was not able to be completed because of time constraints, but it performed poorly as well.

The 0 ms delay had the most throw. This agrees with other studies that have shown that instantaneous or short delays increase throw.

Timing affects fragmentation, so the Kuz-Ram model cannot be complete because it does not incorporate timing into its equations.

## 6. FURTHER STUDIES

This research could be continued and expanded by evaluating of all of the photos taken in late October 2015, and by testing the 0 ms, 1ms, and 10 ms times in additional zones. Full evaluation of the late results was outside of time constraints and graduation deadlines. This would strengthen the conclusions about the effectiveness of those times. Full analysis of these delay times will be completed and published.

This research could be expanded to any number of different quarries, with different rock types. Doing so would further show how rock type differences influence the effectiveness of timing modification. Additionally, testing at a mine with a faster blasting cycle time would allow for photos of the muck to be taken over the course of a few days rather than a few weeks. This could allow for more photos to be taken throughout the mucking process, and it would provide more consistency in the photographs taken across the zones. High-speed video where the face buckets can be seen more clearly would allow for face velocity measurements to be made.

The increased throw that was caused by the 0 ms delay suggests that a study of the timing effects on fragmentation should be completed at a site that does cast blasting.

Finally, given that the Kuz-Ram model is used to estimate fragmentation, but does not incorporate timing as a variable, this research could be extended to create a modification the Kuz-Ram model that incorporates timing.

APPENDIX A.

WIPFRAG PHOTOS AND CHARTS

Figure A. 1: Shot 1, Zone 1, 16ms, DSC04758, Taken April 16, 2015
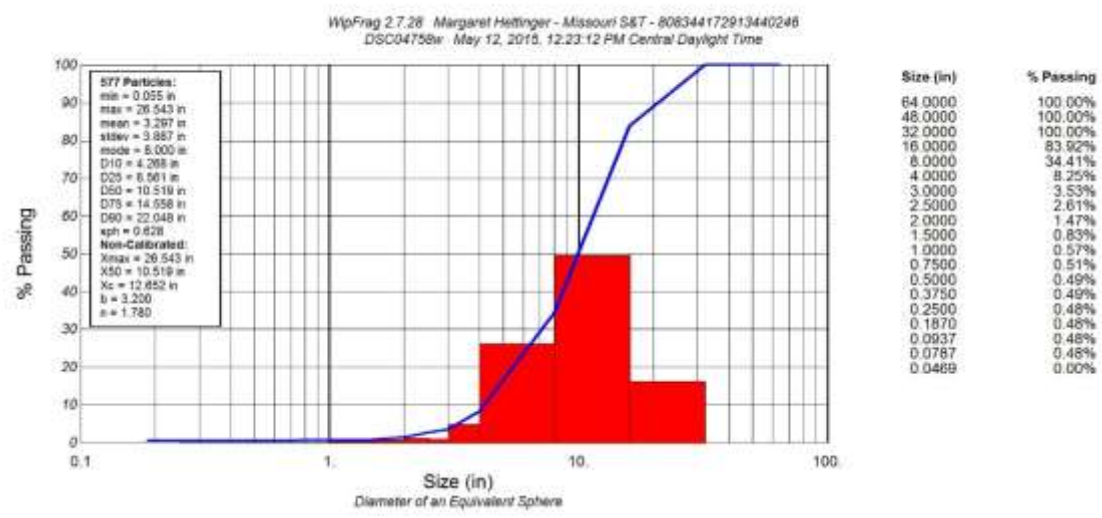


Figure A. 2: Chart for DSC04758

Figure A. 3: Shot 1, Zone 1, 16ms, DSCF1839w, Taken April 24, 2015
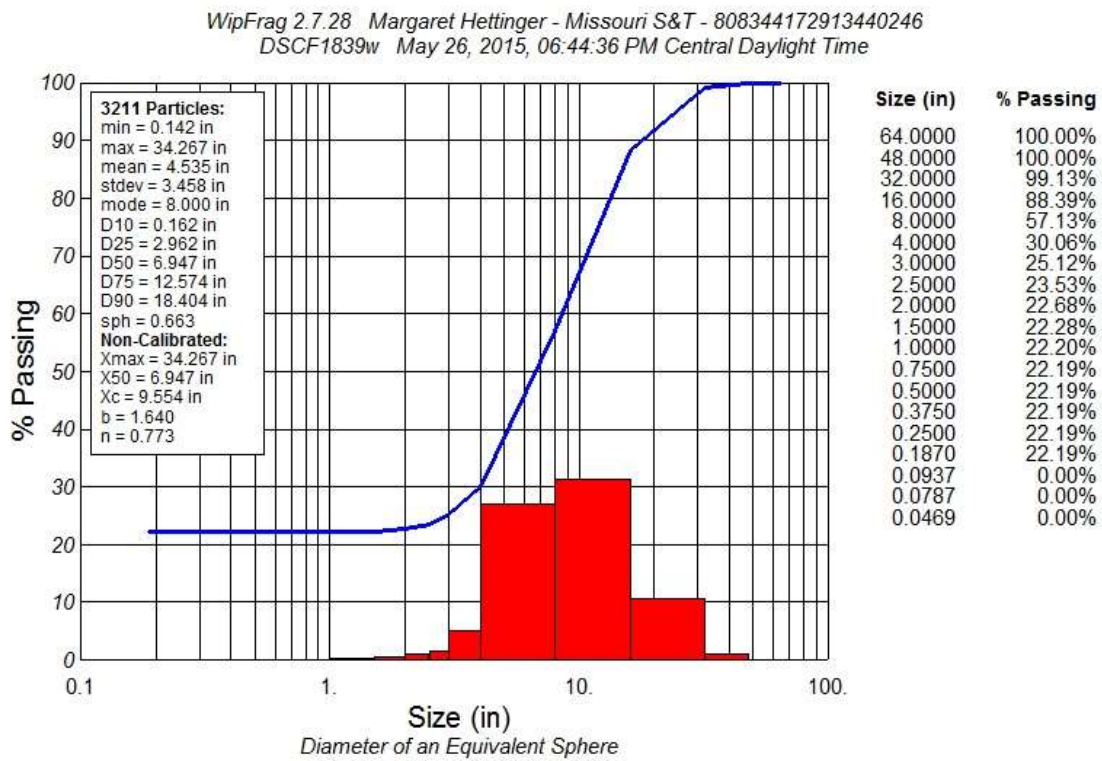


Figure A. 4: Chart for DSCF1839w

Figure A. 5: Shot 1, Zone 1, 16ms, zone1b 5-1-15w, Taken May 1, 2015
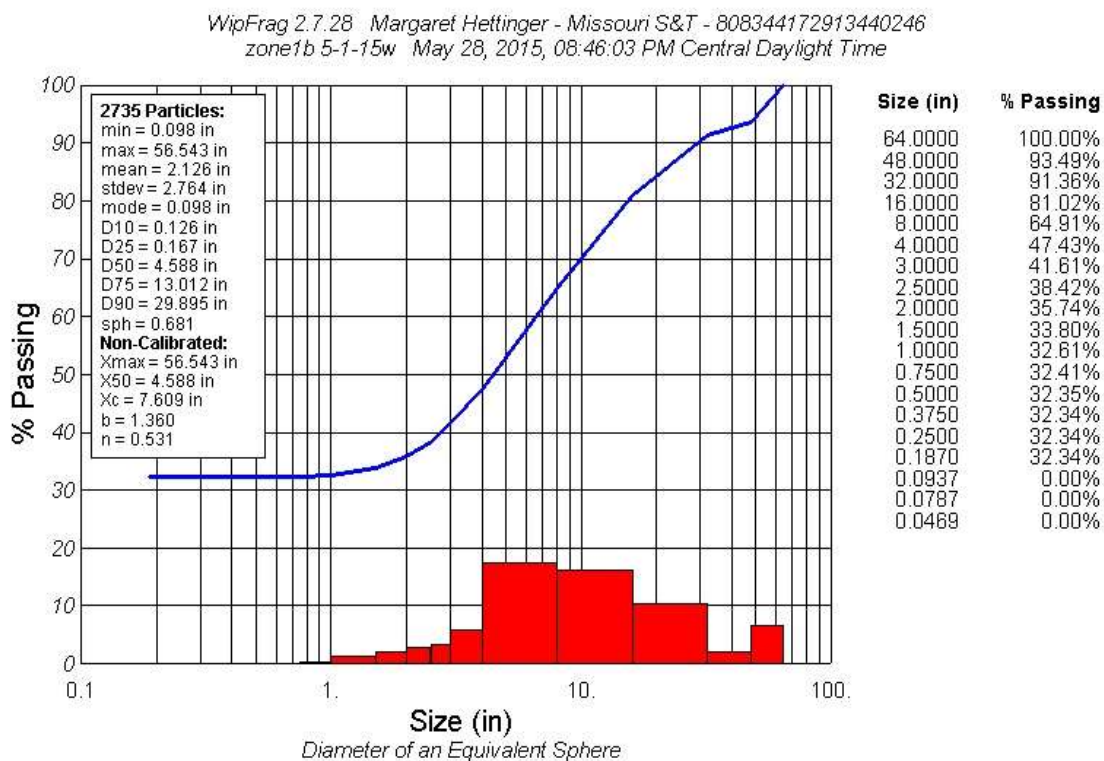


Figure A. 6: Chart for zone1b 5-1-15w

Figure A. 7: Shot 1, Zone 2, 4 ms, DSC04789, Taken April 16, 2015
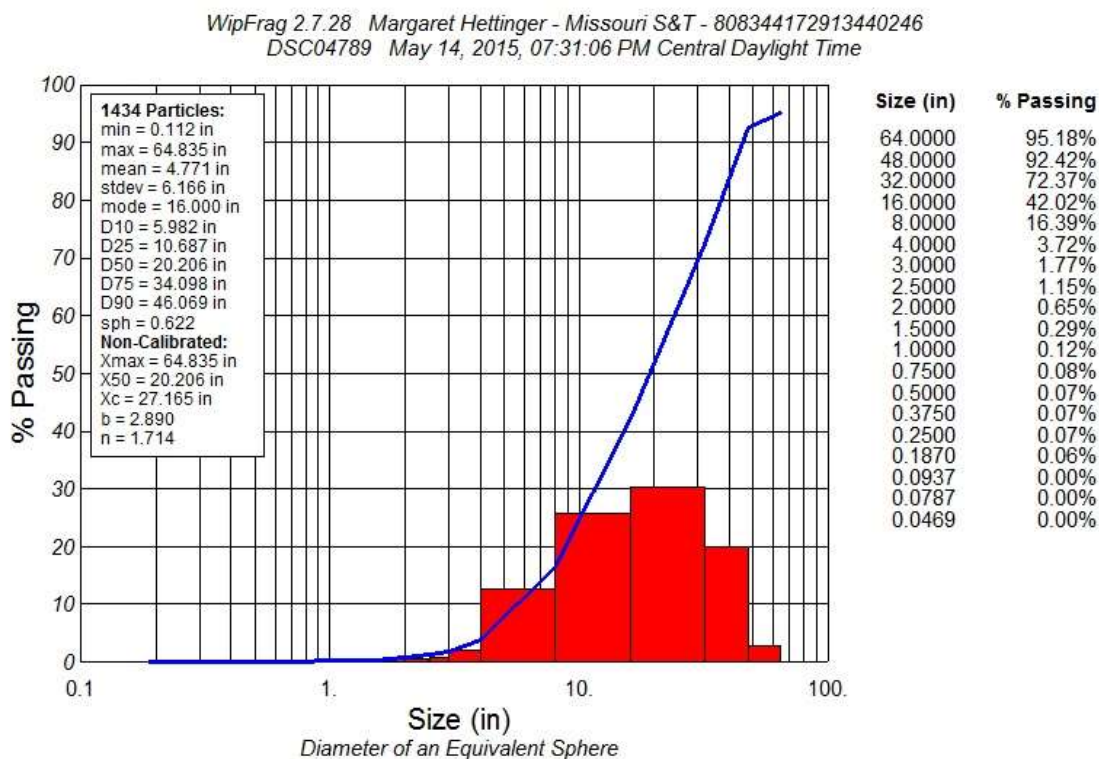
Figure A. 8: Chart for DSC04789



Figure A. 9: Shot 1, Zone 2, 4 ms, DSCF1848w, Taken April 24, 2015
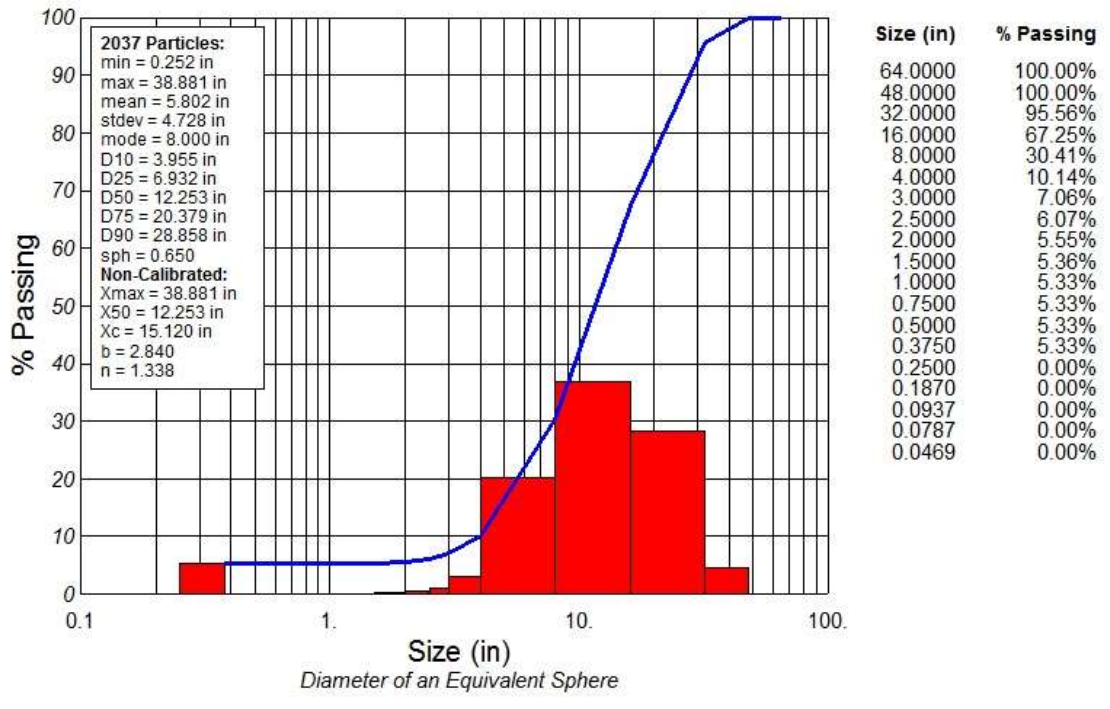
Figure A. 10: Chart for DSCF1848w

Figure A. 11: Shot 1, Zone 2, 4 ms, zone2d 5-1-15, Taken May 1, 2015
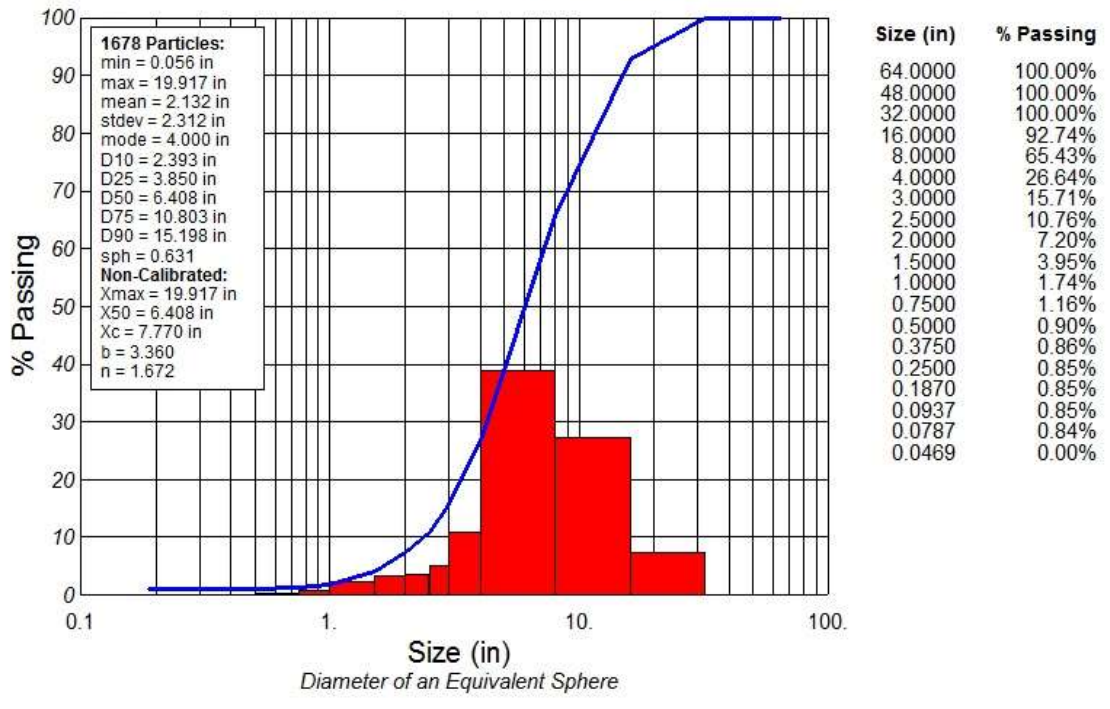
Figure A. 12: Chart for zone2d 5-1-15

Figure A. 13: Shot 2, Zone 1, 4 ms, DSC02034, Taken June 4, 2015
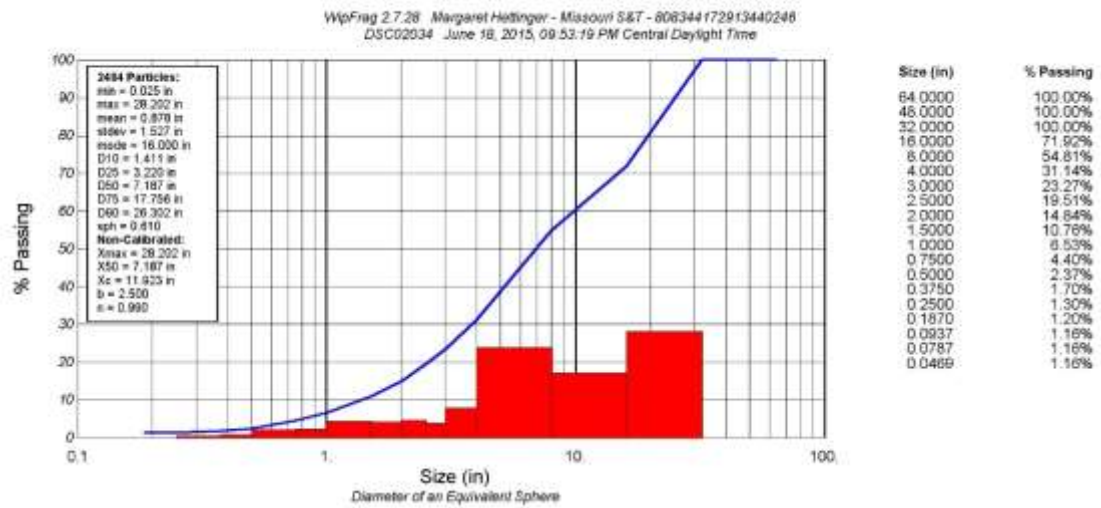


Figure A. 14: Chart for DSC02034

Figure A. 15: Shot 2, Zone 1, 4 ms, #1 Middle, Taken June 10, 2015
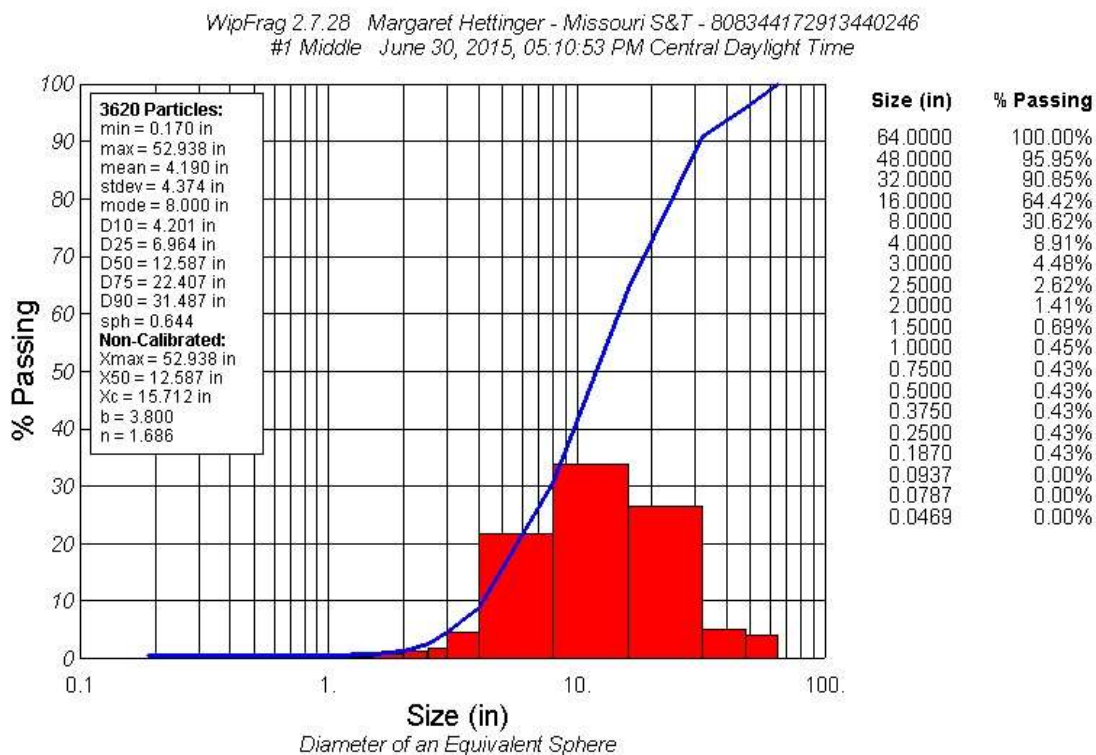
Figure A. 16: Chart for #1 Middle



Figure A. 17: Shot 2, Zone 1, 4 ms, Zn1a 6-25-15, Taken June 25, 2015
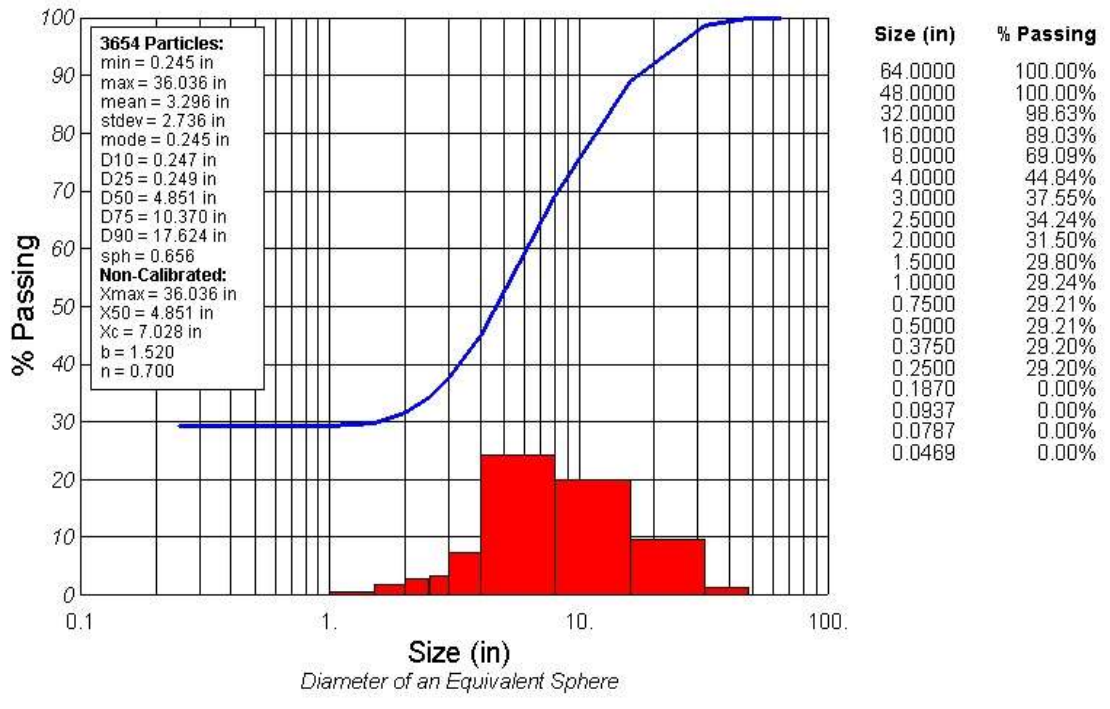
Figure A. 18: Chart for Zn1a 6-25-15

Figure A. 19: Shot 2, Zone 2, 16 ms, DSC02046, Taken June 4, 2015
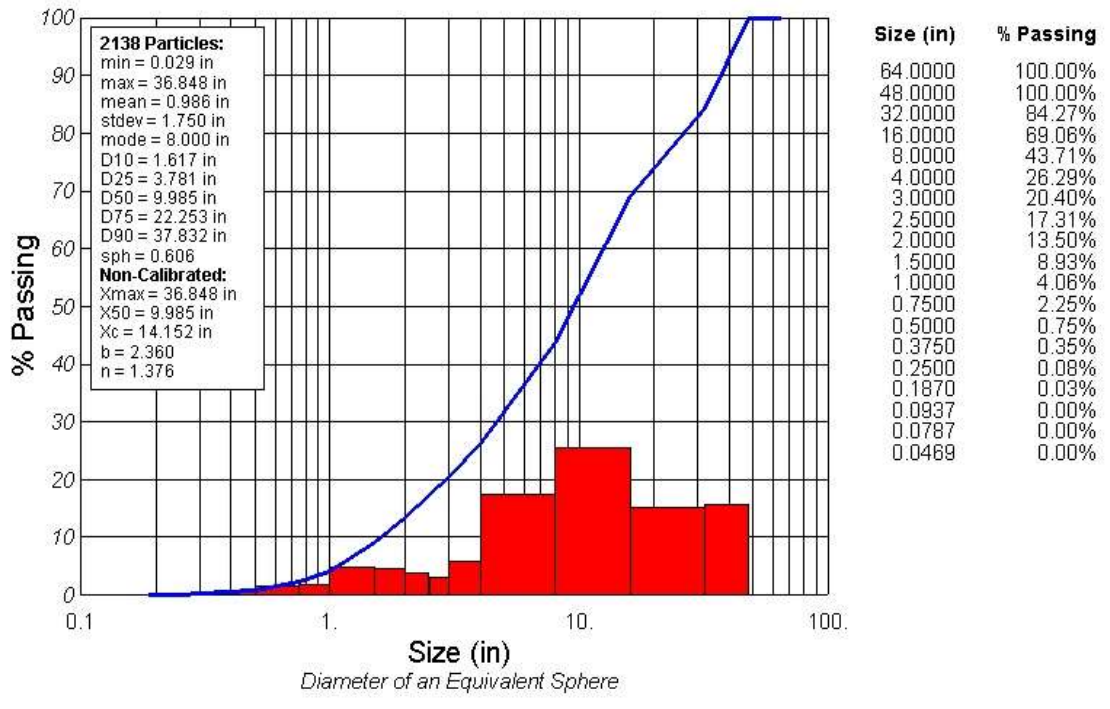
Figure A. 20: Chart for DSC02046

Figure A. 21: Shot 2, Zone 2, 16 ms, #2 Middle, Taken June 10, 2015
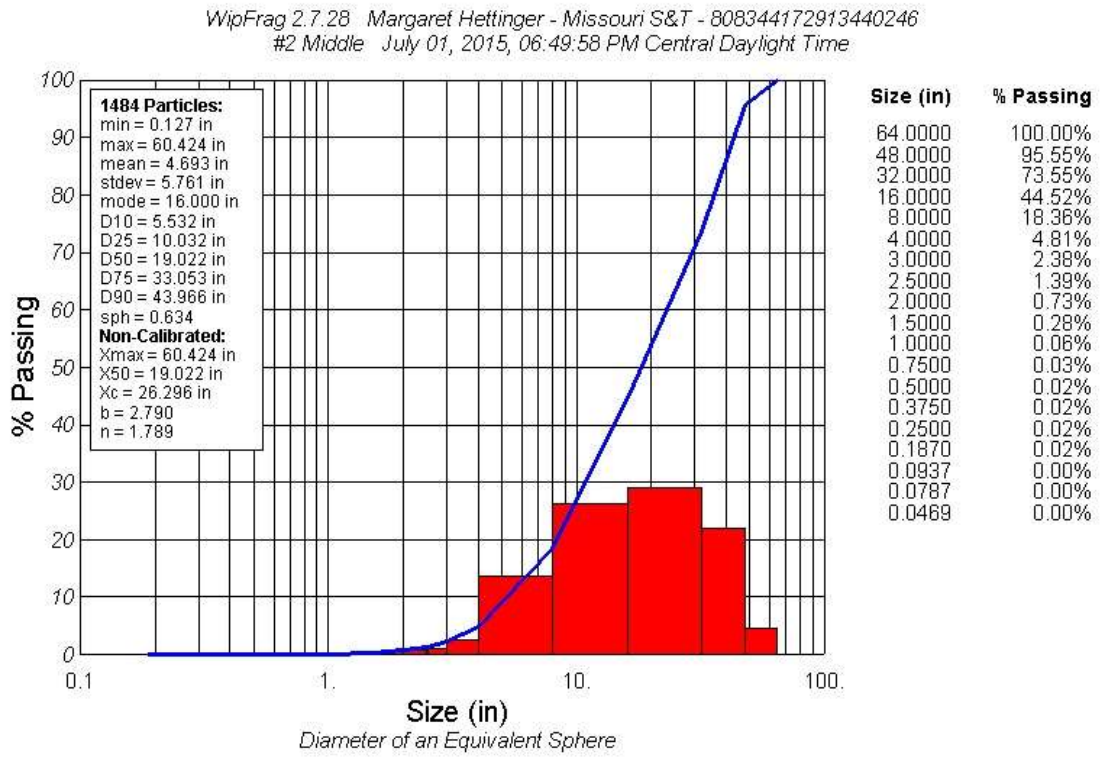
Figure A. 22: Chart for #2 Middle



Figure A. 23: Shot 2, Zone 2, 16 ms, Zn2a 6-25-15, Taken June 25, 2015
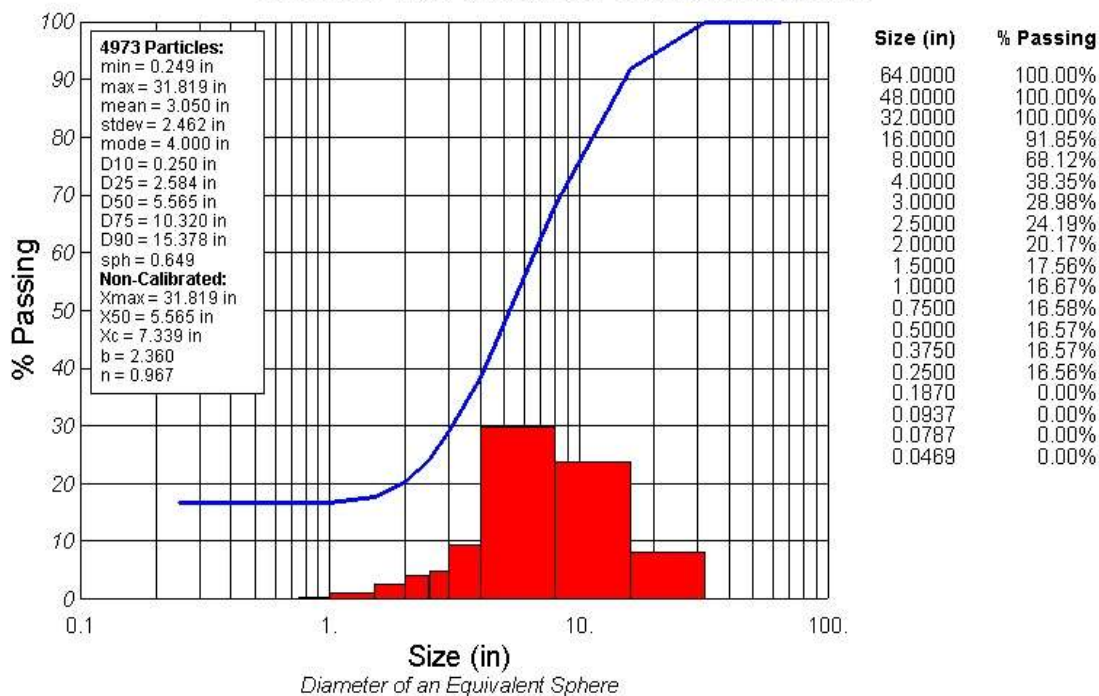
Figure A. 24: Chart for Zn2a 6-25-15

Figure A. 25: Shot 2, Zone 3, 25 ms, DSC02062, Taken June 4, 2015
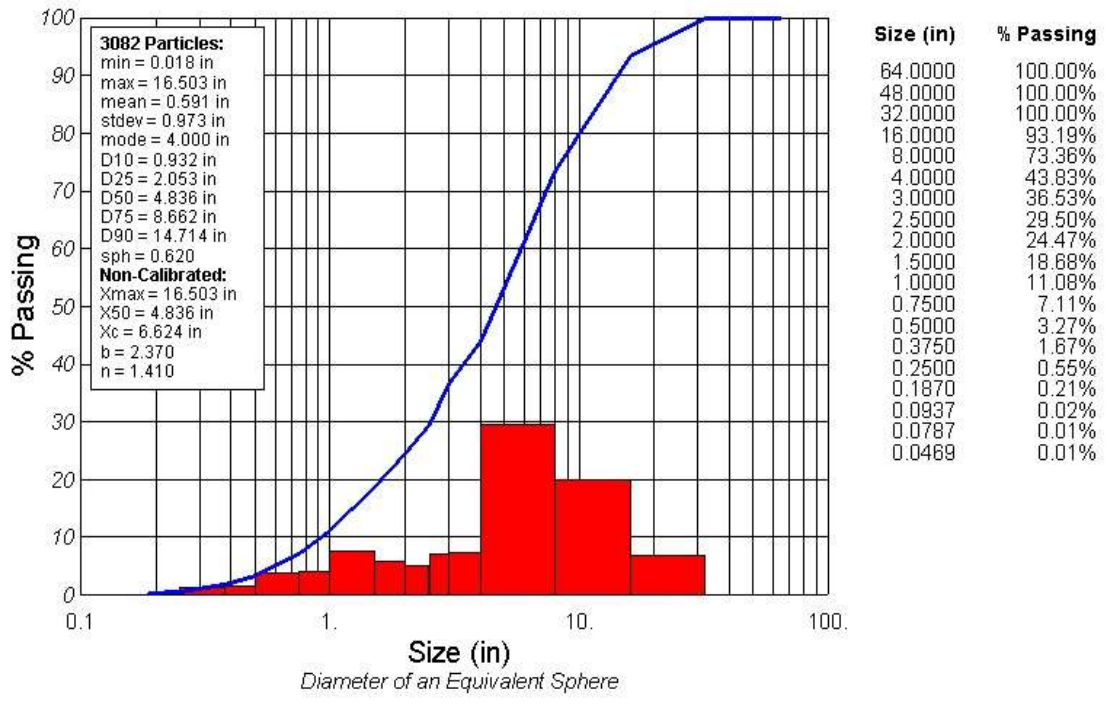
Figure A. 26: Chart for DSC02062



Figure A. 27: Shot 2, Zone 3, 25 ms, Zn3a 6-25-15, Taken June 25, 2015
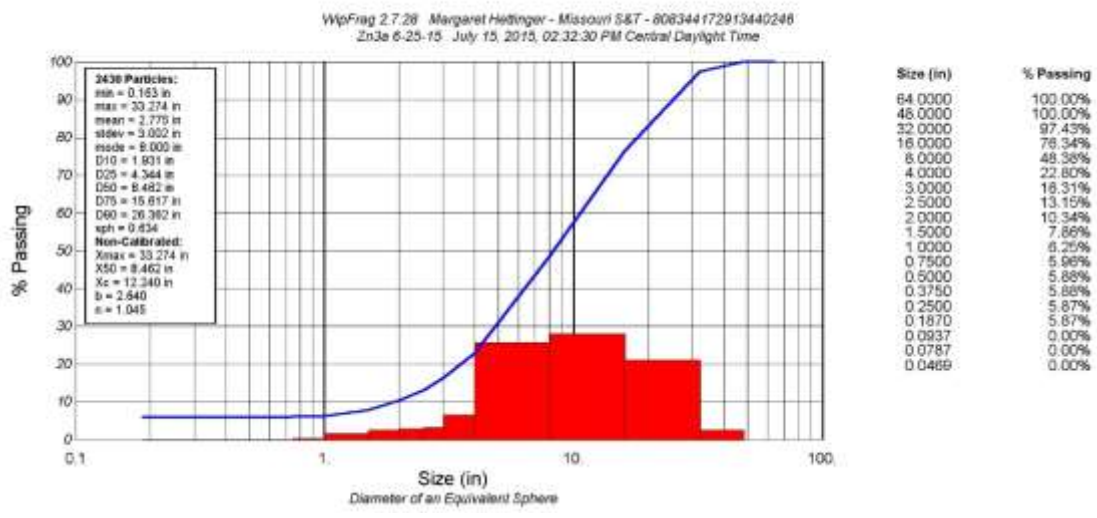
Figure A. 28: Chart for Zn3a 6-25-15



Figure A. 29: Shot 3, Zone 1, 1 ms, DSC02118, Taken July 30, 2015
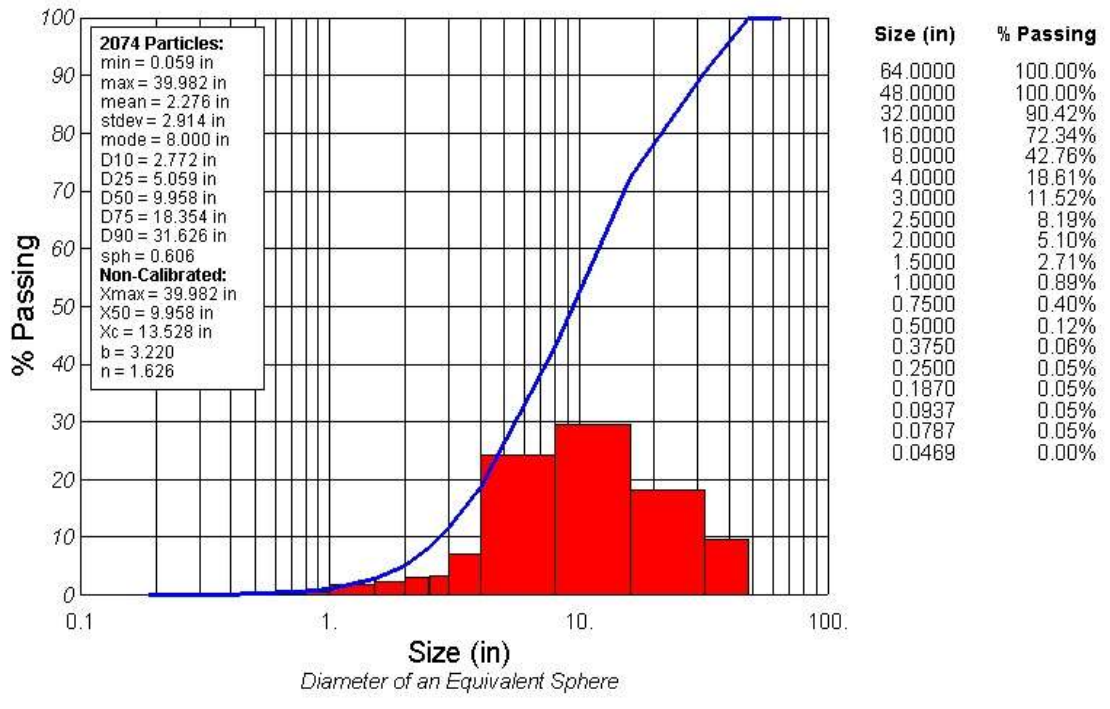
Figure A. 30: Chart for DSC02118

Figure A. 31: Shot 3, Zone 1, 1 ms, Zone 1 A_1598x1063, Taken August 5, 2015
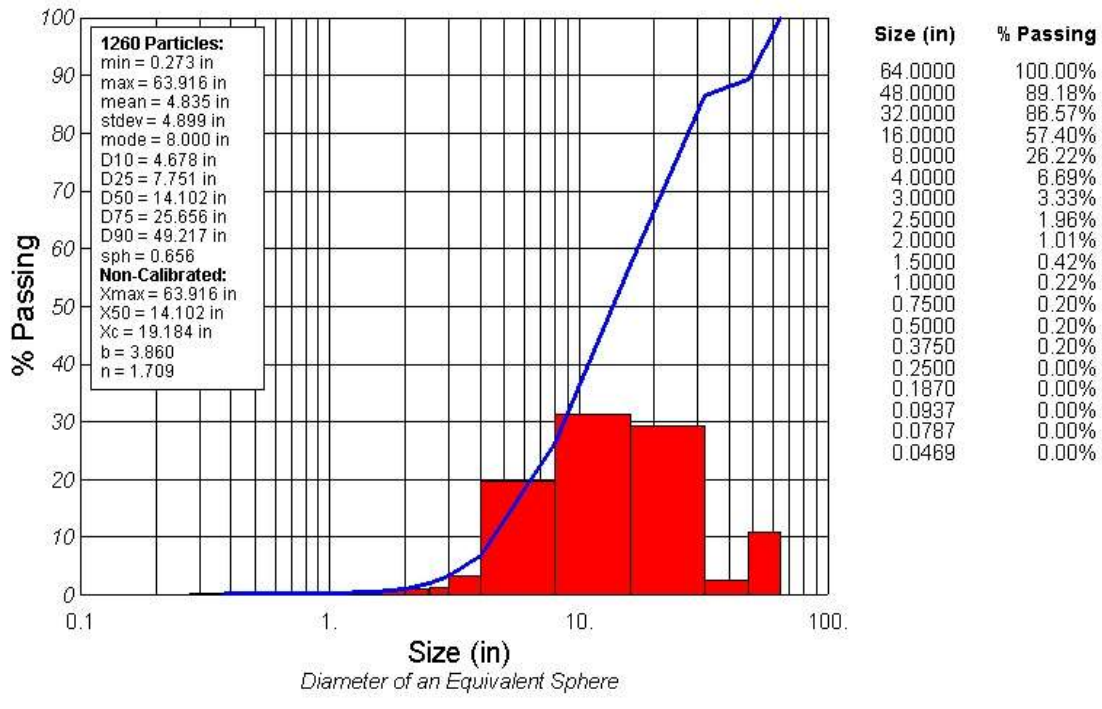
Figure A. 32: Chart for Zone 1 A_1598x1063

Figure A. 33: Shot 3, Zone 1, 1 ms, IMG_0059_1129x1505, Taken August 19, 2015
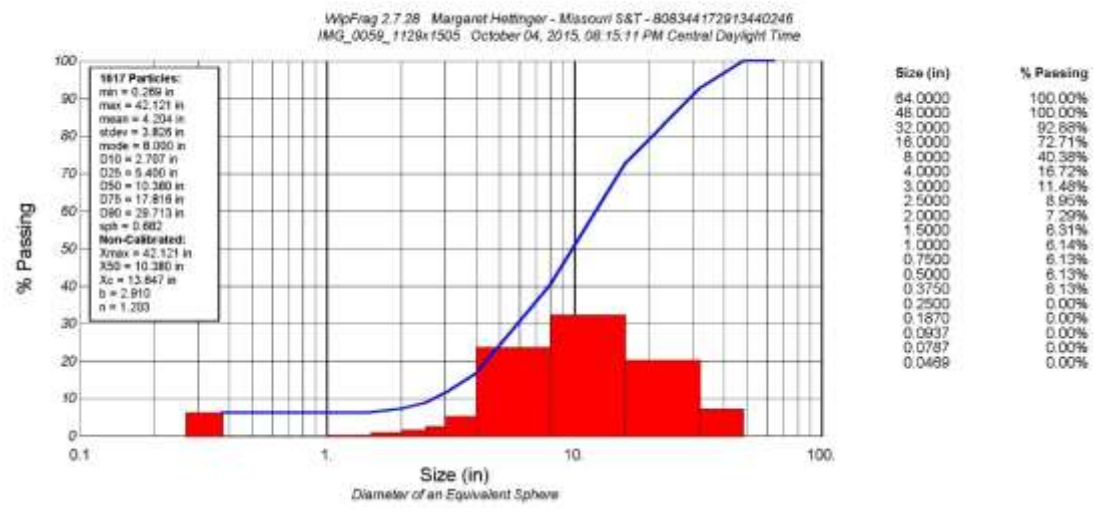
Figure A. 34: Chart for IMG_0059_1129x1505



Figure A. 35: Shot 3, Zone 2, 25 ms, DSC02128w_1835x926, Taken July 30, 2015
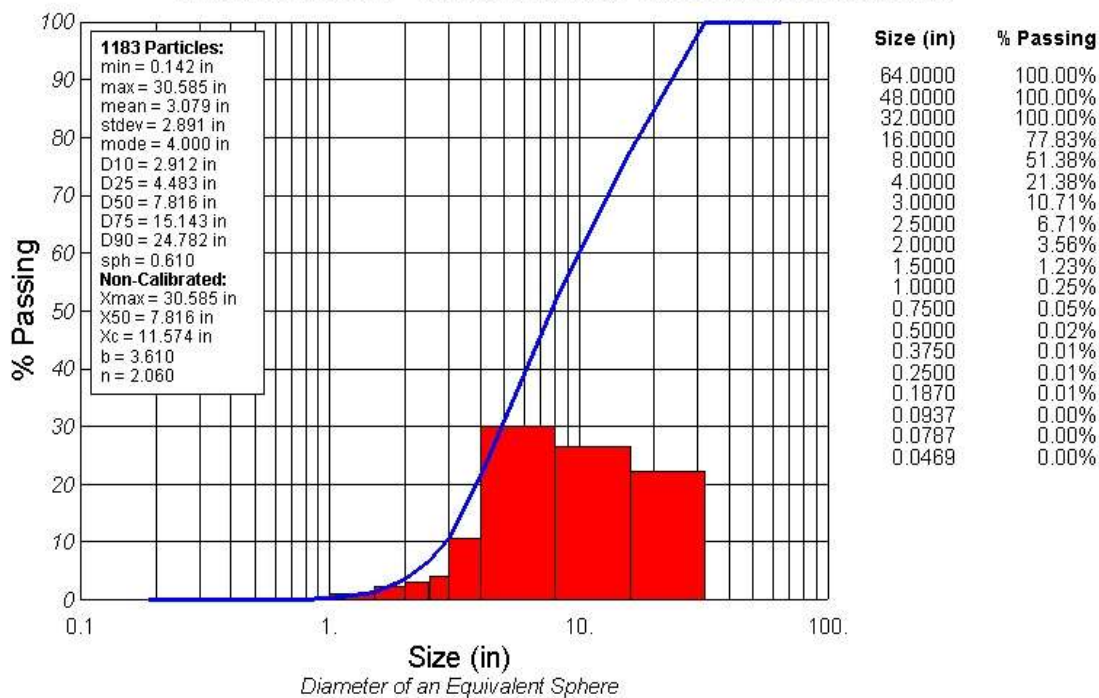
Figure A. 36: Chart for DSC02128w_1835x926

Figure A. 37: Shot 3, Zone 2, 25 ms, Zone 2 A_1598x1063, Taken August 5, 2015
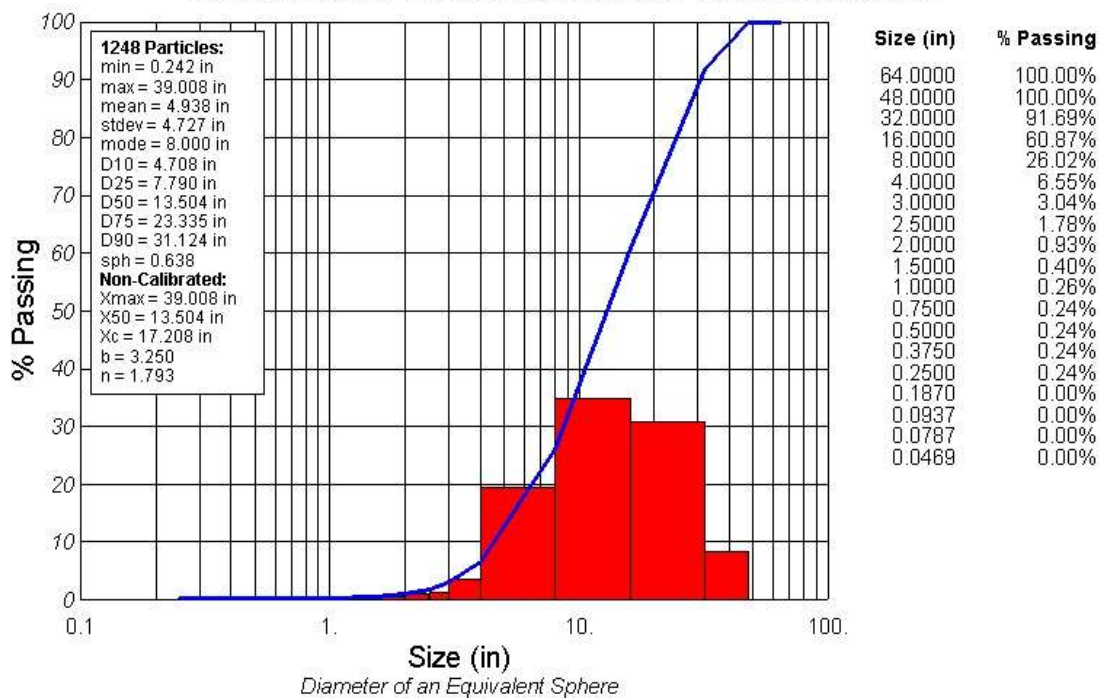
Figure A. 38: Chart for Zone 2 A_1598x1063

Figure A. 39: Shot 3, Zone 2, 25 ms, IMG_0061_1129x1505, Taken August 19, 2015
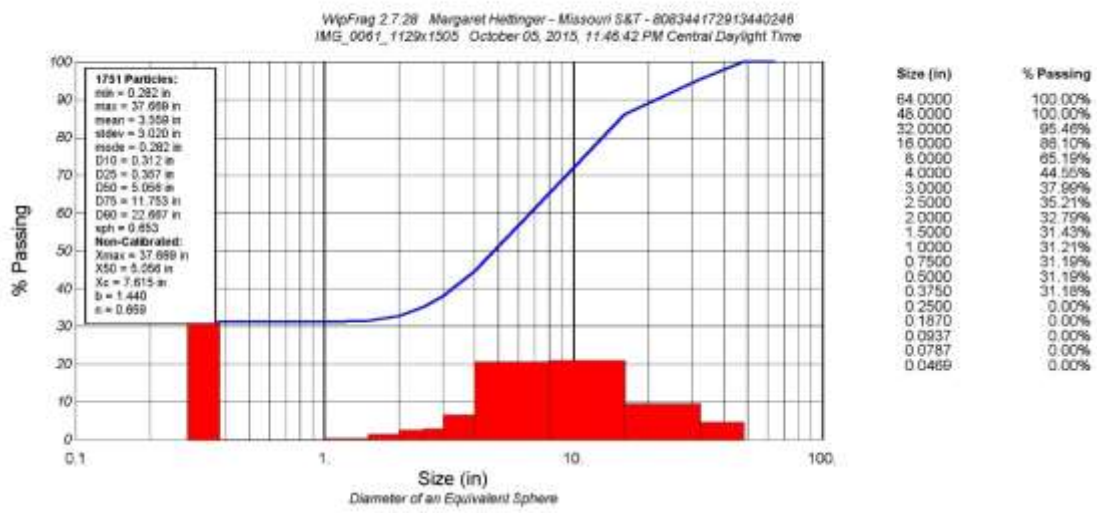
Figure A. 40: Chart for IMG_0061_1129x1505



Figure A. 41: Shot 3, Zone 3, 16 ms, DSC02139_1599x1062, Taken July 30, 2015
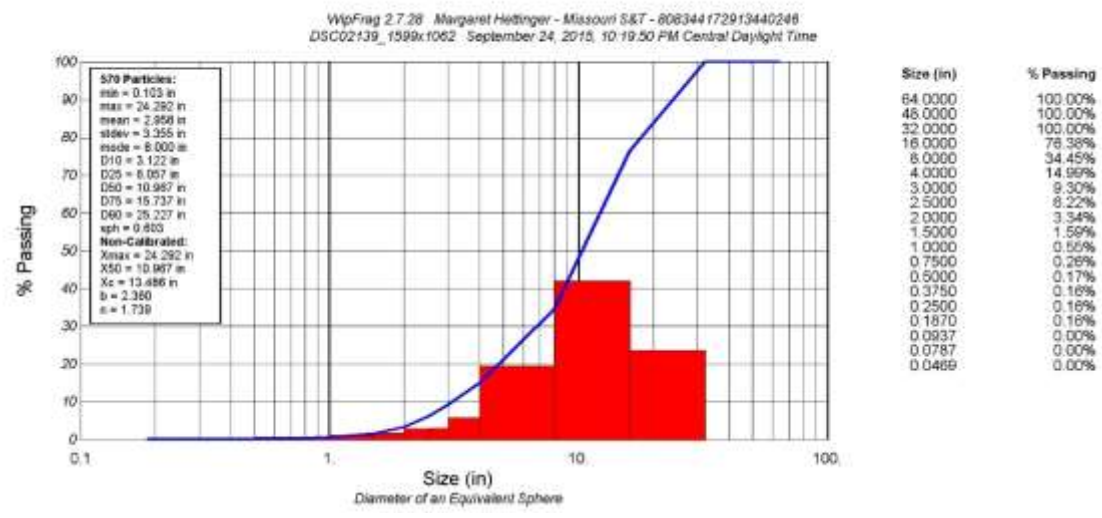
Figure A. 42: Chart for DSC02139_1599x1062

Figure A. 43: Shot 3, Zone 3, 16 ms, IMG_0065_1129x1505, Taken August 19, 2015
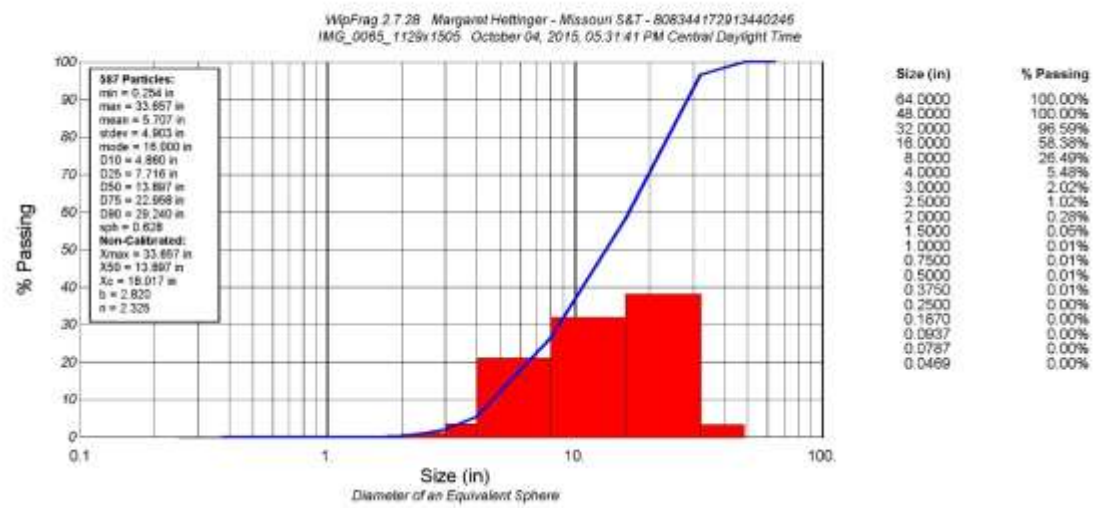


Figure A. 44: Chart for IMG_0065_1129x1505



Figure A. 45: Shot 4, Zone 1, 10 ms, DSC02277_1599x1062, Taken September 15, 2015
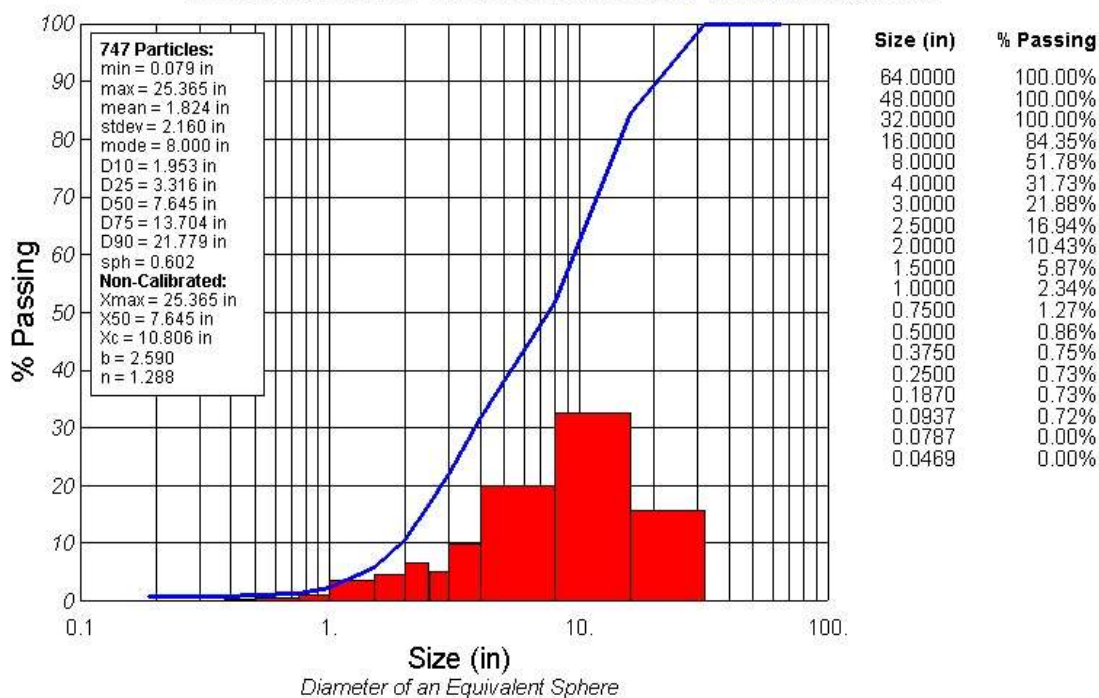
Figure A. 46: Chart for DSC02277_1599x1062

Figure A. 47: Shot 4, Zone 1, 10 ms, IMG_0670_1505x1129, Taken September 29, 2015
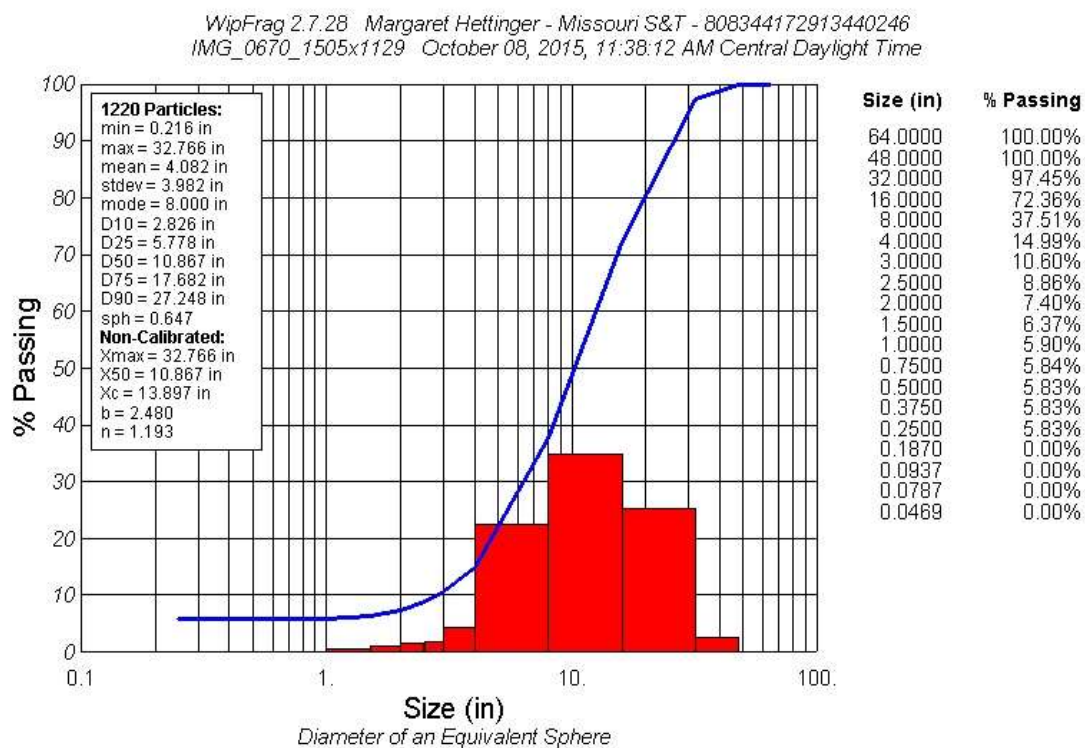
Figure A. 48: Chart for IMG_0670_1505x1129

Figure A. 49: Shot 4, Zone 2, 25 ms, DSC02283_1599x1062, Taken September 15, 2015
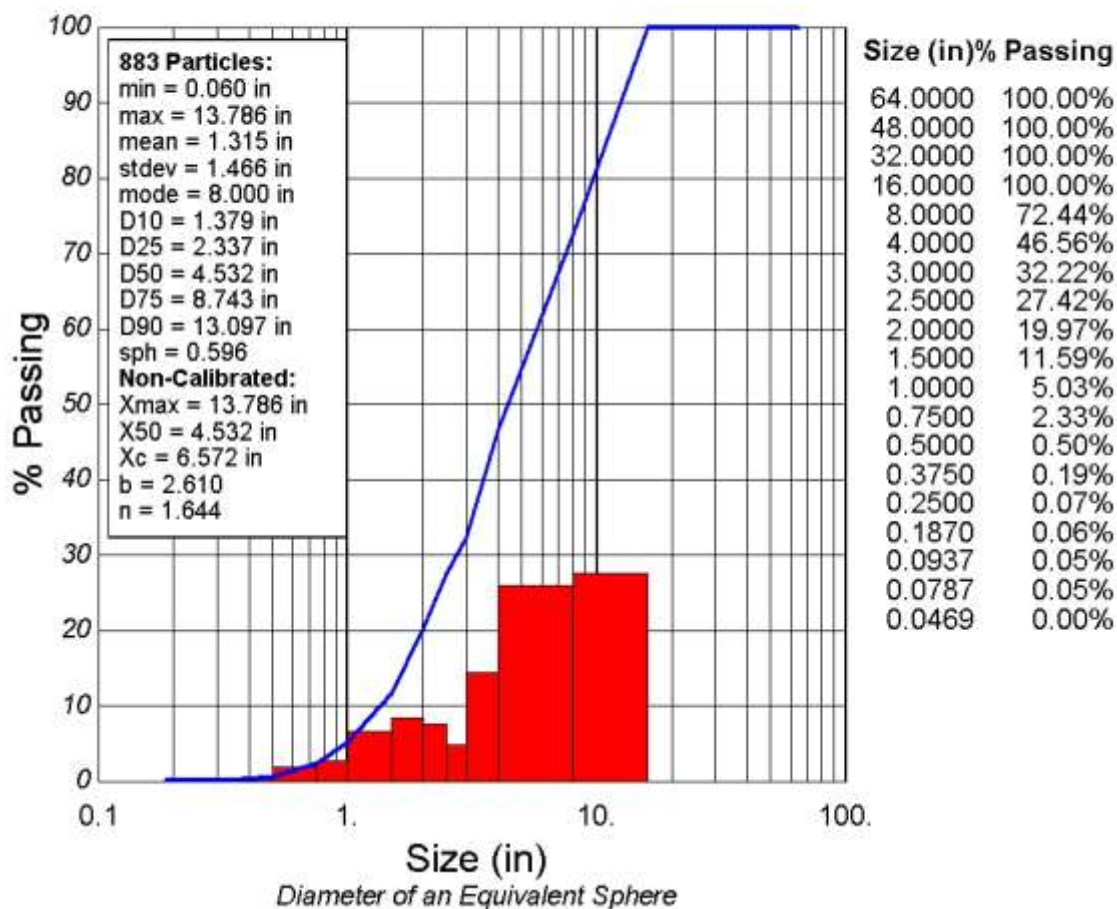
Figure A. 50: Chart for DSC02283_1599x1062

Figure A. 51: Shot 4, Zone 2, 25 ms, IMG_0673_1505x1129, Taken September 29, 2015
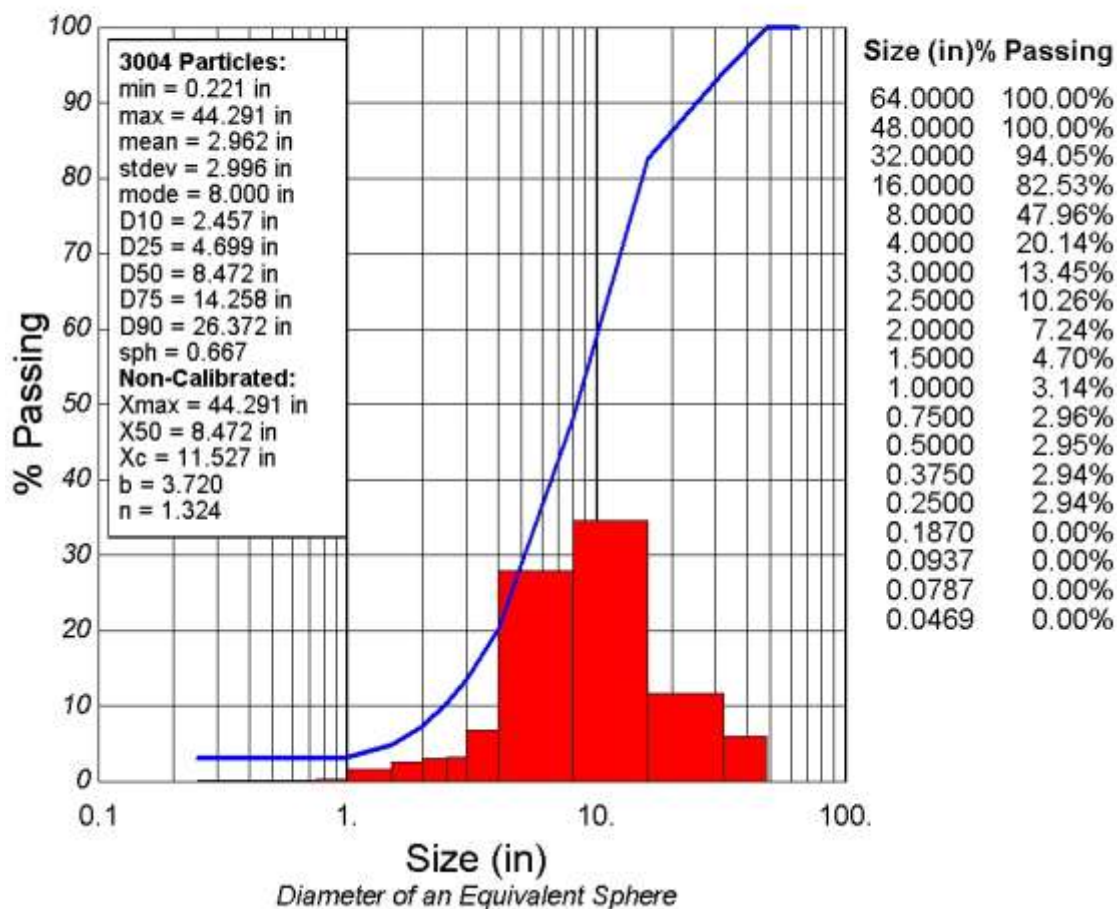
Figure A. 52: Chart for IMG_0673_1505x1129

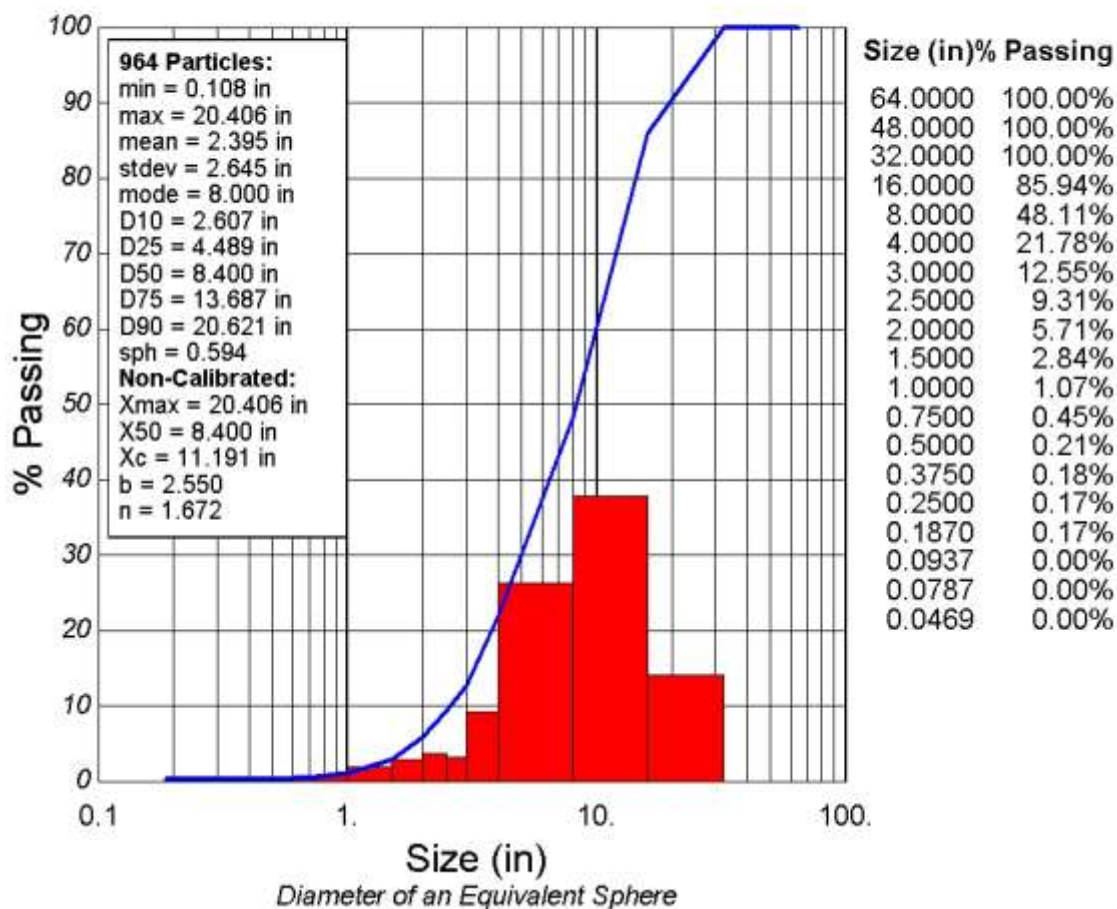Figure A. 53: Shot 4, Zone 3, 0 ms, DSC02294_1599x1062, Taken September 15, 2015

Figure A. 54: Chart for DSC02294_1599x1062

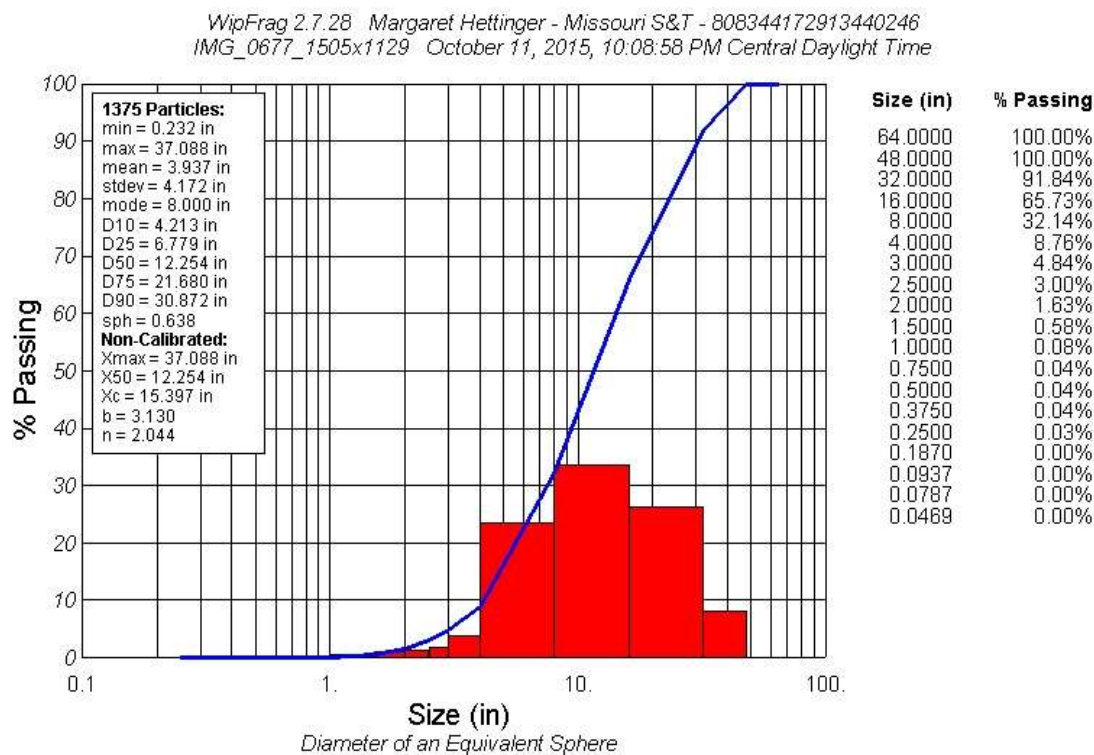Figure A. 55: Shot 4, Zone 3, 0 ms, IMG_0677_1505x1129, Taken September 29, 2015

Figure A. 56: Chart for IMG_0677_1505x1129

APPENDIX B.

EXPLOSIVE INFORMATION AND BLAST REPORTS

Figure B. 1: Titan 1000 SME Product Information

# TITAN® 1000 SD

## Sensitized Bulk Emulsion

**Technical Information**

### Product Description

TITAN 1000 SD is a booster sensitive, high performance, repumpable bulk emulsion explosive specifically formulated to provide superior blasting performance in all open pit and quarry applications where 75 mm (3 in) and larger diameter boreholes are used. TITAN 1000 SD can be used alone, blended with up to 45% ANFO for direct pumping to the bottom of water-filled boreholes; or as the emulsion explosive component for augerable Heavy ANFO blends. The percentage of emulsion in TITAN 1000 SD emulsion/ANFO or TITAN 1000 SD Heavy ANFO blends can be varied to best match specific blasting requirements. Refer to the data table at right for the physical properties of some typical TITAN 1000 SD emulsion/ANFO explosive blends.

### Application Recommendations

- Only ANFO manufactured with emulsion-compatible AN prills is recommended for use in TITAN 1000 SD emulsion/ANFO blends.
- The minimum cast booster recommended to prime TITAN 1000 SD and TITAN 1000 SD emulsion/ANFO blends and TITAN 1000 SD Heavy ANFO blends is 340 g (12 oz).
- ALWAYS double prime when bulk explosive columns exceed 6 m (20 ft) One primer should be positioned near the bottom of the hole and the second nearer the top of the explosive column.
- Do not use detonating cord in borehole diameters less than 159 mm (6¼ in).

## Properties

SBS #1062

| | | 1000 | 1080 | 1070 | 1050 | 1030 | 1020 |
|---|---|---|---|---|---|---|---|
| Percent Emulsion | | 100 | 80 | 70 | 50 | 30 | 20 |
| Density | (g/cc) Avg | 1.20 | 1.23 | 1.24 | 1.27 | 1.15 | 1.05 |
| | (g/cc) Max | 1.24 | 1.28 | 1.30 | 1.30 | 1.18 | 1.08 |
| Energy* | (cal/g) | 880 | 720 | 740 | 771 | 815 | 835 |
| | (cal/cc) | 815 | 885 | 920 | 980 | 935 | 880 |
| Relative Weight Strength** | | 0.77 | 0.82 | 0.84 | 0.88 | 0.93 | 0.95 |
| Relative Bulk Strength** | | 1.13 | 1.23 | 1.27 | 1.36 | 1.30 | 1.22 |
| Velocity* | (m/sec) | 5,600 | 5,400 | 4,800 | 4,700 | 4,400 | 4,200 |
| | (ft/sec) | 18,400 | 17,700 | 15,700 | 15,400 | 14,400 | 13,800 |
| Detonation Pressure* (Kbars) | | 94 | 90 | 71 | 70 | 56 | 46 |
| Gas Volume* (moles/kg) | | 45.4 | 45.0 | 44.8 | 43.5 | 43.3 | 43.2 |
| Water Resistance | | Excellent | Excellent | Excellent | Good | Fair | Poor |
| Minimum Diameter | (mm) | 75 | 90 | 100 | 125 | 115 | 90 |
| | (inches) | 3 | 3.5 | 4 | 5 | 4.5 | 3.5 |
| Loading Method | | Pump | Pump | Pump | Auger | Auger | Auger |

* All Dyno Nobel Inc. energy and gas volume values are calculated using PRODET™, a computer code developed by Dyno Nobel Inc. for its exclusive use. Other computer codes may give different values.
* ANFO = 1.00 @ 0.82 g/cc
* Confined in 150 mm (6 in) diameter at average density

**Hazardous Shipping Description**
Explosive, Blasting, Type E 1.5 UN 0332 II

B-06-06-18-15

**DYNO**
Dyno Nobel
Groundbreaking Performance

Figure B. 2: Titan 1000 SD Product Information

**Dyno Nobel North America BLAST REPORT**

PO NUMBER: JCM 20529

SERVICE SITE LOCATION: Whitesburg     ORDER NO.: 905547

**DYNO**
Dyno Nobel

BLAST NUMBER: 10-2015 Production   BLAST TIME: 1:05 pm     BLAST DATE: 04/16/2015

CUSTOMER: ANDERSON COLUMBIA COM   MINE: JUNCTION CITY MINING     ADDRESS: Talbotton, GA

ROCK TYPE: Granite     Tons/Yd3:     2.27     EXPECTED VIBRATION:     0.060

**LOCATION OF BLAST**

LOCATION OF BLAST IN MINE: North     BENCH: 2nd Bench

BLAST GPS POINTS:     N -032 37 56.59980     & W -084 30 07.30020

**WEATHER**

WEATHER: Overcast     CEILING: <2,000     TEMPERATURE: 58     WIND DIRECTION & SPEED: Northeast   10

**NEAREST NON-OWNED STRUCTURE**

NAME: Roper Residence     GPS Points: N -032 38 38.68800   & W -084 30 51.30000

DISTANCE:     5,688 Ft     DIRECTION:     221°

**SEISMOGRAPH DATA**

| | LOCATION | DISTANCE | GPS POINTS | | CALIBRATION DATE |
|---|---|---|---|---|---|
| 1 | Roper Residence | 5,688  Ft | N -032 38 38.6880 & W -084 30 51.30000 | | 06/16/2009 |

| | L | (F) | T | (F) | V | (F) | AIR (db) | SEISMOGRAPH | SERIAL | OPERATOR |
|---|---|---|---|---|---|---|---|---|---|---|
| 1 | 0.000 | 0 | 0.000 | 0 | 0.000 | 0 | 0 | Seismograph AB96 | 1 | |

**BLAST DATA**

| | | | | EXPLOSIVES SIZE, TYPE & WEIGHT | | |
|---|---|---|---|---|---|---|
| NUMBER OF HOLES (EA) | 85 | | | | | |
| HOLE DIAMETER (IN) | 5.75 | SIZE | | TYPE | | WEIGHT |
| HOLE DEPTH (FT) | 72 | 2.00 LB | 900G | | | 170 |
| FACE HEIGHT (FT) | 69 | 0.75 LB | SPARTAN 350SR | | 63 | 63 ㅁ |
| SUB DRILLING (FT) | 3 | BULK | TITAN 1000 SD | | | 10,900 |
| AVG. STEM FACE HOLES (FT) | 8 | BULK | TITAN 1000 SME | | | $6,405.000 |
| STEM OTHER HOLES (FT) | 8 | | | | | |
| BURDEN FRONT ROW (FT) | 13 | | | | | |
| BURDEN OTHER ROWS (FT) | 13 | | | | | |
| SPACING FRONT ROW (FT) | 17 | | | | | 67538 |
| SPACING OTHER ROWS (FT) | 17 | | | | TOTAL WEIGHT: | 67,538.00 |

DETONATORS USED IN BLAST:   DigiShot     MATS USED: No     STEM TYPE: #6'S

| TYPE | MFG | DATE CODE | USED | TYPE | MFG | DATE CODE | USED |
|---|---|---|---|---|---|---|---|
| BLASTGEL 1070 4 X 20 | Dyno Nobel Global | 04FE15D1 | 680 | DIGISHOT 30 FT | Dyno Nobel Global | 05JA15S1 | 33 |
| DIGISHOT 80FT | Dyno Nobel Global | 05JA15S1 | 2 | DIGISHOT 80FT | Dyno Nobel Global | 09FE15S1 | 40 |
| DIGISHOT 80FT | Dyno Nobel Global | 12JA15S1 | 43 | SPARTAN 350SR | Dyno Nobel Global | 14JA15J2 | 81 |
| DIGISHOT 30 FT | Dyno Nobel Global | 22DE14S1 | 51 | 900G | Dyno Nobel Global | 22SE14W1 | 85 |

CU YDS IN SHOT:   48,008     SCALED DISTANCE FACTOR:   142     % OF ANFO:   0

TONS IN SHOT:   109,189     HOLES/DELAY :   2.0     FUEL OIL % (BULK):   0

MAX LBS/DELAY:   1,600     AVERAGE LBS/HOLE   795

POWDER FACTOR (TONS/LB):     1.62     POWDER FACTOR POUNDS/YD3:     1.41

BLASTERS NAME:  Moore, James P     BLASTERS NUMBER & STATE:   GA 18129     Georgia

BLASTERS SIGNATURE:     SITE SAFETY INSPECTION PERFORMED:     Yes

MINE MGT. SIGNATURE     NUMBER OF PERSONNEL ON SITE:     5

REMARKS :

| START TIME | END TIME | TOTAL TIME | TRUCK NUMBERS |
|---|---|---|---|
| 7:00 AM | 12:00 PM | 05:00 | HT 1190, HT1268 |

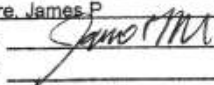Figure B. 3: April 16, 2015, Shot 1 Blast Report

## Dyno Nobel North America BLAST REPORT

**DYNO**
Dyno Nobel

PO NUMBER: JCM 20929
SERVICE SITE LOCATION: Whitesburg      ORDER NO.: 915364

BLAST NUMBER: 14-2015 Production BLAST TIME: 12:50 pm    BLAST DATE: 06/04/2015
CUSTOMER: ANDERSON COLUMBIA COM MINE: JUNCTION CITY MINING    ADDRESS: Talbotton, GA
ROCK TYPE: Granite                    Tons/Yd3:    2.27    EXPECTED VIBRATION:    0.060

### LOCATION OF BLAST

LOCATION OF BLAST IN MINE: North         BENCH: 2nd Bench
BLAST GPS POINTS:   N -032 37 58.99980   & W -084 30 01.99980

### WEATHER

WEATHER: Partly Cloudy    CEILING: <2,000    TEMPERATURE: 78   WIND DIRECTION & SPEED:   North   5

### NEAREST NON-OWNED STRUCTURE

NAME: Roper Residence         GPS Points: N -032 38 38.68800  & W -084 30 51.30000
DISTANCE:    5,826 Ft      DIRECTION:    226°

### SEISMOGRAPH DATA

| | LOCATION | DISTANCE | GPS POINTS | | CALIBRATION DATE |
|---|---|---|---|---|---|
| 1 | Roper Residence | 5,826  Ft | N -032 38 38.6880 & W -084 30 51.30000 | | 06/16/2009 |

| | L | (F) | T | (F) | V | (F) | AIR (db) | SEISMOGRAPH | SERIAL | OPERATOR |
|---|---|---|---|---|---|---|---|---|---|---|
| 1 | 0.000 | 0 | 0.000 | 0 | 0.000 | 0 | 0 | Seismograph AB96 | 1 | |

### BLAST DATA

| | | | EXPLOSIVES SIZE, TYPE & WEIGHT | | |
|---|---|---|---|---|---|
| NUMBER OF HOLES (EA) | 86 | SIZE | TYPE | | WEIGHT |
| HOLE DIAMETER (IN) | 5.75 | | | | |
| HOLE DEPTH (FT) | 73 | 2.00 LB | 900G | | 172 |
| FACE HEIGHT (FT) | 70 | 1.00 LB | BLASTGEL 1070 4 X 20 | | 380.000 |
| SUB DRILLING (FT) | 3 | 0.75 LB | SPARTAN 350SR | | 65.25 |
| AVG. STEM FACE HOLES (FT) | 0 | BULK | TITAN 1000 SD | | 7,120.000 |
| STEM OTHER HOLES (FT) | 0.127 | BULK | TITAN 1000 SME | | $7,284.000 |
| BURDEN FRONT ROW (FT) | 13 | | | | |
| BURDEN OTHER ROWS (FT) | 13 | | | | |
| SPACING FRONT ROW (FT) | 17 | | | | |
| SPACING OTHER ROWS (FT) | 17 | | TOTAL WEIGHT: | | 65,021.250 |

DETONATORS USED IN BLAST:    DigiShot        MATS USED: No    STEM TYPE: #6'S

| TYPE | MFG | DATE CODE | USED | TYPE | MFG | DATE CODE | USED |
|---|---|---|---|---|---|---|---|
| DIGISHOT 30 FT | Dyno Nobel Global | 02FE15S1 | 3 | BLASTGEL 1070 4 X 20 | Dyno Nobel Global | 04FE15D1 | 380 |
| SPARTAN 350SR | Dyno Nobel Global | 04MY15J2 | 87 | DIGISHOT 80FT | Dyno Nobel Global | 04MY15S1 | 40 |
| 900G | Dyno Nobel Global | 05JA15W1 | 86 | DIGISHOT 80FT | Dyno Nobel Global | 06AP15S1 | 46 |
| DIGISHOT 30 FT | Dyno Nobel Global | 09FE15S1 | 84 | | | | |

| | | | | |
|---|---|---|---|---|
| CU YDS IN SHOT: | 49,275 | SCALED DISTANCE FACTOR: | 149 | % OF ANFO:    0 |
| TONS IN SHOT: | 112,075 | HOLES/DELAY : | 2.0 | FUEL OIL % (BULK):    0 |
| MAX LBS/DELAY: | 1,512 | AVERAGE LBS/HOLE | 756 | |

POWDER FACTOR (TONS/LB):         1.72        POWDER FACTOR POUNDS/YD3:         1.32
BLASTERS NAME: Moore, James P        BLASTERS NUMBER & STATE:   GA 18129    Georgia
BLASTERS SIGNATURE: _____        SITE SAFETY INSPECTION PERFORMED:    Yes
MINE MGT. SIGNATURE: _____        NUMBER OF PERSONNEL ON SITE:    5
REMARKS :

| START TIME | END TIME | TOTAL TIME | TRUCK NUMBERS |
|---|---|---|---|
| 7:00 AM | 12:00 PM | 05:00 | |

Figure B. 4: June 4, 2015, Shot 2 Blast Report

# Dyno Nobel North America BLAST REPORT

**DYNO**
Dyno Nobel

PO NUMBER: JCM 21445
SERVICE SITE LOCATION: Whitesburg            ORDER NO.: 926208

BLAST NUMBER: 21-2015 Production BLAST TIME: 1:40 pm     BLAST DATE: 07/30/2015
CUSTOMER: ANDERSON COLUMBIA COM MINE: JUNCTION CITY MINING     ADDRESS: Talbotton, GA
ROCK TYPE: Granite                    Tons/Yd3:        2.27      EXPECTED VIBRATION:      0.060

## LOCATION OF BLAST

LOCATION OF BLAST IN MINE: North          BENCH: 2nd Bench
BLAST GPS POINTS:   N -032 38 02.29980    & W -084 30 01.09980

## WEATHER

WEATHER: Partly Cloudy     CEILING: <2,000     TEMPERATURE: 92  WIND DIRECTION & SPEED: Northeast  5

## NEAREST NON-OWNED STRUCTURE

NAME: Roper Residence                 GPS Points:  N -032 38 38.68800  & W -084 30 51.30000
DISTANCE:      5,658 Ft          DIRECTION:      229°

## SEISMOGRAPH DATA

| | LOCATION | DISTANCE | GPS POINTS | | | CALIBRATION DATE | |
|---|---|---|---|---|---|---|---|
| 1 | Roper Residence | 5,658  Ft | N -032 38 38.6880 & W -084 30 51.30000 | | | 06/16/2009 | |

| | L | (F) | T | (F) | V | (F) | AIR (db) | SEISMOGRAPH | SERIAL | OPERATOR |
|---|---|---|---|---|---|---|---|---|---|---|
| 1 | 0.000 | 0 | 0.000 | 0 | 0.000 | 0 | 0 | Seismograph AB961 | 1 | Vibra-, Tech |

## BLAST DATA

| | | EXPLOSIVES SIZE, TYPE & WEIGHT | | |
|---|---|---|---|---|
| NUMBER OF HOLES (EA) | 85 | SIZE | TYPE | WEIGHT |
| HOLE DIAMETER (IN) | 5.75 | | | |
| HOLE DEPTH (FT) | 72 | 2.00 | 900G | 170 |
| FACE HEIGHT (FT) | 69 | 1.00 | BLASTGEL 1070 4 X 20 | 1,721 |
| SUB DRILLING (FT) | 3 | 0.75 | SPARTAN 350SR | 63.75 |
| AVG. STEM FACE HOLES (FT) | 9 | BULK | TITAN 1000 SD | 6,800 |
| STEM OTHER HOLES (FT) | 9 | BULK | TITAN 1000 SME | 59,049 |
| BURDEN FRONT ROW (FT) | 13 | | | |
| BURDEN OTHER ROWS (FT) | 13 | | | |
| SPACING FRONT ROW (FT) | 17 | | | |
| SPACING OTHER ROWS (FT) | 17 | | TOTAL WEIGHT: | 67,803.75 |

DETONATORS USED IN BLAST:     Electronic        MATS USED: No      STEM TYPE: #6'S

| TYPE | MFG | DATE CODE | USED | TYPE | MFG | DATE CODE | USED |
|---|---|---|---|---|---|---|---|
| 900G | Dyno Nobel Global | 04MY15W1 | 79 | 900G | Dyno Nobel Global | 05JA15W1 | 6 |
| DIGISHOT 30 FT | Dyno Nobel Global | 18MY15S1 | 11 | DIGISHOT 80FT | Dyno Nobel Global | 18MY15S1 | 85 |
| BLASTGEL 1070 4 X 20 | Dyno Nobel Global | 22JY15D1 | 1,720 | DIGISHOT 30 FT | Dyno Nobel Global | 23FE15S1 | 74 |
| SPARTAN 350SR | Dyno Nobel Global | 23JU15J3 | 85 | | | | |

CU YDS IN SHOT:    48,006     SCALED DISTANCE FACTOR:    142          % OF ANFO:      1
TONS IN SHOT:    109,189            HOLES/DELAY :    2          FUEL OIL % (BULK):      0
MAX LBS/DELAY:    1,575          AVERAGE LBS/HOLE    798
POWDER FACTOR (TONS/LB):          1.61          POWDER FACTOR POUNDS/YD3:      1.41
BLASTERS NAME: Moore, James P              BLASTERS NUMBER & STATE:  GA 18129     Georgia
BLASTERS SIGNATURE: _____         SITE SAFETY INSPECTION PERFORMED:      Yes
MINE MGT. SIGNATURE: _____         NUMBER OF PERSONNEL ON SITE:      5
REMARKS : Shot had cracks and voids all through it

| START TIME | END TIME | TOTAL TIME | TRUCK NUMBERS |
|---|---|---|---|
| 7:00 AM | 12:00 PM | 05:00 | |

Figure B. 5: July 30, 2015, Shot 3 Blast Report

# Dyno Nobel North America BLAST REPORT

**DYNO**
**Dyno Nobel**

PO NUMBER: JCM 21888
SERVICE SITE LOCATION: Whitesburg     ORDER NO.: 935010

BLAST NUMBER: 26-2015 production   BLAST TIME: 2:40 pm     BLAST DATE: 09/15/2015
CUSTOMER: ANDERSON COLUMBIA COM   MINE: JUNCTION CITY MINING     ADDRESS: Talbotton, GA
ROCK TYPE: Granite     Tons/Yd3:   2.27     EXPECTED VIBRATION:   0.050

## LOCATION OF BLAST

LOCATION OF BLAST IN MINE: North     BENCH: 2nd Bench
BLAST GPS POINTS: N -032 37 57.49980    &   W -084 30 01.80000

## WEATHER

WEATHER: Partly Cloudy     CEILING: High     TEMPERATURE: 79   WIND DIRECTION & SPEED:   East   8

## NEAREST NON-OWNED STRUCTURE

NAME: Roper Residence     GPS Points: N -032 38 38.68800 & W -084 30 51.30000
DISTANCE:   5,944 Ft     DIRECTION:   225°

## SEISMOGRAPH DATA

| | LOCATION | DISTANCE | GPS POINTS | | CALIBRATION DATE |
|---|---|---|---|---|---|
| 1 | Roper Residence | 5,944 Ft | N -032 38 38.68800 & W -084 30 51.30000 | | 06/16/2009 |

| | L | (F) | T | (F) | V | (F) | AIR (db) | SEISMOGRAPH | SERIAL | OPERATOR |
|---|---|---|---|---|---|---|---|---|---|---|
| 1 | 0.000 | 0 | 0.000 | 0 | 0.000 | 0 | 0 | Seismograph AB96' | 1 | |

## BLAST DATA

| | | EXPLOSIVES SIZE, TYPE & WEIGHT | | |
|---|---|---|---|---|
| NUMBER OF HOLES (EA) | 85 | | | |
| HOLE DIAMETER (IN) | 5.75 | SIZE | TYPE | WEIGHT |
| HOLE DEPTH (FT) | 70 | 2.00 | 900G | 184 |
| FACE HEIGHT (FT) | 67 | 1.00 | BLASTGEL 1070 4 X 20 | 1,540 |
| SUB DRILLING (FT) | 3 | 0.75 | SPARTAN 350SR | 63.75 |
| AVG. STEM FACE HOLES (FT) | 9 | BULK | TITAN 1000 SD | 10,680 |
| STEM OTHER HOLES (FT) | 9 | BULK | TITAN 1000 SME | 58,772 |
| BURDEN FRONT ROW (FT) | 13 | | | |
| BURDEN OTHER ROWS (FT) | 13 | | | |
| SPACING FRONT ROW (FT) | 17 | | | |
| SPACING OTHER ROWS (FT) | 17 | | TOTAL WEIGHT: | 71,239.75 |

DETONATORS USED IN BLAST:   Electronic     MATS USED: No     STEM TYPE: #6'S

| TYPE | MFG | DATE CODE | USED | TYPE | MFG | DATE CODE | USED |
|---|---|---|---|---|---|---|---|
| 900G | Dyno Nobel Global | 13JY15W1 | 92 | SPARTAN 350SR | Dyno Nobel Global | 14AU15J3 | 83 |
| BLASTGEL 1070 4 X 20 | Dyno Nobel Global | 17AU15D1 | 680 | BLASTGEL 1070 4 X 20 | Dyno Nobel Global | 21JY15D1 | 860 |
| SPARTAN 350SR | Dyno Nobel Global | 23JU15J3 | 2 | DIGISHOT 30 FT | Dyno Nobel Global | 27JY15S1 | 85 |
| DIGISHOT DETONATOR 100FT | Dyno Nobel Global | 27JY15S1 | 92 | | | | |

CU YDS IN SHOT: 46,615     SCALED DISTANCE FACTOR: 152     % OF ANFO: 1
TONS IN SHOT: 106,024     HOLES/DELAY: 2     FUEL OIL % (BULK): 0
MAX LBS/DELAY: 1,525     AVERAGE LBS/HOLE 838
POWDER FACTOR (TONS/LB): 1.49     POWDER FACTOR POUNDS/YD3: 1.53
BLASTERS NAME: Moore, James P     BLASTERS NUMBER & STATE: GA 18129   Georgia
BLASTERS SIGNATURE:     SITE SAFETY INSPECTION PERFORMED: Yes
MINE MGT. SIGNATURE:     NUMBER OF PERSONNEL ON SITE: 5
REMARKS: Shot had void and cracks all through it

| START TIME | END TIME | TOTAL TIME | TRUCK NUMBERS |
|---|---|---|---|
| 7:30 AM | 12:00 PM | 04:30 | |

Figure B. 6: September 15, 2015, Shot 4 Blast Report

APPENDIX C.

SEISMOGRAPH AND BORETRACK REPORTS

## Table C.1: DynoConsult Seismograph Summary

| Shot Date | Seismo ID | Seimo Northing | Seismo Easting | Shot Northing | Shot Easting | Location Relative to Shot | Acoustic (dBL) | R PPV | V PPV | T PPV | Max PPV | R Frequency | V Frequency | T Frequency |
|---|---|---|---|---|---|---|---|---|---|---|---|---|---|---|
| 4/16/2015 | 892 | 32°38'2.6" | W84°30'06.7". | N 32°37'56.59980" | W84°30'07.30020" | below in front | 142 | 0.49 | 0.48 | 0.44 | 0.49 | 46.5 | 39.3 | 36.5 |
| 4/16/2015 | 450 | N32°38'3.1" | W84°30'11.3". | N 32°37'56.59980" | W84°30'07.30020" | below in front | 142 | 0.26 | 0.27 | 0.22 | 0.27 | 26.9 | 56.8 | 17.6 |
| 4/16/2015 | 2344 | N32°37'16.6" | W84°29'51". | N 32°37'56.59980" | W84°30'07.30020" | behind (pond) | 133 | 0.43 | 0.48 | 0.49 | 0.49 | 10.2 | 9.3 | 13.1 |
| 6/4/2015 | 450 | N32°37'55.0" | W84°29'52.1". | N 32°38'02.3" | W84°30'01.5" | behind (pond) | <100 | 0.45 | 0.61 | 0.45 | 0.61 | 34.1 | 12.4 | 26.9 |
| 6/4/2015 | 892 | | | N 32°38'02.3" | W84°30'01.5" | | 142 | 0.17 | 0.1 | 0.14 | 0.17 | 19.6 | 18.9 | 18.9 |
| 9/15/2015 | 892 | | | N 32°37'57.49980" | W84°30'01.80000" | behind (pond) | 139 | 2.52 | 1.48 | 1.36 | 2.52 | 34.1 | 23.2 | 46.5 |
| 9/15/2015 | 450 | | | N 32°37'57.49980" | W84°30'01.80000" | in front across pit | 136 | 0.16 | 0.33 | 0.15 | 0.33 | 20.4 | 23.3 | 28.4 |
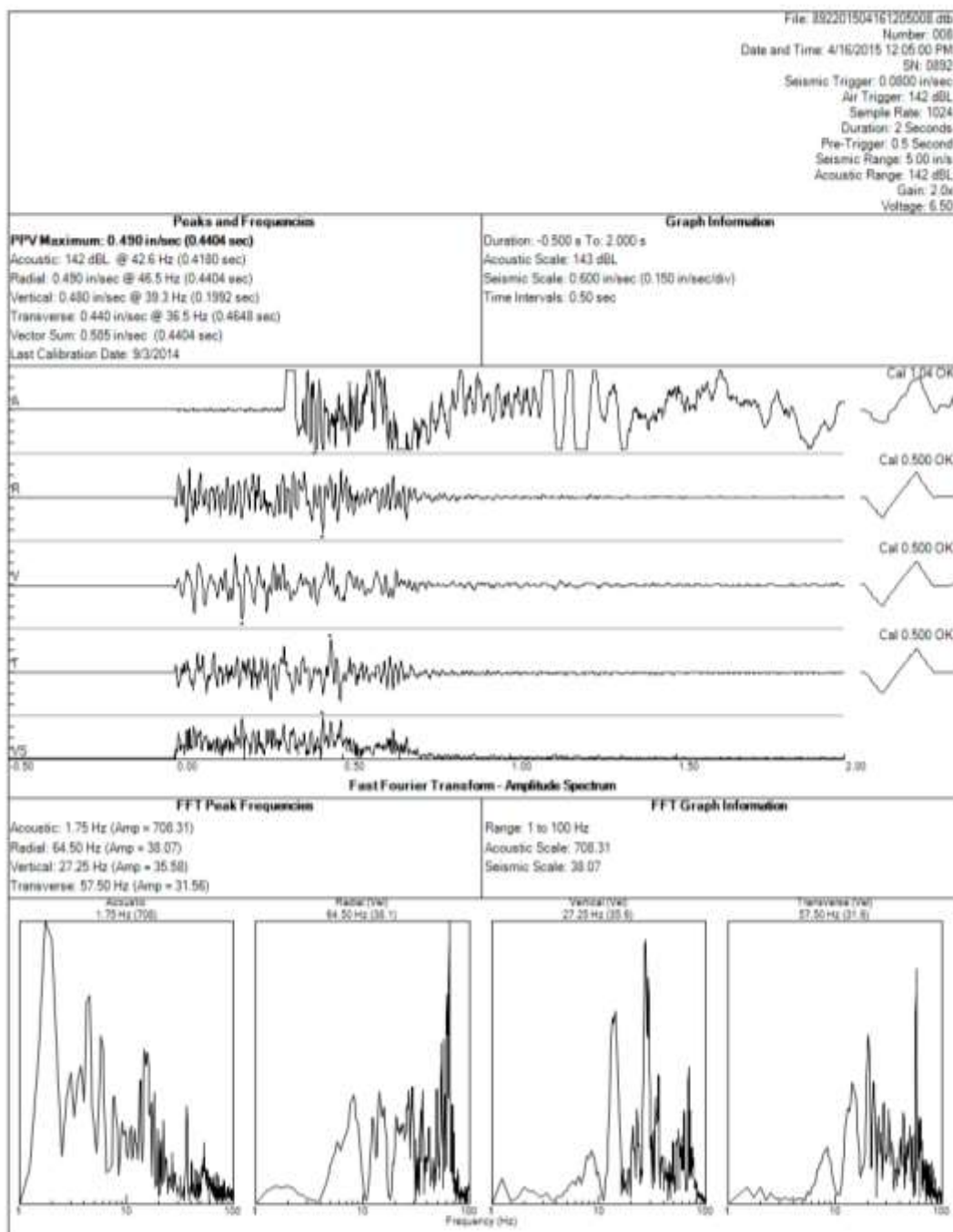
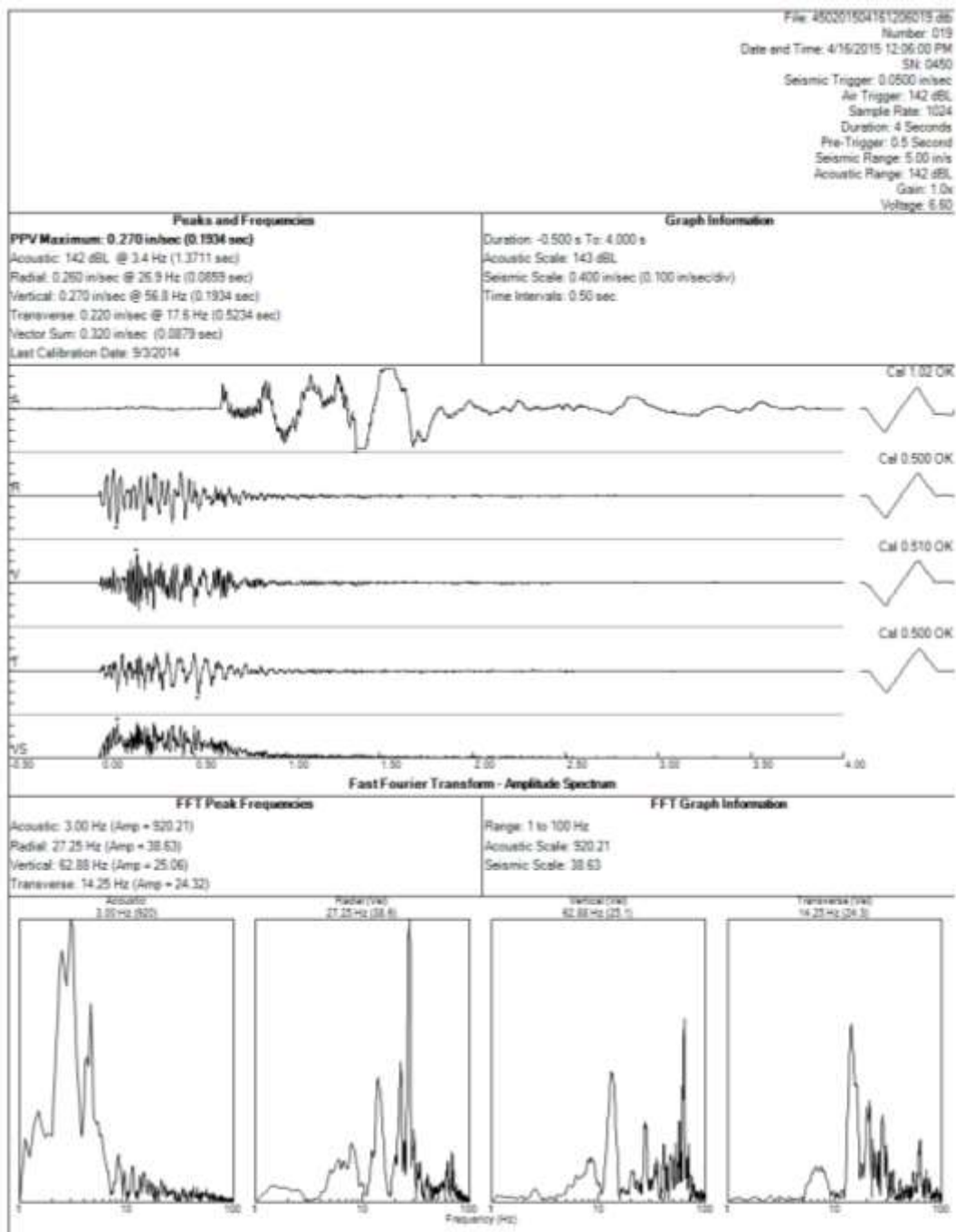Figure C.1: April 14, 2015 892 Seismograph Report

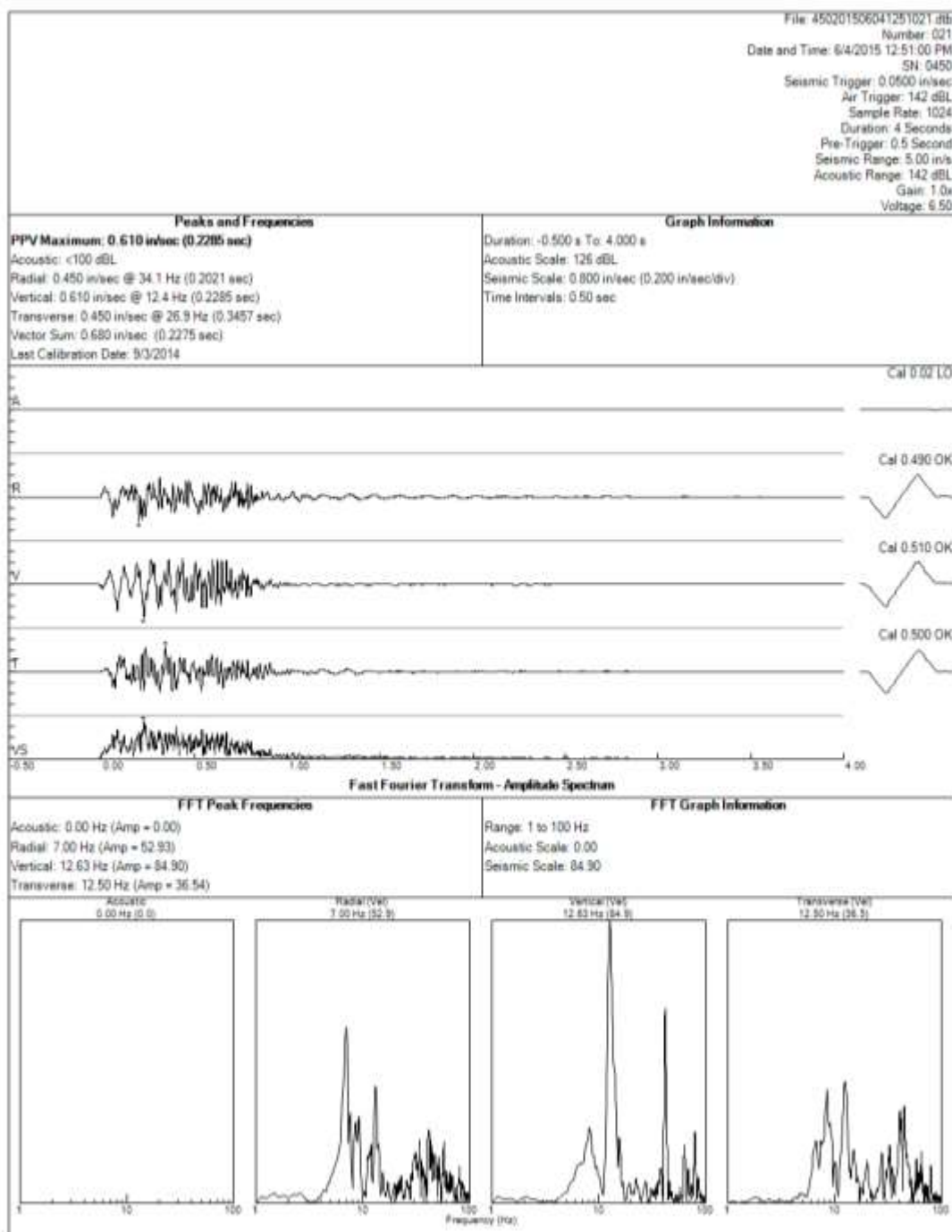Figure C.2: April 14, 2015 450 Seismograph Report

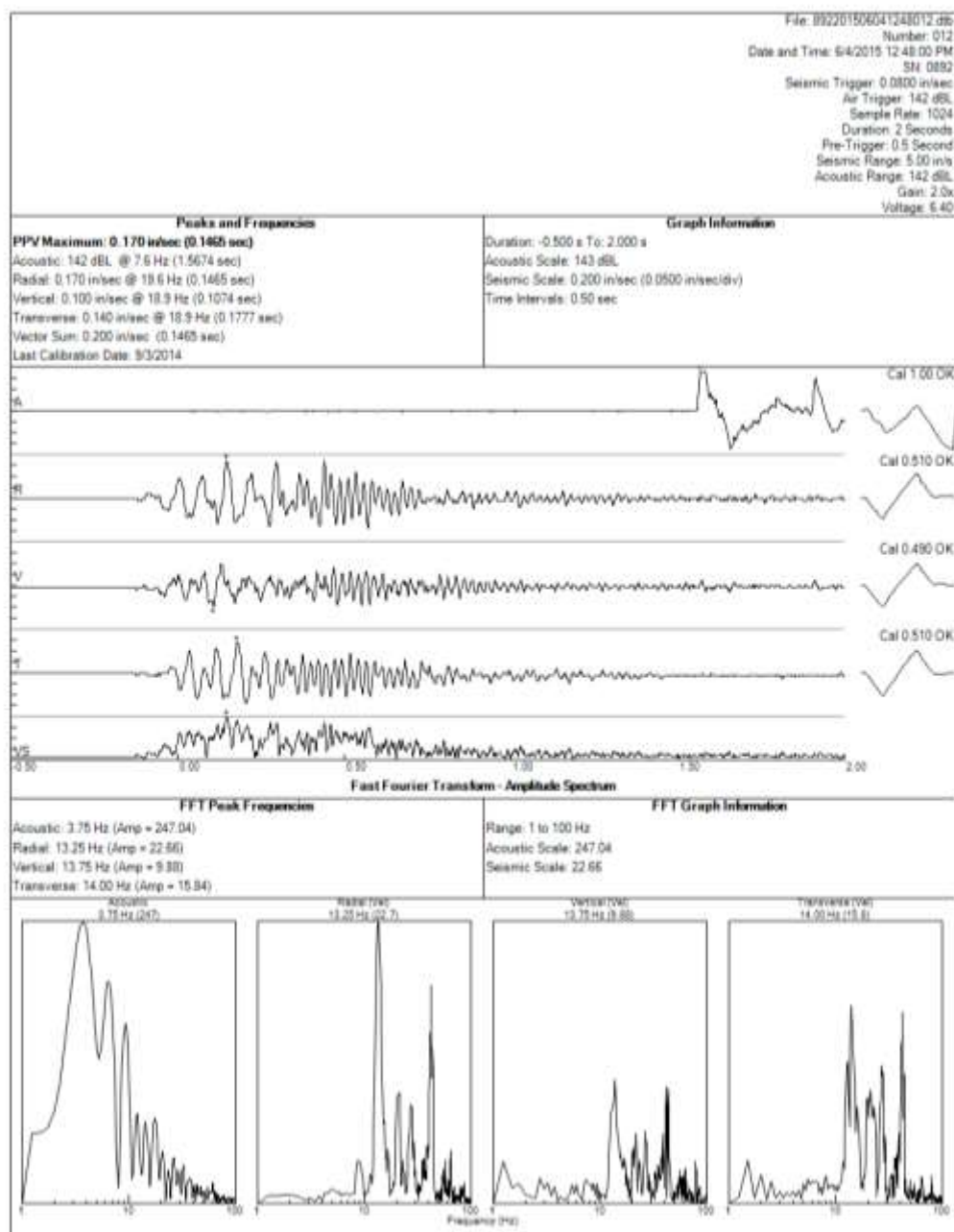Figure C.3: June 4, 2015 450 Seismograph Report

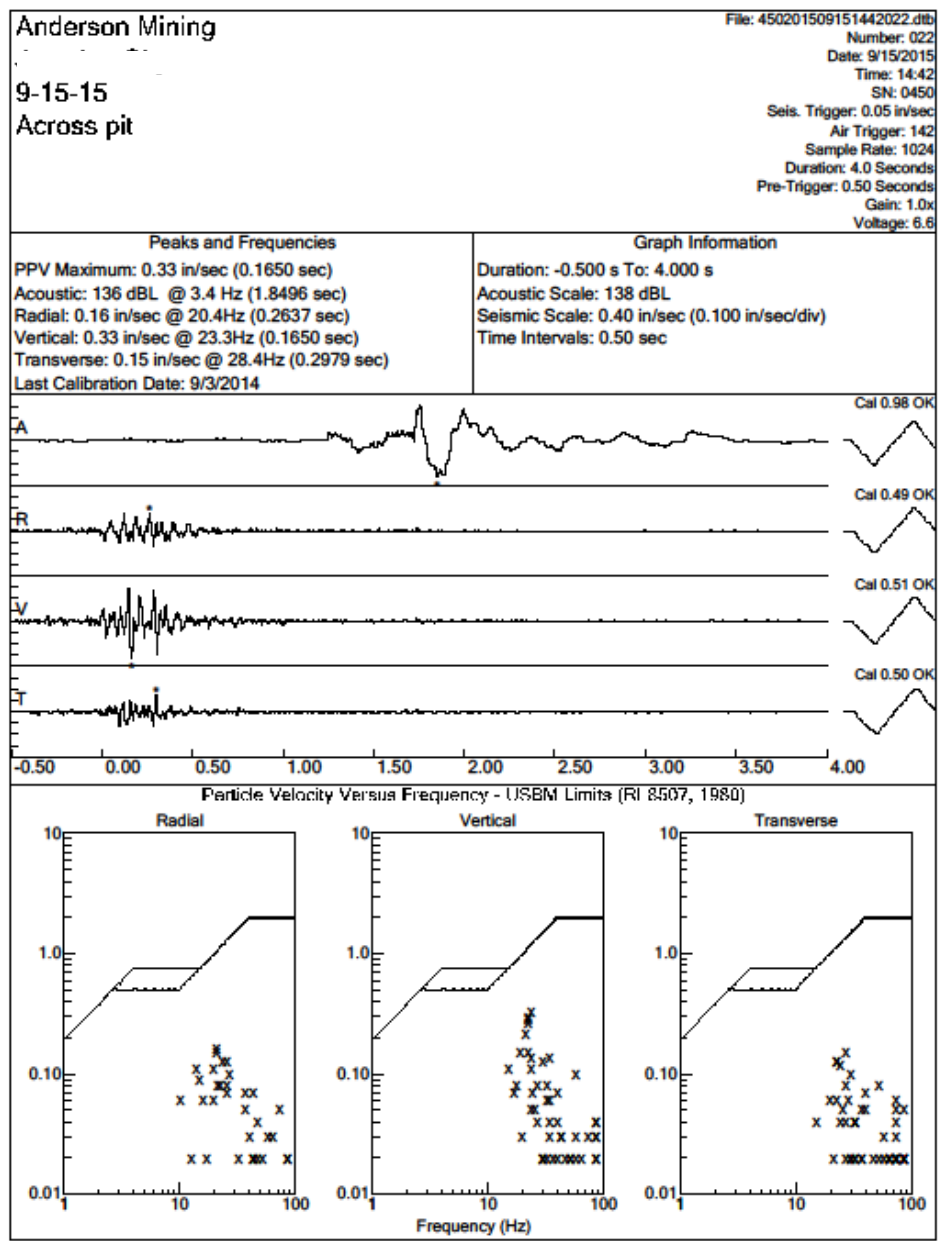Figure C.4: June 4, 2015 892 Seismograph Report

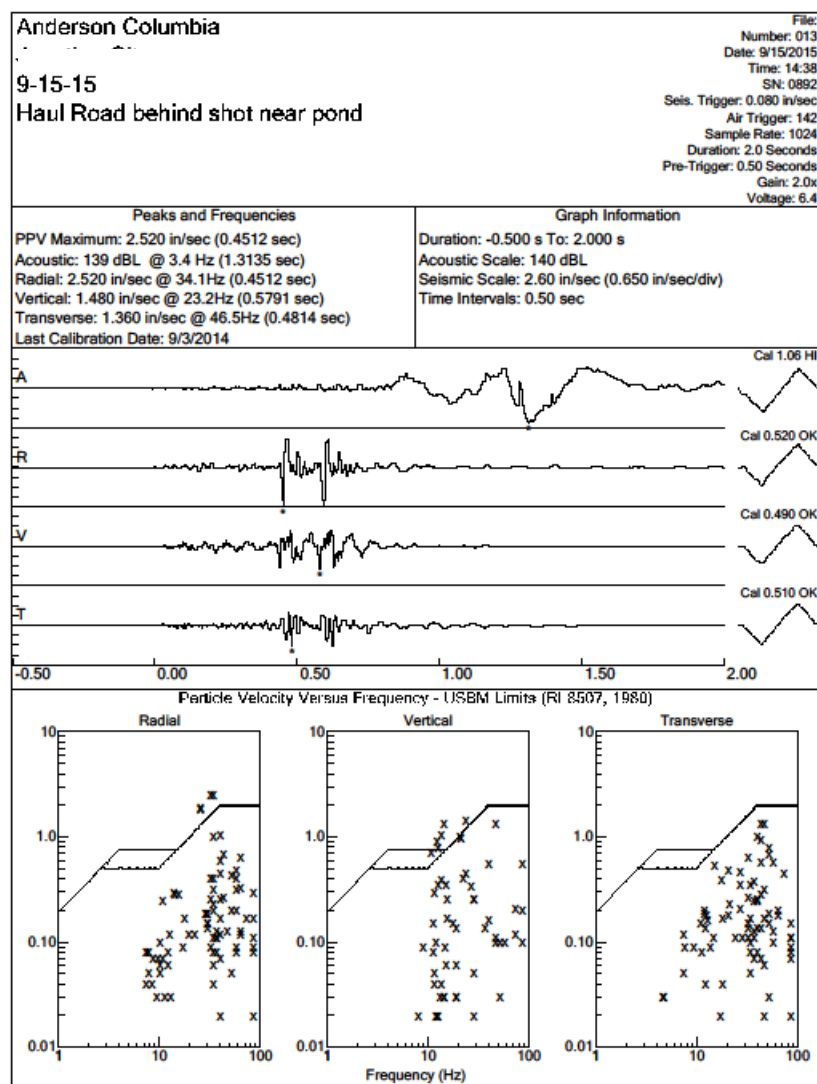Figure C.5: September 15, 2015 450 Seismograph Report

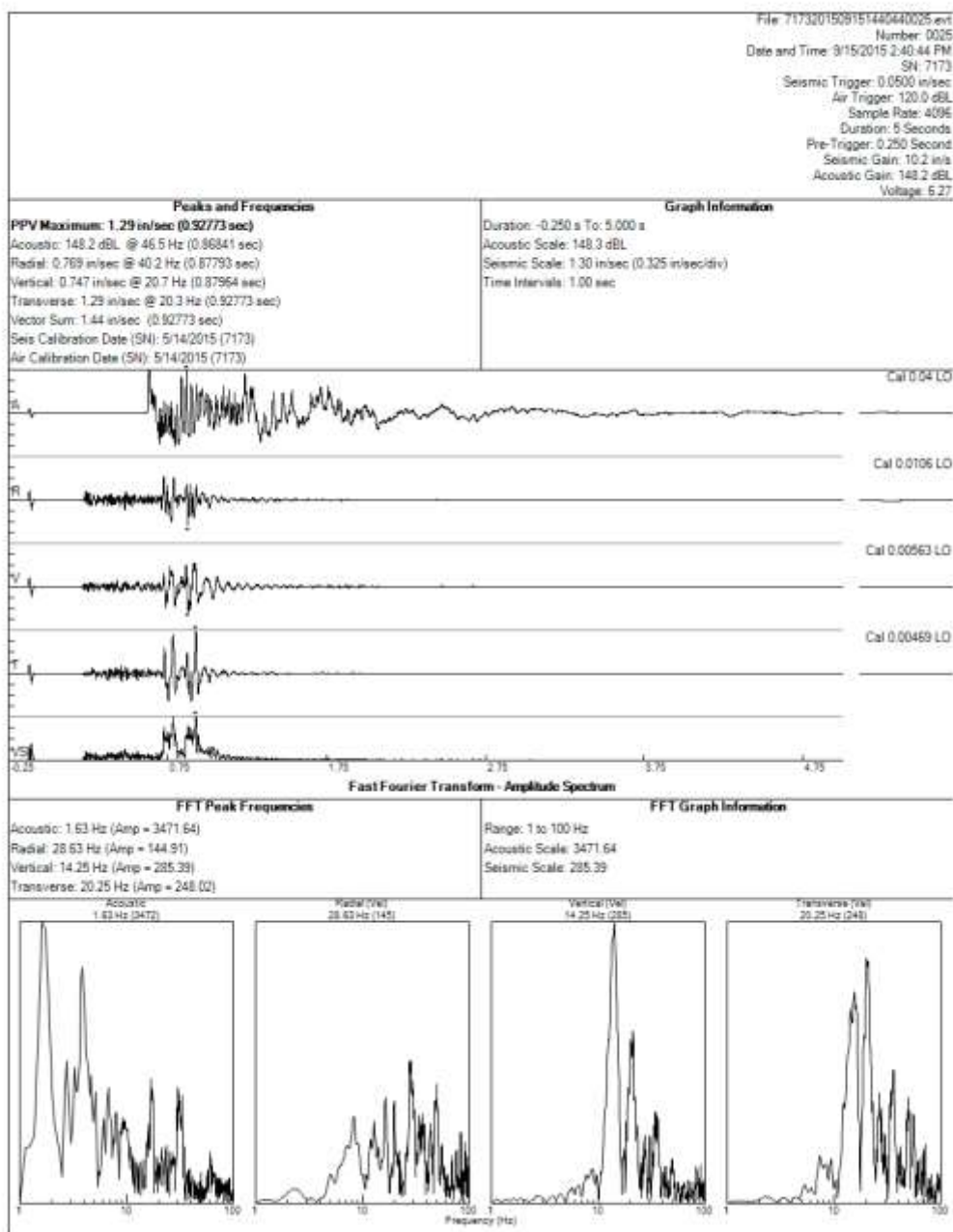Figure C.6: September 15, 2015 892 Seismograph Report

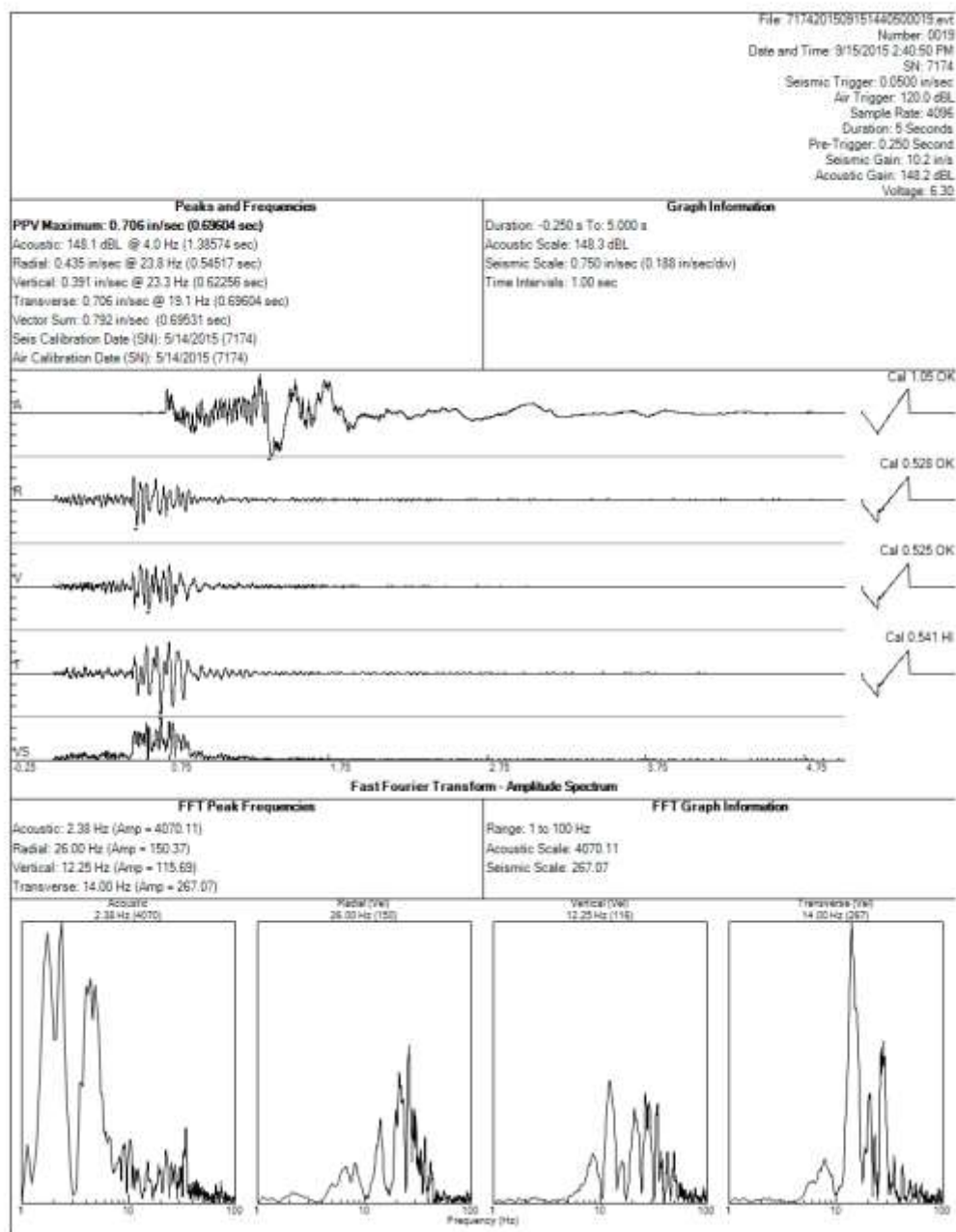Figure C.6: September 15, 2015 7173 Seismograph Report

Figure C.6: September 15, 2015 7174 Seismograph Report

## *Profile Printout*
### Anderson Columbia

Unedited Profile for Borehole   15

Operator:  Andy Hudson

Survey Date 06/03/15

| Depth ft | True Burden ft | Offset ft |
|---|---|---|
| 1.0 | Undefined | 0.0 |
| 2.0 | 9.8 | 0.0 |
| 3.0 | 10.3 | 0.0 |
| 4.0 | 11.6 | 0.0 |
| 5.0 | 12.0 | 0.0 |
| 6.0 | 11.9 | 0.0 |
| 7.0 | 12.1 | 0.0 |
| 8.0 | 12.2 | 0.0 |
| 9.0 | 12.1 | 0.0 |
| 10.0 | 12.0 | 0.0 |
| 11.0 | 11.8 | 0.0 |
| 12.0 | 11.5 | 0.0 |
| 13.0 | 11.5 | 0.0 |
| 14.0 | 11.8 | 0.0 |
| 15.0 | 12.4 | 0.0 |
| 16.0 | 12.7 | 0.0 |
| 17.0 | 12.9 | 0.1 |
| 18.0 | 13.2 | 0.1 |
| 19.0 | 13.6 | 0.1 |
| 20.0 | 14.2 | 0.1 |
| 21.0 | 14.6 | 0.1 |
| 22.0 | 14.5 | 0.1 |
| 23.0 | 14.8 | 0.1 |
| 24.0 | 14.6 | 0.1 |
| 25.0 | 14.4 | 0.1 |
| 26.0 | 14.9 | 0.2 |
| 27.0 | 15.1 | 0.2 |
| 28.0 | 15.1 | 0.2 |
| 29.0 | 15.2 | 0.2 |
| 30.0 | 15.2 | 0.2 |
| 31.0 | 15.1 | 0.2 |
| 32.0 | 15.1 | 0.2 |
| 33.0 | 15.1 | 0.2 |
| 34.0 | 15.1 | 0.2 |
| 35.0 | 15.0 | 0.3 |
| 36.0 | 14.9 | 0.3 |
| 37.0 | 15.0 | 0.3 |
| 38.0 | 14.9 | 0.4 |
| 39.0 | 14.7 | 0.4 |
| 40.0 | 14.9 | 0.4 |

| | |
|---|---|
| Hole Diameter | 5.75 in |
| Hole Length | 72.1 ft |
| Stemming | 8.0 ft |
| Back Fill: | 0.0 ft |
| Subdrill | 1.5 ft |
| Hole Angle | Varies |
| Profile Cross-Section | 978.8 ft² |
| Borehole Volume: | 14622.6 ft3 |
| Minimum Burden | 11.47 ft @12.0 ft |
| Maximum Burden | 18.33 ft @64.7 ft |
| Ave Burden | 14.8 ft |
| Nominal Powder Factor | 0.000 lb/cuy |
| | 0.000 lb/ton |

| Profile Location: | |
|---|---|
| Distance from LM: (ft) | 268.07 |
| Offset from Ref Line: (ft) | -1.39 |
| Borehole Collar: | |
| Northing (ft) | 880.69 (ft) |
| Easting (ft) | 1243.00 (ft) |
| Elevation (ft) | 164.60 (ft) |

Page No : 1

0   4ft   Scale 1:616.2
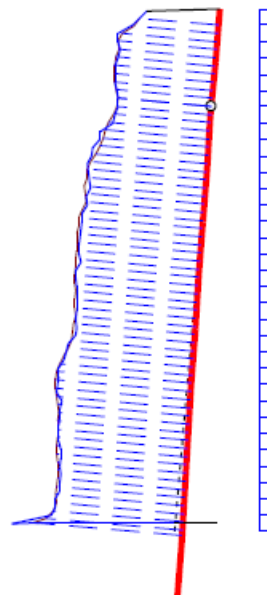
Figure C.7: Example Boretrack Report from Shot 2 Zone 2

APPENDIX D.

SHOT PHOTOGRAPHS

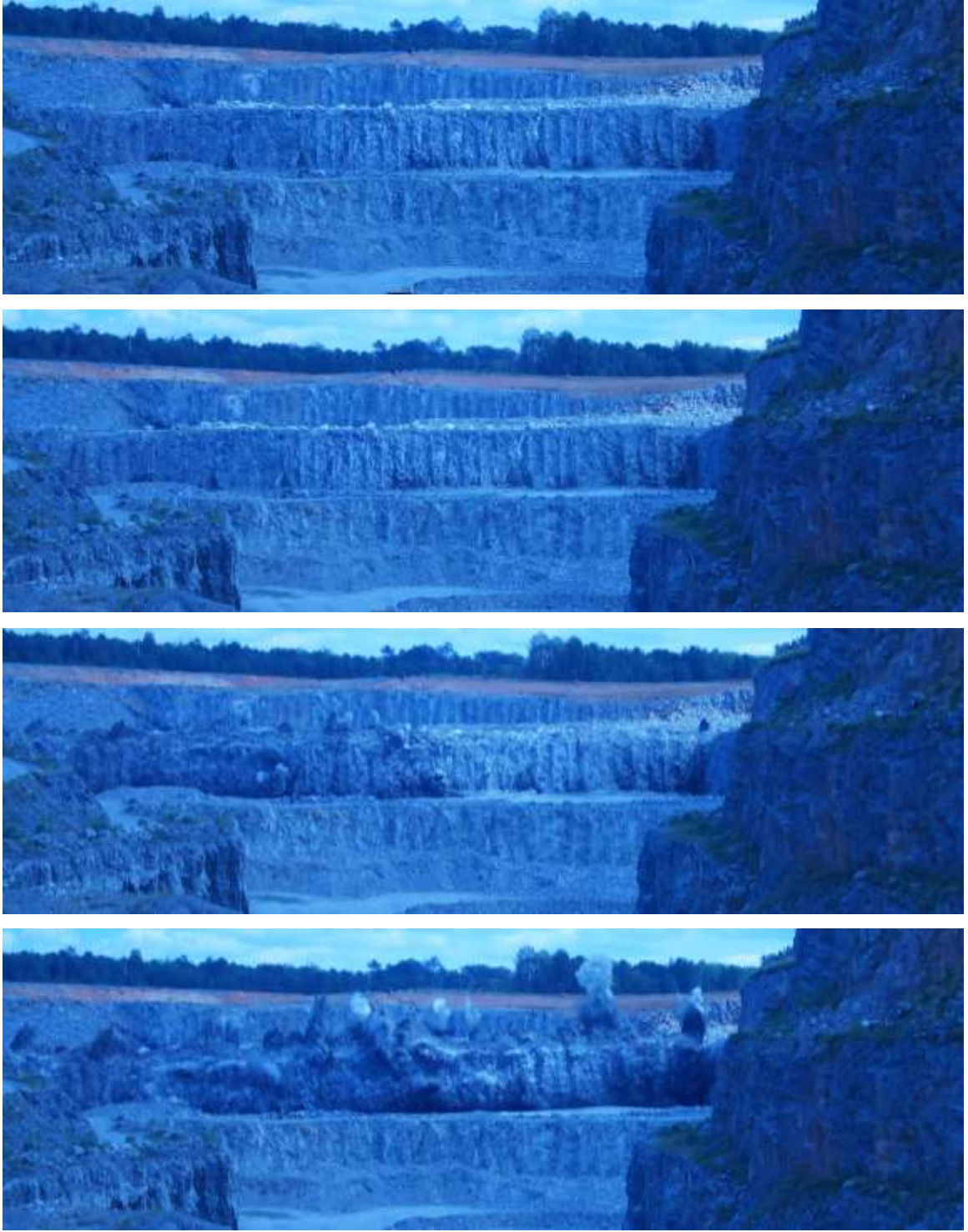Figure E. 1: April 16, 2015, Shot 1 Blast Photographs

Figure E. 2: June 4, 2015, Shot 2 Blast Photographs

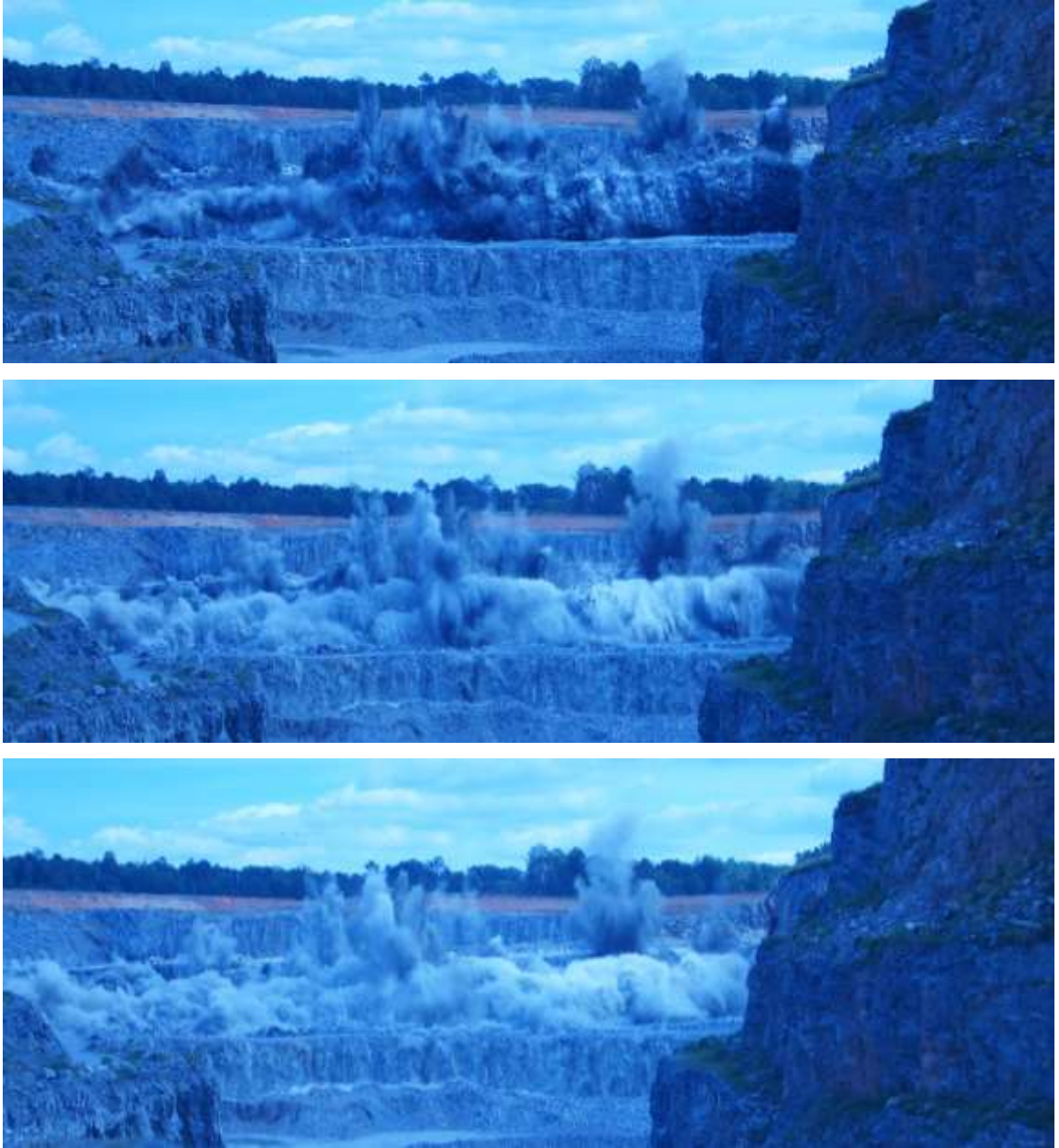Figure E. 3: July 30, 2015, Shot 3 Blast Photographs

Figure E. 4: September 15, 2015, Shot 4 Blast Photographs

# BIBLIOGRAPHY

Abu Bakar, M.Z., Tariq, S.M., Hayat, M.B., Zahoor, M. K., Khan, M.U. "Influence of Geological Discontinuities upon Fragmentation by Blasting." Pakistan Journal of Science. Vol. 65 No. 3. September, 2013.

Cunningham, C.V.B. "The Kuz-Ram fragmentation model - 20 years on." 3rd EFEE Conference Proc., Brighton, England, pp. 201-210. 2005.

Cunningham, C.V.B. "The Kuz—Ram model for prediction of fragmentation from blasting." Proceedings of the first international symposium on rock fragmentation by blasting, Lulea, Sweden. pp. 439–54. 1983.

Floyd, John. "Efficient Blasting Techniques." Blast Dynamics. Course Notes. Reno, NV. May 2013.

Gheibie, S., Aghababaei, H., Hoseinie, S.H., and Pourrahimian, Y. "Modified Kuz—Ram fragmentation model and its use at the Sungun Copper Mine." International Journal of Rock Mechanics and Mining Sciences, Volume 46, Issue 6, September 2009, pp. 967–973.

Grant, John R. "Initiation Systems – What does the Future Hold?" Third International Symposium on Rock Fragmentation by Blasting. The Australasian Institute of Mining and Metallurgy. Brisbane, Queensland. 1990.

ISEE. *Blasters' Handbook 18th Edition*. International Society of Explosives Engineers, Cleveland, OH, 2011.

Johansson, Daniel and Ouchterlony, Finn. "Shock Wave Interactions in Rock Blasting: the Use of Short Delays to Improve Fragmentation in Model-Scale." Rock Mechanics and Rock Engineering, January 2013, Volume 46, Issue 1, pp. 1-18.

Johnson, Catherine E., "Fragmentation Analysis in the Dynamic Stress Wave Collision Regions in Bench Blasting" (2014). Theses and Dissertations--Mining Engineering. Paper 16. http://uknowledge.uky.edu/mng_etds/16.

Katsabanis, P.D., Kim, S., Tawadrous, A., and Sigler, J. "Effect of powder factor and timing on the impact breakage of rocks." ISEE General Proceedings 2008G Volume 2. 2008.

Katsabanis, P.D. and Liu, L. "Delay Requirements for Fragmentation Optimization." *Measurement of Blast Fragmentation.* Balkema, 1996.

Katsabanis, P., Omidi, O., Rielo, O., and Ross, P. "A Review of Timing Requirements for Optimization of Fragmentation". Proceedings of the 40th Conference on Explosives and Blasting Technique. ISEE, Denver, CO, 2014.

Katsabanis, P. D., Tawadrous, A., Braun, C., Kennedy, C. "Timing Effects on Fragmentation." Proceedings of the 32nd Conference on Explosives and Blasting Technique. ISEE, Dallas, TX, 2006.

Motion Metrics. "Portable Analysis PortaMetrics." http://www.motionmetrics.com/portable/. October 2015.

Orica. "I-kon II Detonator." http://www.oricaminingservices.com/us/en/product/products_and_services/electronic_blasting_systems/i-kon_ii/page_the_next_generation/i-kon_ii_detonator/1382. October 2015.

Otterness, R.E., Stagg, M.S. and Rholl, S.A. "Correlation of Shot Design Parameters to Fragmentation." ISEE Annual Conference on Explosives and Blasting Research. pp. 179-191. 1991.

Rossmanith, H. P. "The Mechanics and Physics of Electronic Blasting." Proceedings of the 33rd Conference on Explosives and Blasting Technique. ISEE, Nashville, TN, 2003.

Rossmanith, H.P. "The use of Lagrange diagrams in precise initiation blasting." Part I: Two interacting boreholes. Fragblast, Vol. 6, No. 1, pp. 104–136. 2002.

Sanchidrian, J.A., Segarra, P., Ouchterlony, F. Lopez, L.M. "On the accuracy of fragment size measurement by image analysis in combination with some distribution functions." Rock Mechanics and Rock Engineering. February 2009, Volume 42, Issue 1, pp 95-116.

Sjoberg, J., Schill, M. Hilding, D., Yi, C., Nyberg, U., and Johansson, D. "Computer Simulations of Blasting with Precise Initiation". Eurock, Stockholm, Sweden, 2012.

Split Engineering. "Split-Desktop Software." http://www.spliteng.com/products/splitdesktop-software/. October 2015.

Stagg, M.S. and Nutting, M.J. "Blast Delay Influence on Rock Fragmentation; One-Tenth Scale Tests." USBM IC 9135. pp. 79-95. 1987.

The Physics Hypertextbook. "The Nature of Sound." http://physics.info/sound/. October 2015.

Wagner, Mark. DeVuono, Kevin. WipFrag. Conversation, July 27, 2015.

WipFrag. "WipFrag Manual." North Bay, Ontario, Canada. October 2015.

Worsey, Paul. "1.2 Radial Fracture Mechanics." Course Presentation for Explosives Engineering Environmental Controls for Blasting. Rolla, MO, 2014.

Worsey, Paul. "1.6 Secondary Fragmentation by Collision." Course Presentation for Explosives Engineering Environmental Controls for Blasting. Rolla, MO, 2014, b.

Worsey, Paul. "1.7 Geological Modification Effects on General Blasting Scheme." Course Presentation for Explosives Engineering Environmental Controls for Blasting. Rolla, MO, 2014, c.

Worsey, Paul. "7.3 Optimizing Shots." Course Presentation for Explosives Engineering Blast Design and Technology. Rolla, MO, 2015.

Worsey, Paul. "7.5 Cast Blasting." Course Presentation for Explosives Engineering Blast Design and Technology. Rolla, MO, 2015, b.

Worsey, Paul. "Geotechnical Factors Affecting the Application of Pre-split Blasting to Rock Slopes." Ph.D. Thesis, Department of Mining Engineering, University of Newcastle upon Tyne, August 1981.

Yamamoto, M., Ichijo, T., Inabe, T., Morooka, K., and Kaneko, K. "Experimental and theoretical study on smooth blasting with electronic delay detonators." Fragblast 3: 3-24. 1999.

Yang, Hyung-Sik and Rai, Piyush. "Characterization of fragment size vis-à-vis delay timing in quarry blasts." Powder Technology 211. Pp. 120–126. 2011.

**VITA**

Margaret Ruth Hettinger was born in St. Louis, MO on December 20, 1988. She graduated from the Missouri University of Science and Technology in May 2010 with a Bachelor of Science in Mining Engineering with minors in Explosives Engineering and Writing. After graduation she worked for the Doe Run Company, Dykon Explosive Demolition, and Barrick. In the summer of 2014 she returned to the Missouri University of Science and Technology to pursue a Master of Science in Explosives Engineering and received her MS in December, 2015.